5-2018

Sediment Dynamics and Channel Connectivity on Hillslopes

Xiaoyu Lu
University of Tennessee, xlu14@vols.utk.edu

To the Graduate Council:

I am submitting herewith a dissertation written by Xiaoyu Lu entitled "Sediment Dynamics and Channel Connectivity on Hillslopes." I have examined the final electronic copy of this dissertation for form and content and recommend that it be accepted in partial fulfillment of the requirements for the degree of Doctor of Philosophy, with a major in Geography.

Yingkui Li, Major Professor

We have read this dissertation and recommend its acceptance:

Jonathan M. Harbor, Nicholas N. Nagle, Robert A. Washington-Allen, Daniel C. Yoder

Accepted for the Council:

Dixie L. Thompson

Vice Provost and Dean of the Graduate School

(Original signatures are on file with official student records.)

Sediment Dynamics and Channel Connectivity on Hillslopes

A Dissertation Presented for the

Doctor of Philosophy

Degree

The University of Tennessee, Knoxville

Xiaoyu Lu

May 2018

To my wife Yanan "Nancy" Li, a passionate traveller and dedicated scientist, for the love, support, and understanding.

To my parents Shengchun Lu and Ruilan Zhao for their trust and care along the way.

To my advisor Dr. Yingkui Li, for his immeasurable help on this dissertation and in my life through my PhD program.

Acknowledgments

I would love to thank my advisor, Dr. Yingkui Li, for his mental support and intellectual guidance during my PhD program. Dr. Li is a role model and great inspiration for everyone who seeks to be a scientist, and he leads not with his words, but his actions. I had the privilege to work with Dr. Li for the past 4 years, and learned a great amount from him both in the field and in the lab. He showed me how to work as a scientist, and more importantly, to think as one. Dr. Li is always enthusiastic about geomorphology, and constantly curious about the various processes that shape the Earth; he is also keen on advanced geographic technology, and always trying to incorporate new materials in his teaching. This dissertation could not be done without the guidance of Dr. Li, to whom I am much obliged.

I want to extend my gratitude to my dissertation committee — Drs. Robert Washington-Allen, Nicholas Nagle, Jon Harbor, and Daniel Yoder. They contributed to this dissertation research by sharing their profound domain knowledge, invaluable experience, and insurmountable passion with me. More importantly, they never ceased to intellectually challenge me and encourage me to ask the important questions, to see the big picture, and to be a better scientist.

This dissertation research received financial support from the scholarship and the Thomas Fellowship from University of Tennessee, the Reds Wolman Graduate Research Award from the Geomorphology Specialty Group of the American Association of Geographers, and the Stewart K. McCroskey Memorial Fund and Ralston's Geospatial Award from the Department of Geography. These funds allowed for me to conduct field work, get access to labs and facilities, and attend academic conferences. Additionally, the organizations showed me the importance of giving back, and I am forever grateful for their generous support.

Individuals in the Department of Geography were welcoming and friendly during my program. Specifically, I would like to thank Drs. Shih-lung Shaw, Carol Harden, Yingjie Hu, Sally Horn, Bruce Ralston, Kelsey Ellis, Ron Kalafsky, Ron Foresta, and Melissa Hinten in the Department of Geography for the help throughout my PhD program. I appreciate the support, encouragement, and drinks from graduate students especially Jack McNelis, Rebecca Potter, Yasin Wahid Rabby, Adam Alsamadisi, Maegen Rochner, Kyle Landolt, and Jeremy Auerbach. I am positive that this list is incomplete and there are many others whose name I cannot list here due to limited space.

Special thanks to Lorelei Bryan, Jack Bryan, Rossie Adams, and Ken Adams for being supportive and caring during my time in Knoxville.

Last but not the least, I want to thank my wife Yanan "Nancy" Li. I am lucky to have met Nancy in Knoxville. My life in the graduate school would possibly be somewhat miserable and definitely less fun without her company. She is always there when I need encouragement and support, for that I will always be grateful.

Abstract

The pattern, magnitude, and frequency of hillslope erosion and deposition are spatially varied under the influence of micro-topography and channel geometry. This research investigates the interrelationships between erosion/deposition, micro-topography, and channel connectivity on a hillslope in Loudon, Tennessee using the centimeter (cm) level temporal Digital Elevation Models collected using laser scanning. This research addressed (1) the effect of spatial resolution on the erosion/deposition quantification, and rill delineation; (2) the influences of micro-topographic factors (e.g. slope, roughness, aspect) on erosion and deposition; (3) the relationship between the structural connectivity — depressions and confluence of rills — and the sedimentological connectivity. I conducted (1) visual and quantitative assessments for the erosion and deposition, and the revised automated proximity and conformity analysis for the rill network; (2) quantile regression for micro-topographic factors using segmented rill basins; and (3) cross-correlation analysis using erosion and deposition series along the channels.

Overall, rills are sedimentologically more dynamic than the interrill areas. A larger grid size reduces the detectable changes in both areal and volumetric quantities, and also decreases the total length and number of rills. The offset between delineated rills and the reference increases with larger grid sizes. A larger rill basin has higher erosion and deposition with the magnitude of erosion greater than deposition. The slope has a positive influence on erosion and a negative one on deposition; roughness has a positive influence on deposition and a negative one on erosion. Areas that are more north-facing experience higher erosion and lower deposition. Rill length explains 46% of the variability for erosion and 24% for deposition. The depressions are associated with higher erosion in the downslope direction.

The correlations between the erosion and the confluence are positive; the correlation between the deposition and the sink is positive. Overall, the influence of structural connectivity on the sedimentological connectivity is within 25 cm in both upstream and downstream directions. This research contributes to the understanding in how the sediment movement on hillslopes is governed by topographic variations and channel connectivity, and future work may explore hillslope channels at broader geographical and temporal scales.

Table of Contents

List of Tables

List of Figures

Chapter 1

Introduction

1.1 Overview of this doctoral dissertation research

This doctoral dissertation investigates the inter-relationships between the dynamics of sediment movement and the spatial variations of topographic factors as well as channel connectivity on a rilled hillslope. The sediment movement in this study is defined as the pattern of sediment redistribution both on a planar dimension (spatial pattern) and a longitudinal dimension (sedimentological connectivity). Sedimentological connectivity, defined by Bracken and Croke (2007) as the continuity of sediment transport pathways from source to a sink, describes the coupling between erosion rates and sediment yield and has been used to link the spatially varied sediment transfer mechanism to the channel morphology (Hooke, 2003), runoff transport capacity (Bracken and Croke, 2007), topography (de Vente et al., 2006), vegetation (Sandercock and Hooke, 2011), and abrupt events such as landslides (de Vente et al., 2006). Previous studies in the spatial pattern of sediment redistribution and sedimentological connectivity have focused mainly on the watershed scale, emphasizing fluvial channels and their connection to the hillslopes (Cavalli et al., 2013; Detty and McGuire, 2010). In contrast, limited investigations have been made on hillslope channels such as rills and gullies (Ohde, 2011; Sandercock and Hooke, 2011).

The relatively limitedness of studies on the sedimentological connectivity of hillslope channels is a consequence of the lack of means to accurately quantify and monitor sediment movement within small hillslope channels (rill and ephemeral gullies). The magnitude of the sediment movement in hillslope channels is usually much smaller than that of stream channels, making it difficult to detect landform changes in a short period. With the advance of technologies in remote sensing, the ability to measure topographic change has reached a higher level of accuracy and resolution, allowing for more accurate and precise detection and quantification of sediment movement for hillslope channels. Linking sediment yield, channel change, and topographic variation will provide useful insight into the physical processes that govern sediment yield and channel development on hillslopes and improve our understanding in the practices of land management and soil erosion control.

This research investigates rill erosion, channel connectivity, and sediment dynamics on a hillslope in the East Tennessee. Repeated field surveys were conducted using a terrestrial laser scanner (TLS), and temporal digital elevation models (DEMs) were generated to quantify sediment movement within the channels and the sediment yield from the hillslope. The spatial pattern of sediment movement was used to investigate sedimentological connectivity and channel development and their relationships with micro-topographic factors and channel connectivity.

1.2 Background

1.2.1 Rill erosion on hillslopes

Water-induced soil erosion is one of the most common Earth-surface processes driven by raindrop impact, surface overflow, and mass wasting (Knighton, 1998; Selby, 1982). It accounts for $> 50\%$ of the total soil loss (can reach up to 95% under certain conditions) on the hillslopes (Van Asch, 1983; Morgan et al., 1987). The loss of soil reduces agricultural productivity, causes sedimentation in reservoirs, and contributes to water pollution in streams. Governed by climatic events and geologic conditions, water erosion can also be influenced by other environmental factors including vegetation, topography, land use, and human activities (Wischmeier and Smith, 1978).

Rills are micro-channels on hillslopes that are initially formed during rainfall events. Rills are typically 0.05 – 0.3 m wide and up to 0.3 m deep (Knighton, 1998), and can be as shallow as < 0.02 m in depth with a cross-sectional area as small as 3 cm^2 (Colborne and Staines, 1985). The zones between the rills are called the inter-rill areas, where the erosion is dominated by raindrop impact and unconcentrated sheet wash (Kirkby, 1980; Meyer et al., 1975). Once the flow become concentrated, rills emerge as the venue for collecting sediment detached from inter-rill areas, and transporting the mixture of runoff and sediment removed from rill walls and floors (Foster and Meyer, 1975). Rills are often ephemeral features and can be obliterated by agricultural practices or sudden sediment supply from inter-rill areas or rill sidewalls (Bull and Kirkby, 1997; Kirkby and Bracken, 2009).

During rainfall events, surface soil particles are directly impacted and some of them are detached by the kinetic energy of raindrops. Once the rainfall intensity becomes greater than the soil infiltration rate, the overland flow emerges, concentrates, and travels downslope (Horton, 1933, 1945). The concentrated flow, with substantially greater detachment power, scours the surface and further entrenches the channels. For rills, the development and growth are governed by the equilibrium between the detachment potential, the transport capacity of the flow, and the sediment load (Haan et al., 1994). If the shear stress is higher than the tractive force, rills incise and develop horizontally, eventually grow to an equilibrium width (Foster, 1986). The magnitude of erosion caused by shear stress is controlled by many factors including soil salinity, soil moisture content, shear strength, and the particle size distribution.

Other processes governing the propagation and promotion of channels and within-channel erosion include headwall cutting and sidewall sloughing. The headwall is a discontinuity in the channel profile, representing the transition from channelized flow that are relatively shallow to much narrower and deeper flow (Haan et al., 1994; Harvey et al., 1985). Headwall cutting allows the channel head to slowly migrate upstream, generating a large amount of sediment for the channel. Sidewall sloughing occurs as a consequence of the combined effect of gravitational forces and flow hydraulics. The geometry of the channel cross-section and soil properties including soil moisture content, bulk density, and particle cohesion, govern the resistance to sidewall failure. For rills, sidewall failures occur due to the gravitational forces imposing on an overhang initially created by undercutting (Toy et al., 2002). Hirschi and Barfield (1988) modeled the stability of the sidewall based on the concept of a critical slope, and suggested that the sidewall starts to slough off to form slope that is more stable. During the process, the soil mass that is detached gets deposited into the channel once a critical slope gradient is reached. Crouch (1987) also found that the undercutting process can be sensitive to the slope of the sidewall, resulting in varied erosion rates.

Concentrated flow in channels constantly erode channel bottoms and undercut sidewalls, reducing the stability of the sidewalls (Foster, 1986). Episodic failure events on channel

sidewalls occur when the gravitational stress on the sidewalls exceeds a certain threshold value, and these events drastically increase the sediment supply. Other natural processes such as freeze-thaw and animal activities also accelerate the destabilization of channels. Govers and Poesen (1988) suggested that the sidewall failures within rills contribute to the majority of the erosion, especially when deep-seated failures are present. The headwall and sidewall failures sometimes account for $> 90\%$ of the sediment yield on hillslopes (Betts et al., 2003). The failures can reshape the channel geometry and alter the flow hydraulics. The sidewall failures gradually consume interrill areas and widen the channels, and once the channel width exceeds a threshold (Nearing et al., 1989), channel erosion will be stopped unless an unsteady flow is present (Toy et al., 2002).

1.2.2 Classic approaches

Soil erosion is commonly measured in weight and volume of eroded sediment from a certain area. For small areas, experimental plots can be established either in the field or in the lab, and the runoff and sediment can be collected at the outlet during an observational period (Morgan et al., 1987; Stroosnijder, 2005). This method requires controlled conditions for erosion-related factors (e.g. vegetation, topography, soil type, and rainfall), but measuring the runoff and sediment can be difficult for large areas. Another method is to manually measure the geomorphic changes such as cross-sectional areas and rill lengths at sampling points using micro-topographic profilers, tapes, or rulers (Govers, 1987, 1991a; Govers and Poesen, 1988). One widely used method is to survey the volume of the gullies using cross-sectional profilers at space intervals measured in the fields (Auzet et al., 1995; Casalí et al., 1999; Poesen et al., 2003). Erosion pins are also used to assess the erosion within the gullies by measuring the elevation changes along the cross-sections (Oostwoud Wijdenes and Bryan, 2001; Vandekerckhove et al., 2001).

The attempts to expand the erosion rates measured from experimental plots to larger landscape produced unsatisfactory results (Boardman, 2006). Previous literature found that compared to the measurements made in agricultural fields, data collected in the experimental plots generally overestimate the erosion values and show more skewed distribution (Evans,

1995; Govers, 1991b). Evans (1995) suggested that this discrepancy results from the limited sampled area of plots; also, plots failed to account for the complex topography which contributes to spatially varied erosion rates and local deposition. However, in the natural landscape, the transformation from rills to gullies are often observed (Casalí et al., 2006; Desmet and Govers, 1997; Gao, 2013; Knighton, 1998; Selby, 1982), making it necessary to bridge the gap with a method which produces comparable measurements.

Another factor that cannot be assessed using the "sediment collection" method is the spatial redistribution of material, especially the material deposited (Boardman, 2006). In natural landscape, deposition tends to occur at the foot of hillslopes when a sudden decrease in slope gradient coincides with increased drainage area (Nachtergaele et al., 2002; Poesen et al., 2003, 1998), in front of vegetation patches (Meyer et al., 1995; Steegen et al., 2000; Takken et al., 1999), at areas with a sudden increase in surface roughness (Papanicolaou et al., 2001), and in local depressions within the landscape (Poesen et al., 2003). Therefore, amount of sediment leaving a drainage area is always less than that detached, as a part of the sediment deposited before reaching the outlet (Morgan et al., 1987). The "sediment collection" method measures "net loss", the difference between the detached sediment and the sediment deposited. Questions such as where the material moves to, where the materials deposit, and what caused the deposition, are not answered. It is possible to trace the movement of sediment in the field by recording erosion and deposition using tracer substance including paint (Kirkby and Kirkby, 1974), ^{137}Cs (Walling and Quine, 1990; Walling et al., 1990), and mineral magnetics (Coutts et al., 1968; De Ploey, 1969). However, these methods are expensive and time-consuming, and the assumptions on which some of the methods are based is still questionable (Dalgleish and Foster, 1996; Foster et al., 1994).

The methods based on measuring rill or gully morphology are usually time-consuming and labor-intensive. Also, the elevation information collected using erosion pins or cross-sections is dependent upon whether the measured cross section is representative or not (Casalí et al., 2015, 2006). Other studies on soil erosion also suggested that both natural characteristics and human errors associated with measurement are accountable for a great degree of unexplained variability (Nearing, 2000; Nearing et al., 1989; Todisco et al.,

2012). Further, the data collected using erosion pins are susceptible to contamination from disturbance of various sources, and the researcher always bear the risk of theft and vandalism (Haigh, 1977). The disruptive nature of the methods brings further complication into the attempts to link erosion and channel geometry with sediment yield.

1.2.3 Recent opportunities

The main concern preventing the use of elevation data for erosion studies has been the limited ability to account for uncertainty, and the lack of a method to provide spatial and temporal resolution on a proper scale without introducing the measurer disturbance (Govers, 1991b). In recent years, the ability for more accurate measurement has advanced with the improved accuracy and finer resolution brought by new technologies, including advanced photogrammetry, unmanned aerial system, and laser scanning. These technologies are comparatively efficient and are capable to produce high-resolution topography with three-dimensional features (Everaerts, 2008; Heritage and Large, 2009; Rieke-Zapp and Nearing, 2005; Shan and Toth, 2008). Laser scanning – also known as LiDAR (Light Detection and Ranging) – allows for rapid acquisition of high-resolution topographic data (Lefsky et al., 2002). As the lens of the scanner is able to rotate both horizontally and vertically, the scanner can generate a three-dimensional virtual environment (Jensen, 2009). Originally designed for surveying and engineering applications, laser scanning has shown its capability in various environment-related studies (Heritage and Large, 2009).

TLS is suitable for small scale (rill to gully) soil erosion research, and existing applications of TLS in past studies demonstrated its advantages (Schneider et al., 2012; Vinci et al., 2015). First, TLS units are able to produce DEMs with spatial resolution at the centimeter or sub-centimeter level, and research has successfully produced protocols for TLS in geomorphological applications, and suggested a reliable horizontal accuracy of $\pm$ 1 cm, and a vertical accuracy of approximately $\pm$ 1.5 cm (Eltner and Baumgart, 2015; Heritage and Hetherington, 2007). The three dimensionality of TLS further allows for geomorphic change detection for features that are not suitable for airborne and space-borne sensors (for example, cliffs (Gulyaev and Buckeridge, 2004), steep hillslopes (Wawrzyniec et al., 2007),

and channel bank undercut (Chu-Agor et al., 2008)). TLS also allows the measurement to be performed at a distance. Consequently, the safety of the researcher is more secured and the absence of direct human impact minimizes the error from human disturbance. Therefore, TLS is widely used in studies of various types of dynamic environments, including cliff (Lague et al., 2013; Olsen et al., 2009) and landslide (Bitelli et al., 2004; Jaboyedoff et al., 2012; Jones, 2006). This feature of TLS also allows the measurement to be performed for areas with limited accessibility. For example, Hancock et al. (2008) used a TLS to survey a hillslope at Rix's Creek Coal Mine in Singleton, Australia across a pond that prevents access for field measurement.

Development in the field of geomatics provides useful tools to detect features and quantify the geomorphologic processes. Progress has been made to quantify the uncertainty associated with the TLS-generated elevation data on a cell-to-cell basis, which is affected by factors including roughness, point density, and slope (Brasington et al., 2012; Lane et al., 2003; Wheaton, 2008). Such improvement allows for a more accurate way to quantitatively map the erosion and deposition pattern associated with various processes (Prosdocimi et al., 2015; Tarolli and Dalla Fontana, 2009). Brodu and Lague (2012) developed a method to use multi-scale 3-d properties for classification of geomorphic features. Lague et al. (2013) developed a method that calculates the difference between temporal TLS dataset in a spatial perspective at various scales and found it useful in dynamic environment with spatially varied erosion and deposition.

The quantitative analysis of erosional landscapes is dependent upon successful definition, extraction, and calculation of important geomorphic factors (Bishop et al., 2012; James et al., 2012; Tarolli, 2014). Studies have successfully used fine resolution elevation data to extract stream networks (Charrier and Li, 2012; Passalacqua et al., 2010), landslide scars (Baldo et al., 2009; Glenn et al., 2006; Jaboyedoff et al., 2012; Tarolli et al., 2012), gullies (Perroy et al., 2010), and channel heads (Passalacqua et al., 2012; Tarolli and Dalla Fontana, 2008, 2009). High-resolution elevation data have exhibited great potential in advancing our knowledge in the physical processes (Bremer and Sass, 2012; Chen et al., 2006; Tarolli, 2014; Vaze and Teng, 2007). In the meantime, the limitations of high-resolution topographic

data are discussed in several studies (Barber and Shortridge, 2005; Charrier and Li, 2012; Tarolli, 2014; Yang et al., 2014; Zhang et al., 2008). Conceptual frameworks of quantitative geomorphometric analyses suggested that the morphology of drainage basins and channels can be characterized using parameters calculated based on elevation data (Horton, 1932, 1945; Moore et al., 1991). A good example is the study of gullies on hillslopes. Gullies initiate once the magnitude and duration of concentrated surface runoff exceed a threshold value, causing substantial magnitude of sediment loss. This thresholding nature of gully initiation is considered a transition between diffusive processes and convergent channel processes (Tarboton et al., 1991; Tarolli et al., 2009). The direct link is established between this value and the geomorphic thresholds, as a function of slope steepness and the contributing area (Horton, 1945; Montgomery and Foufoula-Georgiou, 1993; Poesen et al., 1998; Vandaele et al., 1996).

The elevation data with high-resolution and accuracy produced using TLS can be used to derive certain geomorphic factors and allows for linking these factors to erosion and deposition on the hillslope. For example, surface roughness, or the micro-topographic variation of the elevation, plays a critical role in affecting flow path formation, flow erosion, infiltration rates, surface depositional storage, and hydraulic resistance (Abrahams and Parsons, 1991; Cogo et al., 1984; Darboux and Huang, 2005; Gómez and Nearing, 2005). Various soil erosion models, including the Revised Universal Soil Loss Equation (RUSLE) (Renard et al., 1997), and the Water Erosion Prediction Project (WEPP) (Nearing et al., 1989), include a surface roughness factor in the model framework. Surface roughness was measured using profilers in the past, but the profiler has limitations as it only covers a narrow band along the cross section, and is of limited field portability (Bertuzzi et al., 1990; Huang and Bradford, 1990; McCarroll and Nesje, 1996). Until recently, the use of TLS has enabled research to assess the impact of roughness from a spatial perspective, and improved the prediction of the erosion based on this topographic information (Eitel et al., 2011; Lague et al., 2013; Nield et al., 2013; Sankey et al., 2012).

1.2.4 Sedimentological connectivity in hillslope channels

The sedimentological connectivity is defined as "the transfer of sediment from one location to another and the potential for any particle to move through the system" (Bracken and Croke, 2007; Hooke, 2003), and determines whether the erosion and sediment yield within an upland drainage system are coupled or not. The sedimentological connectivity, influenced by the connectivity of both topography and hydrology, varies for different drainage basins (Michaelides and Wainwright, 2002; Morgan et al., 1987; Walling, 1999). The sedimentological connectivity is often conceptualized as the "sediment delivery ratio" in literatures (Haan et al., 1994; Walling, 1983; Williams and Berndt, 1976). In many studies, a "black box" approach was commonly adopted for the "sediment delivery" concept, with limited understanding of the spatial and temporal patterns of sediment routing. Although some approaches such as the sediment tracing (Walling and Quine, 1990; Wilkinson et al., 2013) help understand this topic, current knowledge regarding the sedimentological connectivity is still limited due to the complex interaction between various factors, including climate, soil, vegetation, and topography (Bracken and Croke, 2007).

The development in hi-resolution remote sensing technology allows for the examination of the topic of sedimentological connectivity at finer scales. One opportunity is the improved ability to detect, monitor, quantify, and assess fine-scale (plot or even smaller) geomorphic changes. The classic "sediment collection" method relies on the "coupling" assumption, that the higher erosion rates on upland areas always translate to similar, or at least comparable level of increase in sediment yield within fluvial channels (Harvey, 2001). The presumed connectivity between different geomorphologic components guarantees the transmission of energy and material within the system. In other situations when erosion rate and sediment yield are not coupled, the sediment yield is often over-estimated, suggesting that sediment cannot transport throughout the system without energy loss, but was partially deposited at a certain intermediate stage (Boardman, 2006). Harvey (2001) suggested that this type of non-coupled, or "buffered" systems are featured with spatially restricted local changes.

The current knowledge of sedimentological connectivity is mainly derived at the scale of watersheds, which is a synthesized system of both hillslopes and fluvial channel systems (Bracken and Croke, 2007; Cavalli et al., 2013; Detty and McGuire, 2010; Hooke, 2003; López-Vicente et al., 2015; Vigiak et al., 2012). In these studies, the hillslopes were often considered as a unit delivering sediment into the fluvial channels, but the connectivity of hillslope channels was not given much attention, possibly due to a lack of accurate methods to measure and track the sediment movement. A few studies have applied the concept of connectivity to upland channels, and the majority of these literatures focused on the gullies (de Vente et al., 2006; Sandercock and Hooke, 2011), with only a few investigations on the sedimentological connectivity for a rilled hillslope (Huang et al., 1996; Penuela Fernandez et al., 2014). Literatures proposed two types of connectivity: topographic/structural connectivity that describes the continuity of the terrain, and sedimentological connectivity that describes how well sediment particles are routed throughout the system (Fryirs, 2013; Brierley et al., 2006).

The knowledge of the sedimentological connectivity within hillslope channels, especially rills, is still lacking. Further work is also necessary to examine the influence of structural connectivity on the sedimentological connectivity. Experiments for rill formation and development studies are often conceptualized as a scenario where rills emerge on a freshly engineered hillslope with uniform surface geometry (usually either in a field plot or an experimental plot). These experiments emphasize sediment yield at the early phase of hillslope channel development when rills emerge and grow, until the geometry of the cross-sections is somewhat stabilized. Only a few studies investigated how the erosion rate and sediment yield change after the locations of the rills are defined (Kavvas and Govindaraju, 1992). However, studies suggest that rills are negative-feedback or self-stabilizing systems that the emergence of new rills results in a cumulative effect of uniform erosion across a hillslope (Bull and Kirkby, 1997). Also, both lab-based and field-based experimental studies have demonstrated that the erosion rate and sediment delivery on the hillslope surface are significantly affected by the presence of rills (Kavvas and Govindaraju, 1992; Meyer et al., 1975). Similar to fluvial channels, the coupling of the hillslope channels is governed by the balance between the sediment load and the transport capacity. Some of the factors affecting the coupling, such as channel connectivity, the temporal variation of surface runoff, and the

abrupt increase in sediment supply due to episodical events such as sidewall failures also apply to the hillslope channels, although the effects are likely to be scale-dependent. Thus, understanding the sedimentological connectivity, and how the influences of different factors differ at various scales is critical for a better knowledge of the physical processes driven hillslope erosion, sediment yield, and channel evolution.

1.3 Research objectives

The overall goal of this dissertation research is to assess the spatial variation of the sedimentological redistribution within a rilled hillslope by analyzing the impact of micro-topographic factors and structural connectivity on the sedimentological connectivity. The central objectives of this study include:

i To examine the effect of DEM resolution on the quantification of erosion and deposition. The measurements of erosion and deposition based on DEMs are scale-dependent, and quantifying the effect of DEM resolution on these measurements provide useful guidance for future studies.

ii To identify micro-topographic factors that control the dynamics of erosion and deposition. Understanding the roles of different factors on erosion and deposition improve the knowledge in the mechanisms of fine-scale sediment movement.

iii To assess the spatial variation of sedimentological connectivity and how structural connectivity affect the variation. This research investigates the correlation between the structural connectivity and the sedimentological connectivity, and examines the spatial extent of such relationships.

This dissertation research is helpful for revealing the relationship between sedimentological connectivity and topography, channel geometry, and precipitation. The research aims to test the following hypotheses:

Hypothesis 1 DEM-based measurements of sediment erosion, deposition, and summary metrics of delineated channels decrease with the increased DEM grid size.

Hypothesis 2 The amount of erosion is positively related to slope, aspect, contributing area, and the channel density; within-channel deposition is related positively to roughness but negatively to the contributing area.

Hypothesis 3 The structural (dis)connectivity, including depressions and channel confluence, controls the sedimentological connectivity — depressions lead to local deposition and confluences of rills result in higher erosion.

1.4 Study area

The study site (35°37'33"N, 84°13'00"W, Figure 1.1) is an engineered hillslope located on the terraces of the Little Tennessee River that contributes to the Fort Loudoun Lake Watershed in East Tennessee. This area has a Humid Subtropical climate (Cfa in the Köppen climate classification) with hot summers, mild winters, and year-round precipitation. The frequent rainfall events interact with the local geology and topography, causing intensive soil erosion throughout the state, impairing the agricultural productivity and fragmenting the landscape (Barnhardt, 1988; Dotterweich et al., 2014; Harden and Mathews, 2000). One hillslope with well-developed rill networks is selected to observe the evolution of a rilled landscape. Located in natural settings with limited human disturbance, the site suffered intensive soil loss, and is still affected by the erosion. No physical boundaries were installed, therefore the erodible materials are unlikely to be exhausted and long-term observation of erosion is possible (Boix-Fayos et al., 2006).

The annual precipitation in the study area is around 1300 mm, and the annual temperature is around 15°C according to US Climate Data (http://www.usclimatedata.com/). The study site is located in the Southern Limestone/Dolomite Valleys and Low Rolling Hills sub-ecoregion, a region composed predominantly of shale. The slope is around 20 m long and was initially created by post-construction land abandonment, set at a ratio of 2:1 (horizontal: vertical). As Google Earth historic images suggest, the site has been exposed as a bare surface since at least 2007. Although vegetation strips were installed at the foot of the hillslope to control sediment delivery, the hillslope surface has been free of

vegetation and is characterized by well-developed rill networks formed in 2007 according to historical images in Google Earth. The bed material in our study site is shale.

1.5 Methods

1.5.1 Data acquisition

This research relies on the successful acquisition and processing of fine-resolution ($\sim$ 1 cm) temporal DEMs. I used a FARO Focus3D X 330 laser scanner which has a 360° horizontal and 300° vertical scanning view, and a ranging accuracy of $\pm$ 2 mm at 50 m according to the manufacturer's specifications. The scanner uses a class 1 laser (wavelength: 1550 nm) and is able to acquire three-dimensional features within 330 meters at a rate of 976000 pulses per second. In field surveys, I mount the scanner on a tripod with dual-axis compensation function activated. All field surveys are performed during daytime with clear-sky condition, and at least two days after any prior precipitation event. I repeated the field survey every few months, and for each survey, at least 3 scans at different locations across the site are performed to minimize occlusion caused by surface roughness or uncertainty introduced by the positioning of TLS. The number of scans depends on the complexity and the extent of the site, but the scan locations are selected at approximate uniform distribution, and I try to re-occupy the same scan location for every field survey. I used 5 spherical reference targets (ATS Scan Reference System) of a diameter of 139 mm for intra-survey registration. I did not use the targets for geo-referencing between time-series surveys because it would be difficult to re-locate the targets at the same position every time in dynamic environments (Lague et al., 2013; Schürch et al., 2011). The scanning procedure started with a full 360 scan at a low resolution ($\sim$ 5 cm at 50 m) followed by scans only on the area of interest at a much higher resolution ($\sim$ 1 cm at 50 m). The locations of each scan and each spherical targets were recorded using a GeoExplorer 6000 Series GeoXH^{TM} handheld differential GPS (dGPS) that has a location accuracy of less than 1 cm.

Climate data were collected as daily records and propagated in accordance with the interval between any two consecutive field surveys. The data were obtained from the

US Climate Data (http://www.usclimatedata.com/). The US Climate Data offers daily precipitation and temperature dataset, and the station at the Lenoir City is approximately 28 km away from our study site.

1.5.2 Data processing

Registration and geo-referencing were performed using the FARO SCENE software (https://www.faro.com/products/product-design/faro-scene/). I conducted the intra-survey registration using a target-based method. The location of all scans and reference targets recorded by the dGPS were input by the user, and the software uses an automated procedure to register the scans on a target-to-target basis. The between-survey geo-referencing was performed using the GPS records and the user manually aligns the scans using features with regular geometry (e.g. buildings). Once scans were well-aligned, they were exported as point cloud files in binary format. I used the method proposed by Brodu and Lague (2012) to classify and separate vegetation from the terrain surface using CloudCompare(http://www.cloudcompare.org/), a free software specially developed for processing and analyzing point cloud files. To produce the DEM raster using the point cloud files, a bilinear interpolation was used, as this method is not computing-intensive, and less sensitive to randomness and errors associated with the dataset compared to other methods (Haile and Rientjes, 2005; Wang et al., 2015). As the extents of the study areas in this research were all within 20 m $\times$ 20 m, a local Cartesian projection was used, as it is generally used for large-scale mapping purposes without much consideration of the curvature of the earth (Kennedy and Kopp, 2002).

1.5.3 Data analyses

The analyses of the data were performed in accordance with the three separate tasks:

Task 1. To evaluate the effect of spatial resolution on the analyses

I used different grid size for the mapping of erosion and deposition, and quantification of the sediment yield, to examine how spatial resolution affects the propagation of sediment budget from both an areal and volumetric perspective. I used multiple methods to extract channel networks, and compare the sensitivity to DEM grid size of different models. The DEM of the finest resolution was used as the reference. The analyses of sensitivity to resolution are not only based on a numerical basis, and also on spatial patterns. For the extraction of channel systems (rills in this research), I compared multiple methods, including morphology-based methods (Horn, 1981; Roth and La Barbera, 1997; Tarolli et al., 2012), and quantity-based methods (Broscoe, 1959; Tarboton et al., 1991). The channel systems extracted using different DEMs were compared to the reference using the Revised Automated Proximity and Conformity Analysis method (Li et al., 2008; Napieralski et al., 2006). This method is suitable for our purpose as it was originally designed for quantitatively compare the offset between linear features.

Task 2. To examine how topographic factors affect the dynamics of erosion and deposition

This research further examines the influence of different factors on the erosion and deposition events after the frequency and the magnitude of erosion and deposition are quantified using the DEM of Difference (DoD) method. The study area is divided according to drainage divide and contributing area into segments of rill basins, and the erosion and deposition within each segment can be quantified. The topographic factors including slope, area, contributing area, are be calculated using ArcGIS 10.4.

Statistical methods were used to investigate the relationship between erosion/deposition and topographic indices including slope, aspect, contributing area and potential between-variable high correlation, and channel density. This research used the group k-fold cross validation method that is able to handle spatial auto-correlation, and the quantile regression to quantitatively assess the relationship of these topographic factors with the erosion and

deposition. The analyses also included the determination of relative importance between various variables.

Task 3. To assess the influence of structural connectivity on the spatial variation of sedimentological connectivity

I used the DEM of Difference (DoD) to quantify the amount of sediment that was eroded and deposited in the channels (Knapen et al., 2007). The time-series of the DEMs produced were imported to ArcGIS 10.4 and the Geomorphic Change Detection package (Wheaton et al., 2010) was used for the propagation of uncertainties. The spatial distribution of erosion and deposition hotspots within the study area were mapped, and the volume of sediment change was quantified. The sediment yield was calculated as the net sediment loss, or the difference between erosion and deposition. The sediment delivery ratio was calculated as the ratio of eroded volume to the sediment yield.

The channels were delineated at our study site using the Arc Hydro Tools in ArcGIS 10.4 (Maidment, 2002). I extracted the longitudinal profiles of major rill channels. The channels were segmented along the profile, and the local depressions within the study area and the confluence of channels was used to quantify the structural connectivity of the channels. The cross-correlation between the structural and sedimentological connectivity was examined. I picked several locations along the channel to measure the change of the cross-sections and used visual analysis on the change of the cross-sectional area to determine whether the channels were widening and whether it's deepening. Through comparison between the temporal variations of the cross-sections of channels, the trend of channel change along the rill profile can be determined.

1.6 Dissertation outline

This dissertation is organized based on the manuscript format, with chapters 2 – 4 as three individual manuscripts targeted for different academic journals.

Chapter 2 focuses on the effect of spatial resolution on the erosion/deposition monitoring and quantification on hillslopes. This chapter discusses the effect of spatial resolution in the study of erosion and deposition on hillslopes, as well as the delineation of channel features.

Chapter 3 focuses on the impact of micro-topographic variations on erosion and deposition by identifying representative topographic indices that best predict erosion and deposition within the hillslope. This chapter aims to quantify erosion and deposition within a hillslope, identify the important micro-topographic factors that influence the erosion and deposition, and predict erosion and deposition values in our study site using the quantile regression model.

Chapter 4 aims to examine the relationship between the local depressions, rill confluence, and sedimentological connectivity. I also investigated the spatial extent of such influences, to reveal the scale of the impact of topographic (dis)connectivity on sedimentological connectivity.

Chapter 5 summarizes the major findings of this research, and presents major conclusions derived from Chapter 2 – 4. I also discussed potential topics that might be of interest for future work.

Exemplary Python scripts associated with this research are provided in Appendices.

References

Abrahams, A. D. and Parsons, A. J. (1991). Resistance to overland flow on desert pavement and its implications for sediment transport modeling. *Water Resources Research*, 27(8):1827–1836.

Auzet, A. V., Boiffin, J., and Ludwig, B. (1995). Concentrated flow erosion in cultivated catchments: influence of soil surface state. *Earth Surface Processes and Landforms*, 20(8):759–767.

Baldo, M., Bicocchi, C., Chiocchini, U., Giordan, D., and Lollino, G. (2009). LIDAR monitoring of mass wasting processes: The Radicofani landslide, Province of Siena, Central Italy. *Geomorphology*, 105(3):193–201.

Barber, C. P. and Shortridge, A. (2005). Lidar elevation data for surface hydrologic modeling: Resolution and representation issues. *Cartography and Geographic Information Science*, 32(4):401–410.

Barnhardt, M. L. (1988). Historical sedimentation in west Tennessee gullies. *Southeastern Geographer*, 28(1):1–18.

Bertuzzi, P., Caussignac, J. M., Stengel, P., Morel, G., Lorendeau, J. Y., and Pelloux, G. (1990). An automated, noncontact laser profile meter for measuring soil roughness in situ. *Soil Science*, 149(3):169–178.

Betts, H. D., Trustrum, N. A., and Rose, R. C. D. (2003). Geomorphic changes in a complex gully system measured from sequential digital elevation models, and implications for management. *Earth Surface Processes and Landforms*, 28(10):1043–1058.

Bishop, M. P., James, L. A., Shroder, J. F., and Walsh, S. J. (2012). Geospatial technologies and digital geomorphological mapping: Concepts, issues and research. *Geomorphology*, 137(1):5–26.

Bitelli, G., Dubbini, M., and Zanutta, A. (2004). Terrestrial laser scanning and digital photogrammetry techniques to monitor landslide bodies. *XXth ISPRS Congress: Proceedings of Commission V*, 35(Part B 5):246–251.

Boardman, J. (2006). Soil erosion science: Reflections on the limitations of current approaches. *Catena*, 68(2–3):73–86.

Boix-Fayos, C., Martínez-Mena, M., Arnau-Rosalén, E., Calvo-Cases, A., Castillo, V., and Albaladejo, J. (2006). Measuring soil erosion by field plots: Understanding the sources of variation. *Earth-Science Reviews*, 78(3–4):267–285.

Bracken, L. J. and Croke, J. (2007). The concept of hydrological connectivity and its contribution to understanding runoff-dominated geomorphic systems. *Hydrological Processes*, 21(13):1749–1763.

Brasington, J., Vericat, D., and Rychkov, I. (2012). Modeling river bed morphology, roughness, and surface sedimentology using high resolution terrestrial laser scanning. *Water Resources Research*, 48(11):W11519.

Bremer, M. and Sass, O. (2012). Combining airborne and terrestrial laser scanning for quantifying erosion and deposition by a debris flow event. *Geomorphology*, 138(1):49–60.

Brierley, G., Fryirs, K., and Jain, V. (2006). Landscape connectivity: the geographic basis of geomorphic applications. *Area*, 38(2):165–174.

Brodu, N. and Lague, D. (2012). 3D terrestrial lidar data classification of complex natural scenes using a multi-scale dimensionality criterion: Applications in geomorphology. *ISPRS Journal of Photogrammetry and Remote Sensing*, 68:121–134.

Broscoe, A. (1959). Quantitative analysis of longitudinal stream profiles of small watersheds. Technical Report 389–402, U.S. Geological Survey, New York.

Bull, L. J. and Kirkby, M. J. (1997). Gully processes and modelling. *Progress in Physical Geography*, 21(3):354–374.

Casalí, J., Giménez, R., and Campo-Bescós, M. A. (2015). Gully geometry: what are we measuring? *Soil*, 1:509–513.

Casalí, J., Loizu, J., Campo, M. A., De Santisteban, L. M., and Álvarez-Mozos, J. (2006). Accuracy of methods for field assessment of rill and ephemeral gully erosion. *Catena*, 67(2):128–138.

Casalí, J., López, J. J., and Giráldez, J. V. (1999). Ephemeral gully erosion in southern Navarra (Spain). *Catena*, 36(1):65–84.

Cavalli, M., Trevisani, S., Comiti, F., and Marchi, L. (2013). Geomorphometric assessment of spatial sediment connectivity in small Alpine catchments. *Geomorphology*, 188:31–41.

Charrier, R. and Li, Y. (2012). Assessing resolution and source effects of digital elevation models on automated floodplain delineation: A case study from the Camp Creek Watershed, Missouri. *Applied Geography*, 34:38–46.

Chen, R., Chang, K., Angelier, J., Chan, Y., Deffontaines, B., Lee, C., and Lin, M. (2006). Topographical changes revealed by high-resolution airborne LiDAR data: The 1999 Tsaoling landslide induced by the Chi-Chi earthquake. *Engineering Geology*, 88(3):160–172.

Chu-Agor, M. L., Fox, G. A., Cancienne, R. M., and Wilson, G. V. (2008). Seepage caused tension failures and erosion undercutting of hillslopes. *Journal of hydrology*, 359(3):247–259.

Cogo, N. P., Moldenhauer, W. C., and Foster, G. R. (1984). Soil loss reductions from conservation tillage practices. *Soil Science Society of America Journal*, 48(2):368–373.

Colborne, G. J. N. and Staines, S. J. (1985). Soil erosion in south Somerset. *The Journal of Agricultural Science*, 104(01):107–112.

Coutts, J. R. H., Kandil, M. F., and Tinsley, J. (1968). Use of Radioactive 59Fe for Tracing Soil Particle Movement. *Journal of Soil Science*, 19(2):325–341.

Crouch, R. J. (1987). The relationship of gully sidewall shape to sediment production. *Soil Research*, 25(4):531–539.

Dalgleish, H. Y. and Foster, I. D. L. (1996). 137Cs losses from a loamy surface water gleyed soil (Inceptisol); a laboratory simulation experiment. *Catena*, 26(3):227–245.

Darboux, F. and Huang, C.-h. (2005). Does soil surface roughness increase or decrease water and particle transfers? *Soil Science Society of America Journal*, 69(3):748–756.

De Ploey, J. (1969). *L'érosion pluviale: expériences à l'aide de sables traceurs et bilans morphogéniques*, volume 7. Acta Geographica Lovaniensia.

de Vente, J., Poesen, J., Bazzoffi, P., Rompaey, A. V., and Verstraeten, G. (2006). Predicting catchment sediment yield in Mediterranean environments: the importance of sediment sources and connectivity in Italian drainage basins. *Earth Surface Processes and Landforms*, 31(8):1017–1034.

Desmet, P. J. J. and Govers, G. (1997). Two-dimensional modelling of the within-field variation in rill and gully geometry and location related to topography. *Catena*, 29(3):283–306.

Detty, J. M. and McGuire, K. J. (2010). Topographic controls on shallow groundwater dynamics: implications of hydrologic connectivity between hillslopes and riparian zones in a till mantled catchment. *Hydrological Processes*, 24(16):2222–2236.

Dotterweich, M., Ivester, A. H., Hanson, P. R., Larsen, D., and Dye, D. H. (2014). Natural and human-induced prehistoric and historical soil erosion and landscape development in Southwestern Tennessee, USA. *Anthropocene*, 8:6–24.

Eitel, J. U. H., Williams, C. J., Vierling, L. A., Al-Hamdan, O. Z., and Pierson, F. B. (2011). Suitability of terrestrial laser scanning for studying surface roughness effects on concentrated flow erosion processes in rangelands. *Catena*, 87(3):398–407.

Eltner, A. and Baumgart, P. (2015). Accuracy constraints of terrestrial Lidar data for soil erosion measurement: Application to a Mediterranean field plot. *Geomorphology*, 245:243–254.

Evans, R. (1995). Some methods of directly assessing water erosion of cultivated land-a comparison of measurements made on plots and in fields. *Progress in Physical Geography*, 19(1):115–129.

Everaerts, J. (2008). The use of unmanned aerial vehicles (UAVs) for remote sensing and mapping. *The International Archives of the Photogrammetry, Remote Sensing and Spatial Information Sciences*, 37:1187–1192.

Foster, G. R. (1986). Understanding ephemeral gully erosion. *Soil Conservation*, 2:90–125.

Foster, G. R. and Meyer, L. D. (1975). Mathematical simulation of upland erosion by fundamental erosion mechanics. In *Present and prospective technology for predicting*

sediment yields and sources, pages 190–207, Southern Region, New Orleans, Louisiana. US Department of Agriculture, Agricultural Research Services.

Foster, I. D. L., Dalgleish, H., Dearing, J. A., and Jones, E. D. (1994). Quantifying soil erosion and sediment transport in drainage basins; some observations on the use of 137Cs. In *Variability in stream erosion and sediment transport*, volume 224, pages 55–64, Canberra, Australia. IAHS Press.

Fryirs, K. A. (2013). (Dis) Connectivity in catchment sediment cascades: a fresh look at the sediment delivery problem. *Earth Surface Processes and Landforms*, 38(1):30–46.

Gao, P. (2013). Rill and Gully Development Processes. In Shroder, J. F., editor, *Treatise on Geomorphology*, volume 7, pages 122–131. Academic Press, San Diego.

Glenn, N. F., Streutker, D. R., Chadwick, D. J., Thackray, G. D., and Dorsch, S. J. (2006). Analysis of LiDAR-derived topographic information for characterizing and differentiating landslide morphology and activity. *Geomorphology*, 73(1):131–148.

Gómez, J. A. and Nearing, M. A. (2005). Runoff and sediment losses from rough and smooth soil surfaces in a laboratory experiment. *Catena*, 59(3):253–266.

Govers, G. (1987). Initiation of motion in overland flow. *Sedimentology*, 34(6):1157–1164.

Govers, G. (1991a). Rill erosion on arable land in Central Belgium: Rates, controls and predictability. *Catena*, 18(2):133–155.

Govers, G. (1991b). Time-dependency of runoff velocity and erosion the effect of the initial soil moisture profile. *Earth Surface Processes and Landforms*, 16(8):713–729.

Govers, G. and Poesen, J. (1988). Assessment of the interrill and rill contributions to total soil loss from an upland field plot. *Geomorphology*, 1(4):343–354.

Gulyaev, S. A. and Buckeridge, J. S. (2004). Terrestrial methods for monitoring cliff erosion in an urban environment. *Journal of Coastal Research*, pages 871–878.

Haan, C. T., Barfield, B. J., and Hayes, J. C. (1994). *Design Hydrology and Sedimentology for Small Catchments*. Academic Press, London.

Haigh, M. J. (1977). The use of erosion pins in the study of slope evolution. *British Geomorphological Research Group Technical Bulletin*, 18:31–49.

Haile, A. T. and Rientjes, T. H. M. (2005). Effects of LiDAR DEM resolution in flood modelling: a model sensitivity study for the city of Tegucigalpa, Honduras. In *ISPRS WG III/3, III/4*, volume 36, pages 168–173, Enshede, the Netherlands.

Hancock, G. R., Crawter, D., Fityus, S. G., Chandler, J., and Wells, T. (2008). The measurement and modelling of rill erosion at angle of repose slopes in mine spoil. *Earth Surface Processes and Landforms*, 33(7):1006–1020.

Harden, C. P. and Mathews, L. (2000). Rainfall response of degraded soil following reforestation in the Copper Basin, Tennessee, USA. *Environmental Management*, 26(2):163–174.

Harvey, A. M. (2001). Coupling between hillslopes and channels in upland fluvial systems: implications for landscape sensitivity, illustrated from the Howgill Fells, northwest England. *Catena*, 42(2):225–250.

Harvey, M. D., Watson, C. C., and Schumm, S. A. (1985). Gully erosion. Technical report, Denver, USA.

Heritage, G. and Hetherington, D. (2007). Towards a protocol for laser scanning in fluvial geomorphology. *Earth Surface Processes and Landforms*, 32(1):66–74.

Heritage, G. and Large, A. (2009). *Laser Scanning for the Environmental Sciences*. John Wiley & Sons, London.

Hirschi, M. C. and Barfield, B. J. (1988). KYERMO – A Physically Based Research Erosion Model Part I. Model Development. *Transactions of the ASAE*, 31(3):804–813.

Hooke, J. (2003). Coarse sediment connectivity in river channel systems: a conceptual framework and methodology. *Geomorphology*, 56(1):79–94.

Horn, B. K. P. (1981). Hill shading and the reflectance map. *Proceedings of the IEEE*, 69(1):14–47.

Horton, R. E. (1932). Drainage-basin characteristics. *Eos, Transactions American Geophysical Union*, 13(1):350–361.

Horton, R. E. (1933). The role of infiltration in the hydrologic cycle. *Eos, Transactions American Geophysical Union*, 14(1):446–460.

Horton, R. E. (1945). Erosional development of streams and their drainage basins; hydrophysical approach to quantitative morphology. *Geological society of America bulletin*, 56(3):275–370.

Huang, C.-h. and Bradford, J. M. (1990). Portable laser scanner for measuring soil surface roughness. *Soil Science Society of America Journal*, 54(5):1402–1406.

Huang, C.-h., Laflen, J. M., and Bradford, J. M. (1996). Evaluation of the detachment-transport coupling concept in the WEPP rill erosion equation. *Soil Science Society of America Journal*, 60(3):734–739.

Jaboyedoff, M., Oppikofer, T., Abellán, A., Derron, M.-H., Loye, A., Metzger, R., and Pedrazzini, A. (2012). Use of LIDAR in landslide investigations: a review. *Natural hazards*, 61(1):5–28.

James, L. A., Hodgson, M. E., Ghoshal, S., and Latiolais, M. M. (2012). Geomorphic change detection using historic maps and DEM differencing: The temporal dimension of geospatial analysis. *Geomorphology*, 137(1):181–198.

Jensen, J. R. (2009). *Remote sensing of the environment: An earth resource perspective*. Prentice-Hall Inc., New York, New York, USA.

Jones, L. D. (2006). Monitoring landslides in hazardous terrain using terrestrial LiDAR: an example from Montserrat. *Quarterly journal of engineering geology and hydrogeology*, 39(4):371–373.

Kavvas, M. L. and Govindaraju, R. S. (1992). Hydrodynamic averaging of overland flow and soil erosion over rilled hillslopes. In *Erosion, debris flows and environment in mountain regions*, number 209, pages 101–111, Chengdu, China. IAHS Publ.

Kennedy, M. and Kopp, S. (2002). *Understanding map projections*. ESRI.

Kirkby, A. and Kirkby, M. J. (1974). Surface wash at the semi-arid break in slope. *Zeitschrift fuer Geomorphologie, Supplement Volumes.*, 21:1521–2176.

Kirkby, M. J. (1980). *Modelling water erosion processes*. John Wiley & Sons, Chichester, UK.

Kirkby, M. J. and Bracken, L. J. (2009). Gully processes and gully dynamics. *Earth Surface Processes and Landforms*, 34(14):1841–1851.

Knapen, A., Poesen, J., and De Baets, S. (2007). Seasonal variations in soil erosion resistance during concentrated flow for a loess-derived soil under two contrasting tillage practices. *Soil and Tillage Research*, 94(2):425–440.

Knighton, D. (1998). *Fluvial Forms and Processes: A New Perspective*. Number Ed. 2. Edward Arnold, London, UK.

Lague, D., Brodu, N., and Leroux, J. (2013). Accurate 3D comparison of complex topography with terrestrial laser scanner: Application to the Rangitikei canyon (N-Z). *ISPRS Journal of Photogrammetry and Remote Sensing*, 82:10–26.

Lane, S. N., Westaway, R. M., and Murray Hicks, D. (2003). Estimation of erosion and deposition volumes in a large, gravel-bed, braided river using synoptic remote sensing. *Earth Surface Processes and Landforms*, 28(3):249–271.

Lefsky, M. A., Cohen, W. B., Parker, G. G., and Harding, D. J. (2002). Lidar Remote Sensing for Ecosystem Studies. *BioScience*, 52(1):19–30.

Li, Y., Napieralski, J., and Harbor, J. (2008). A revised automated proximity and conformity analysis method to compare predicted and observed spatial boundaries of geologic phenomena. *Computers & Geosciences*, 34(12):1806–1814.

López-Vicente, M., Quijano, L., Palazón, L., Gaspar, L., and Izquierdo, A. N. (2015). Assessment of soil redistribution at catchment scale by coupling a soil erosion model and a sediment connectivity index (Central Spanish Pre-Pyrenees). *Cuadernos de investigación geográfica*, 41:127–147.

Maidment, D. R. (2002). *Arc Hydro: GIS for water resources*, volume 1. ESRI, Inc.

McCarroll, D. and Nesje, A. (1996). Rock surface roughness as an indicator of degree of rock surface weathering. *Earth Surface Processes and Landforms*, 21(10):963–977.

Meyer, L. D., Dabney, S. M., and Harmon, W. C. (1995). Sediment-trapping effectiveness of stiff-grass hedges. *Transactions of the ASAE*, 38(3):809–815.

Meyer, L. D., Foster, G. R., and Romkens, M. J. M. (1975). Source of soil eroded by water from upland slopes. *Present and prospective technology for predicting sediment yields and sources*, 177(ARS-S-40):189.

Michaelides, K. and Wainwright, J. (2002). Modelling the effects of hillslope-channel coupling on catchment hydrological response. *Earth Surface Processes and Landforms*, 27(13):1441–1457.

Montgomery, D. R. and Foufoula-Georgiou, E. (1993). Channel network source representation using digital elevation models. *Water Resources Research*, 29(12):3925–3934.

Moore, I. D., Grayson, R. B., and Ladson, A. R. (1991). Digital terrain modelling: a review of hydrological, geomorphological, and biological applications. *Hydrological Processes*, 5(1):3–30.

Morgan, R. P. C., Martin, L., and Noble, C. A. (1987). *Soil erosion in the United Kingdom: a case study from mid-Bedfordshire*. Silsoe College, Cranfield Institute of Technology.

Nachtergaele, J., Poesen, J., Wijdenes, D. O., and Vandekerckhove, L. (2002). Medium-term evolution of a gully developed in a loess-derived soil. *Geomorphology*, 46(3):223–239.

Napieralski, J., Li, Y., and Harbor, J. (2006). Comparing predicted and observed spatial boundaries of geologic phenomena: Automated Proximity and Conformity Analysis applied to ice sheet reconstructions. *Computers & Geosciences*, 32(1):124–134.

Nearing, M. A. (2000). Evaluating soil erosion models using measured plot data: accounting for variability in the data. *Earth Surface Processes and Landforms*, 25(9):1035–1043.

Nearing, M. A., Foster, G. R., Lane, L. J., and Finkner, S. C. (1989). A process-based soil erosion model for USDA-Water Erosion Prediction Project technology. *Transactions of the ASAE*, 32(5):1587–1593.

Nield, J. M., King, J., Wiggs, G. F. S., Leyland, J., Bryant, R. G., Chiverrell, R. C., Darby, S. E., Eckardt, F. D., Thomas, D. S. G., and Vircavs, L. H. (2013). Estimating aerodynamic roughness over complex surface terrain. *Journal of Geophysical Research: Atmospheres*, 118(23):12948–12961.

Ohde, N. R. (2011). *Ephemeral gullies and ecosystems services: Social and biophysical factors*. PhD thesis.

Olsen, M. J., Johnstone, E., Driscoll, N., Ashford, S. A., and Kuester, F. (2009). Terrestrial laser scanning of extended cliff sections in dynamic environments: Parameter analysis. *Journal of surveying engineering*, 135(4):161–169.

Oostwoud Wijdenes, D. J. and Bryan, R. (2001). Gully-head erosion processes on a semi-arid valley floor in Kenya: a case study into temporal variation and sediment budgeting. *Earth Surface Processes and Landforms*, 26(9):911–933.

Papanicolaou, A. N., Diplas, P., Dancey, C. L., and Balakrishnan, M. (2001). Surface roughness effects in near-bed turbulence: Implications to sediment entrainment. *Journal of Engineering Mechanics*, 127(3):211–218.

Passalacqua, P., Belmont, P., and Foufoula-Georgiou, E. (2012). Automatic geomorphic feature extraction from lidar in flat and engineered landscapes. *Water Resources Research*, 48(3):W03528.

Passalacqua, P., Tarolli, P., and Foufoula-Georgiou, E. (2010). Testing space-scale methodologies for automatic geomorphic feature extraction from lidar in a complex mountainous landscape. *Water Resources Research*, 46(11):W11535.

Penuela Fernandez, A., Rocio Rodriguez Pleguezuelo, C., Javaux, M., and Bielders, C. L. (2014). Effect of sheet and rill erosion on overland flow connectivity in bare agricultural plots. In *EGU General Assembly Conference Abstracts*, volume 16.

Perroy, R. L., Bookhagen, B., Asner, G. P., and Chadwick, O. A. (2010). Comparison of gully erosion estimates using airborne and ground-based LiDAR on Santa Cruz Island, California. *Geomorphology*, 118(3):288–300.

Poesen, J., Nachtergaele, J., Verstraeten, G., and Valentin, C. (2003). Gully erosion and environmental change: importance and research needs. *Catena*, 50(2):91–133.

Poesen, J., Vandaele, K., and van Wesemael, B. (1998). Gully erosion: importance and model implications. In Boardman, J. and Favis-Mortlock, D., editors, *Modelling Soil Erosion by Water*, volume I-55, pages 285–311. Springer-Verlag, Berlin.

Prosdocimi, M., Calligaro, S., Sofia, G., Dalla Fontana, G., and Tarolli, P. (2015). Bank erosion in agricultural drainage networks: new challenges from structure-from-motion photogrammetry for post-event analysis. *Earth Surface Processes and Landforms*, 40(14):1891–1906.

Renard, K. G., Foster, G. R., Weesies, G. A., McCool, D. K., and Yoder, D. C. (1997). Predicting soil erosion by water: a guide to conservation planning with the Revised Universal Soil Loss Equation (RUSLE). Technical report, U.S. Department of Agriculture, Washington DC.

Rieke-Zapp, D. H. and Nearing, M. A. (2005). Digital close range photogrammetry for measurement of soil erosion. *The Photogrammetric Record*, 20(109):69–87.

Roth, G. and La Barbera, P. (1997). Morphological characterization of channel initiation. *Physics and Chemistry of the Earth*, 22(3–4):329–332.

Sandercock, P. J. and Hooke, J. M. (2011). Vegetation effects on sediment connectivity and processes in an ephemeral channel in SE Spain. *Journal of Arid Environments*, 75(3):239–254.

Sankey, J. B., Ravi, S., Wallace, C. S. A., Webb, R. H., and Huxman, T. E. (2012). Quantifying soil surface change in degraded drylands: Shrub encroachment and effects of fire and vegetation removal in a desert grassland. *Journal of Geophysical Research: Biogeosciences*, 117:G02025.

Schneider, A., Gerke, H. H., Maurer, T., Seifert, S., Nenov, R., and Hüttl, R. F. (2012). Evaluation of remotely-sensed DEMs and modification based on plausibility rules and initial sediment budgets of an artificially-created catchment. *Earth Surface Processes and Landforms*, 37(7):708–725.

Schürch, P., Densmore, A. L., Rosser, N. J., Lim, M., and McArdell, B. W. (2011). Detection of surface change in complex topography using terrestrial laser scanning: application to the Illgraben debris-flow channel. *Earth Surface Processes and Landforms*, 36(14):1847–1859.

Selby, M. J. (1982). *Hillslope Materials and Processes*. Oxford University Press, New York.

Shan, J. and Toth, C. K. (2008). *Topographic laser ranging and scanning: principles and processing*. CRC Press, Boca Raton, FL.

Steegen, A., Govers, G., Nachtergaele, J., Takken, I., Beuselinck, L., and Poesen, J. (2000). Sediment export by water from an agricultural catchment in the Loam Belt of central Belgium. *Geomorphology*, 33(1):25–36.

Stroosnijder, L. (2005). Measurement of erosion: Is it possible? *Catena*, 64(2–3):162–173.

Takken, I., Beuselinck, L., Nachtergaele, J., Govers, G., Poesen, J., and Degraer, G. (1999). Spatial evaluation of a physically-based distributed erosion model (LISEM). *Catena*, 37(3–4):431–447.

Tarboton, D. G., Bras, R. L., and Rodriguez-Iturbe, I. (1991). On the extraction of channel networks from digital elevation data. *Hydrological Processes*, 5(1):81–100.

Tarolli, P. (2014). High-resolution topography for understanding Earth surface processes: opportunities and challenges. *Geomorphology*, 216:295–312.

Tarolli, P., Arrowsmith, J. R., and Vivoni, E. R. (2009). Understanding earth surface processes from remotely sensed digital terrain models. *Geomorphology*, 113(1):1–3.

Tarolli, P. and Dalla Fontana, G. (2008). Analysis of the headwater basins' morphology by high resolution LiDAR-derived DTM. *International Archives of the Photogrammetry, Remote Sensing and Spatial Information Sciences*, 36(5/C55):297–306.

Tarolli, P. and Dalla Fontana, G. (2009). Hillslope-to-valley transition morphology: new opportunities from high resolution DTMs. *Geomorphology*, 113(1):47–56.

Tarolli, P., Sofia, G., and Dalla Fontana, G. (2012). Geomorphic features extraction from high-resolution topography: landslide crowns and bank erosion. *Natural hazards*, 61(1):65–83.

Todisco, F., Vergni, L., Mannocchi, F., and Bomba, C. (2012). Calibration of the soil loss measurement method at the Masse experimental station. *Catena*, 91:4–9.

Toy, T. J., Foster, G. R., and Renard, K. G. (2002). *Soil erosion: processes, prediction, measurement, and control*. John Wiley & Sons, New York.

Van Asch, T. W. J. (1983). Water erosion on slopes in some land units in a Mediterranean area. *Catena supplement*, 4:129–140.

Vandaele, K., Poesen, J., Govers, G., and van Wesemael, B. (1996). Geomorphic threshold conditions for ephemeral gully incision. *Geomorphology*, 16(2):161–173.

Vandekerckhove, L., Poesen, J., Wijdenes, D. O., and Gyssels, G. (2001). Short-term bank gully retreat rates in Mediterranean environments. *Catena*, 44(2):133–161.

Vaze, J. and Teng, J. (2007). High resolution LiDAR DEM-how good is it. In *the Proceedings of the MODSIM 2007 International Congress on Modelling and Simulation*, pages 692–698.

Vigiak, O., Borselli, L., Newham, L. T. H., McInnes, J., and Roberts, A. M. (2012). Comparison of conceptual landscape metrics to define hillslope-scale sediment delivery ratio. *Geomorphology*, 138(1):74–88.

Vinci, A., Brigante, R., Todisco, F., Mannocchi, F., and Radicioni, F. (2015). Measuring rill erosion by laser scanning. *Catena*, 124:97–108.

Walling, D. E. (1983). The sediment delivery problem. *Journal of hydrology*, 65(1-3):209–237.

Walling, D. E. (1999). Linking land use, erosion and sediment yields in river basins. *Hydrobiologia*, (410):223–240.

Walling, D. E. and Quine, T. A. (1990). Calibration of caesium-137 measurements to provide quantitative erosion rate data. *Land Degradation & Development*, 2(3):161–175.

Walling, D. E., Quine, T. A., Boardman, J., Foster, I. D. L., and Dearing, J. A. (1990). Use of caesium-137 to investigate patterns and rates of soil erosion on arable fields. In *Soil erosion on agricultural land. Proceedings of a workshop sponsored by the British Geomorphological Research Group, Coventry, UK, January 1989.*, pages 33–53. John Wiley & Sons Ltd.

Wang, B., Shi, W., and Liu, E. (2015). Robust methods for assessing the accuracy of linear interpolated DEM. *International Journal of Applied Earth Observation and Geoinformation*, 34:198–206.

Wawrzyniec, T. F., McFadden, L. D., Ellwein, A., Meyer, G., Scuderi, L., McAuliffe, J., and Fawcett, P. (2007). Chronotopographic analysis directly from point-cloud data: A method for detecting small, seasonal hillslope change, Black Mesa Escarpment, NE Arizona. *Geosphere*, 3(6):550–567.

Wheaton, J. M. (2008). *Uncertainty in morphological sediment budgeting of rivers*. PhD thesis, UK.

Wheaton, J. M., Brasington, J., Darby, S. E., and Sear, D. A. (2010). Accounting for uncertainty in DEMs from repeat topographic surveys: improved sediment budgets. *Earth Surface Processes and Landforms*, 35(2):136–156.

Wilkinson, S. N., Hancock, G. J., Bartley, R., Hawdon, A. A., and Keen, R. J. (2013). Using sediment tracing to assess processes and spatial patterns of erosion in grazed rangelands, Burdekin River basin, Australia. *Agriculture, ecosystems & environment*, 180:90–102.

Williams, J. R. and Berndt, H. D. (1976). Sediment yield prediction based on watershed hydrology. *American Society of Agricultural Engineering*, 20(6):1100–1104.

Wischmeier, W. H. and Smith, D. D. (1978). Predicting rainfall erosion losses-A guide to conservation planning. (20782).

Yang, P., Ames, D. P., Fonseca, A., Anderson, D., Shrestha, R., Glenn, N. F., and Cao, Y. (2014). What is the effect of LiDAR-derived DEM resolution on large-scale watershed model results? *Environmental Modelling & Software*, 58:48–57.

Zhang, J. X., Chang, K.-T., and Wu, J. Q. (2008). Effects of DEM resolution and source on soil erosion modelling: a case study using the WEPP model. *International Journal of Geographical Information Science*, 22(8):925–942.

Appendix for Chapter 1

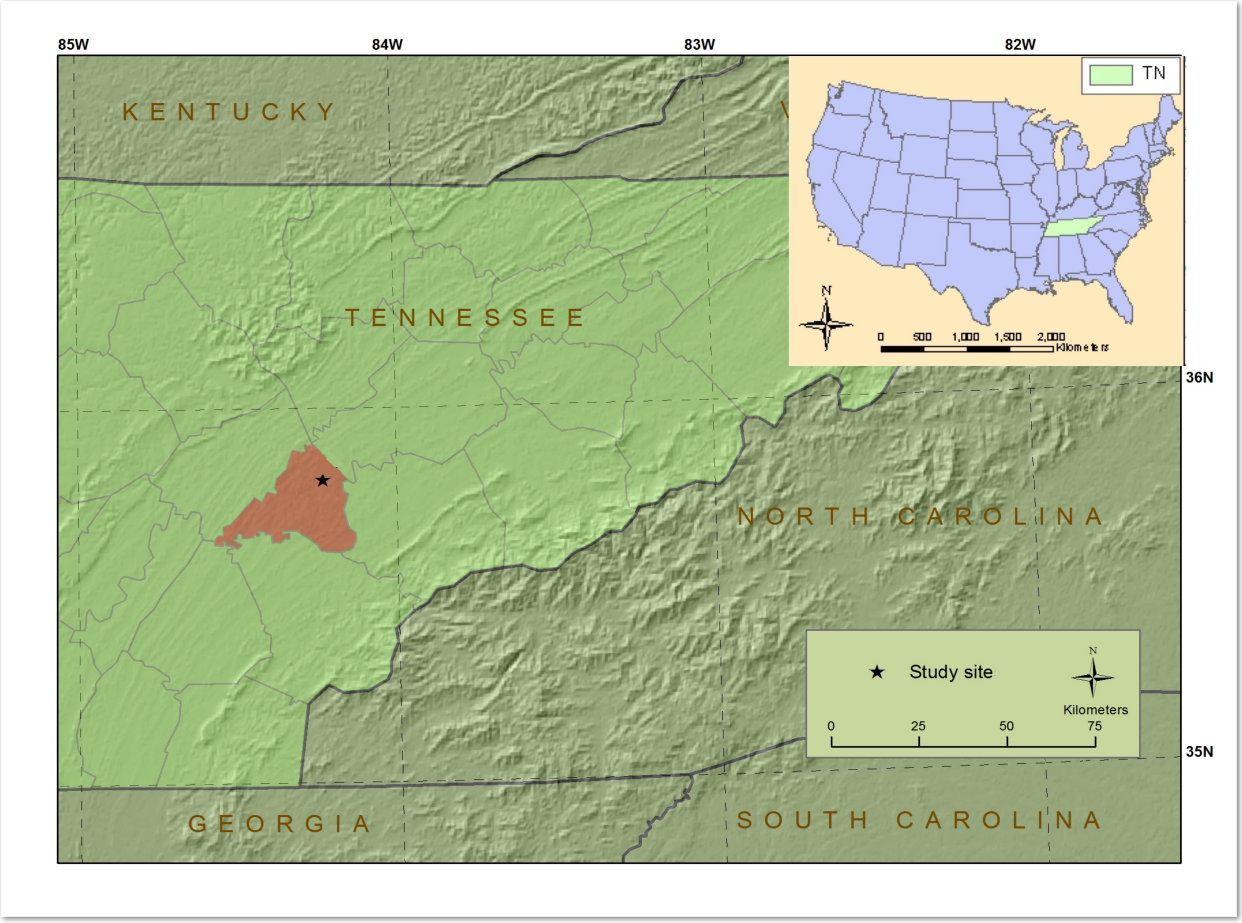

Figure 1.1: Study site in Loudon, Tennessee. Red color represents the county boundary.

Chapter 2

The effect of grid size on the quantification of erosion, deposition, and rill network on a hillslope

This chapter is based on a paper published by Lu et al., 2017:

Lu, X., Li, Y., Washington-Allen, R. A., Li, Y., Li, H., and Hu, Q. (2017). The effect of grid size on the quantification of erosion, deposition, and rill network. *International Soil and Water Conservation Research*, 5(3):241 – 251. The use of "we" in this chapter refers to all co-authors on the manuscript. My primary contribution to this work include (i) forming the research idea; (ii) collecting, processing, and analyzing the data; (iii) gathering and organizing the literature; (iv) producing the necessary tables and figures; (v) writing the manuscript.

Abstract

Hillslope rill/interrill erosion has been investigated mainly based on the collection of sediment and runoff from certain outlet locations. Recent advances in terrestrial laser scanning provide high-resolution of elevation data to centimeter levels, and temporal digital elevation models (DEMs) enabled the detection and quantification of sediment redistribution. Erosion and deposition are spatially heterogeneous across hillslopes, and when using a DEM to study the spatial pattern of the processes, the choice of resolution is critical. This study investigates the influence of grid size on the sediment change calculation and rill network delineation based on two surveys that were conducted using a terrestrial laser scanner at a hillslope with well-developed rills in 2014 and 2015. Temporal DEMs were produced and differenced to quantify changes and delineate rill networks. We investigated DEM pairs of incremental grid sizes (1-cm, 2-cm, 5-cm, 8-cm, 10-cm, 15-cm, 20-cm, and 30-cm) for DEM difference and rill network delineation. We used the 1-cm DEM as the reference to compare the results produced from other DEMs. Our results suggest that erosion mainly occurs on the rill sidewalls, and deposition on the rill floors, with patches of erosion/deposition within interrill areas. Both the area and volume of detectable change decreases as the grid size increases, while the area and volume of erosion are less sensitive compared to those of deposition. The total length and number of rills decrease with the increased grid size, whereas the average length of rills increased. The mean offset between delineated rill network and the reference increased toward larger grid sizes. In contrast to the erosion and deposition detected within rills, minor changes are detected in interrill areas, indicating either no topographic changes occur or the changes are too small to be detected in interill areas by our finest 1-cm DEMs. We recommend future studies to use the finest possible grid size that can be achieved.

2.1 Introduction

Water erosion on hillslopes is one of the dominant Earth-surface processes driven by the rainfall impacts and concentrated surface runoff (Knighton, 1998). During a rainfall event, the soil particles on the ground are detached by the rainfall impact and splashed to all directions with a tendency toward the downslope direction. Once the rainfall intensity exceeds the soil's infiltration capability, surface runoff appears, concentrates, and flows toward the foot of the hillslope (Horton, 1945). During this process, rills emerge as micro-channels to dissect the hillslope into rill and interill areas. Rills are the venues to transport sediments detached from both rills and interrill areas through concentrated flow. Rills are micro-relief channels (Knighton, 1998) that are usually < 0.3 m in depth and < 0.3 m in width (Gao, 2013; Nearing et al., 1997). They are mostly ephemeral features and can be easily removed by conventional tillage (Nearing et al., 1997; Haan et al., 1994).

Classic approaches for studying hillslope erosion either measure the sediment collected at the bottom of a plot, or measure the changes in surface elevation. The first method collects all or part of the flow and sediment during a period, and measures the weight or the volume (Stroosnijder, 2005). One limitation of this method is that it only measures the net value of sediment delivery, without accounting for the spatial variability of sediment movement (Boardman, 2006). The second method examines the changes in elevation over an area and/or the channel geometry (usually width and depth), and it is commonly used for areas that are longer than 100 m (such as gullied hillslopes)(Stroosnijder, 2005). The changes in elevation or channel geometry are usually measured using erosion pins or tapes. This method requires expertise in identifying "representative" locations, thus may be subjective with human bias. The relatively low spatial resolution of data collected using this method is also not sufficient to capture the continuous nature of sediment redistribution.

The development of digital elevation models (DEMs) has led to innovative instrument and software developments to detect and quantify the topographic characteristics of landforms, such as elevation, slope, profile/curvature, aspect, and roughness (Moore et al., 1991; Pike, 2002; Pike et al., 2009). Recent advances in remote sensing instruments,

particularly the use of terrestrial laser scanning (TLS) systems, have provided measurements of unprecedented accuracy and fine resolution that allow for the rapid collection of data for the three-dimensional (3-D) surface reconstruction and modeling (Heritage and Hetherington, 2007). Various fields have witnessed an increasing trend in applying TLS to a wide range of topics, such as geology, glaciology, hydrology, biogeochemistry, and terrestrial ecology (Eitel et al., 2011; Smith, 2015). The point cloud that is collected by TLS can be directly analyzed for metrics of interest, or converted to a triangulated irregular network (TIN), or raster-based DEM with resolutions that are greater than the TLS's laser spot size (usually in mm) and range accuracies of a few millimeters (may be varied for different scanner systems). The DEM, TIN, or point cloud generated using TLS is suitable for quantifying hydrologic and geomorphic variables of a specific area in a more automatic and flexible fashion (Cavalli et al., 2013; Pirotti and Tarolli, 2010; Starek et al., 2013; Tarolli et al., 2015; Vinci et al., 2015).

Many studies have used TLS to investigate rill/interrill erosion in experiment plots and the natural environment (Eltner et al., 2013; Eltner and Baumgart, 2015; Vinci et al., 2015, 2016), see Table 2.1. The DEMs produced by TLS can be used to discriminate the spatial pattern of erosion and deposition (Eitel et al., 2011), derive geomorphometric indices (e.g. surface roughness, in Eitel et al. (2011)), and provide high resolution topographic inputs for modeling efforts (Hancock et al. 2008). For example, Eitel et al. (2011) used TLS to test the effect of surface roughness in concentrated flow processes. Vinci et al. (2015) used TLS-produced DEMs to extract rill networks and calculate the rill morphometric characteristics in an experiment plot. They found that TLS has advantages in measuring certain indices (e.g. rill length, eroded volume) compared to manual surveys. Zhang et al. (2016) used the TLS-surveyed DEM to quantify rill morphology. Eltner and Baumgart (2015) investigated the accuracy constraints of TLS in a controlled experiment condition and suggested that with the propagated error from multiple sources (including registration, surface roughness, systematic error, and interpolation), the minimal threshold of vertical change detection is 1.5 cm. Hancock et al. (2008) used TLS to produce a DEM of the angle-of-repose of slope in mine spoil for the input of the SIBERIA landscape model.

Some critical issues still exist in TLS-based rill/interrill erosion studies, such as the choice of scanner spacing at a certain range and the point spacing necessary to detect surface features and their changes. A few airborne LiDAR and TLS studies have discussed the effect of DEM grid size on the detection and analysis of land surface features (Woolard and Colby, 2002), especially the delineation and morphology of rill networks (Vinci et al., 2015; Zhang et al., 2016), but none of these studies have systematically analyzed the effect of grid size for change detection and feature geometry in rill/interrill erosion studies. A few studies have shown a resolution threshold, that beyond a certain resolution, any finer resolution no longer improves the range accuracy of airborne LiDAR systems (García-Quijano et al., 2008). This threshold effect is important to TLS systems as the amount of erosion on a hillslope is spatially heterogeneous, and the TLS's ability to detect rill networks and the spatial pattern of erosion/deposition may be limited by the grid size of observation for these features. For example, a finer resolution may not be a better representation for a type of geomorphic features compared to a coarser resolution, especially when the level of noise (random local variance) is high. On the other hand, a coarser resolution might filter the random local noise, but it is also possible to over-generalize the features of interest, reducing the accuracy of mapping and detecting a certain type of features (Lechner et al., 2008, 2009; Woodcock and Strahler, 1987).

The effect of TLS point spacing and the grid size of TLS-derived DEMs has been investigated in various water- and erosion-related studies, including erosion modeling (Zhang et al., 2008), watershed modeling (Yang et al., 2014), and delineation of stream network (Charrier and Li, 2012). The purpose of this study is to assess the effect of DEM resolution on the quantification of hillslope erosion and deposition, and on the delineation of rill network through a case study from a rilled hillslope in Loudon, Tennessee. The results of this study provide insights into the determination of an optimal DEM resolution and guidance for future TLS-based erosion studies.

2.2 Material and Methods

2.2.1 Study Site

This study was conducted at an engineered hillslope on a terrace of the Little Tennessee River (35°37'32.52"N, 84°12'59.69"W, Figure 2.1) in Loudon County, Tennessee. The annual precipitation in this area is 1300 mm, and the annual temperature is 15 C. The study site is within the Southern Limestone/Dolomite Valleys and Low Rolling Hills sub-ecoregion, a region dominated by shale as parent materials. The dominant soil type is Waynesboro Loam with moderately low runoff potential according to US Department of Agriculture Natural Resources Conservation Service Web Soil Survey (http://websoilsurvey.sc.egov.usda.gov/). Land use/land cover in this region includes agriculture, urban, industrial, forest, and grassland.

Historical aerial photos and satellite images in Google Earth show that the hillslope was formed during the construction of the facility of Christensen Yacht in 2007, and the original soil structure was likely to be disturbed. To control erosion, bluestem (*Schizachyrium scoparium*) grass was planted on the top of the hill and also as a dense strip at the bottom of the slope. A small pond was formed at the foot of the hillslope that contains broadleaf cattail (*Typha latifolia*). The length of the hillslope is about 20-m with a slope of 27° facing southwest (257° clockwise from due north). The altitude of the hillslope section extends from approximately 255 m a.s.l. to 263 m a.s.l. The surface of the hillslope is covered with sparse vegetation patches, and the overland flow during precipitation events created a vast rill network on the slope (Figure 2.2). The very upper part of the hillslope does not have well-formed rills, indicating a lesser chance of frequent incoming runoff from top of the hillslope as a consequence of grass cover on the top of the hillslope. This study focuses on a mostly vegetation-free and about 20 m by 20 m square section that extends from the top to the foot of the hillslope.

2.2.2 Data acquisition

We used a 1550-nm wavelength FARO Focus3D X 330 TLS that was mounted on a tripod with dual-axis compensation. The Focus3D has a 360° horizontal and 307° vertical scanning view, a laser spot size of 2.25-mm at exit with 0.19 mrad (0.011°) beam divergence, a ranging accuracy of ± 2 mm at 50-m distance, with a customizable scan spacing. This TLS is able to acquire 3-D features within a radius of 330 meters at a maximum rate of 976000 pulses per second. This scanner unit is not equipped with a collimator, thus the diameter of the laser beam increases with increasing distance between the scanner and the intercepting surface. The ranging distance in our case varies from $\sim$ 10 to 20 m, and the spot size at the intercepting surface ranges from 4.15 to 6.05 mm using the methods suggested by Pesci et al. (2011).

We surveyed the study site on December 10th, 2014 and November 12th, 2015. Prior to scanning, 5 spherical reference targets (ATS Scan Reference System) with diameters of 139-mm were placed around the slope as uniformly as we could for registration between different scans within a single survey (Figure 2.2). We used a Trimble GeoExplorer 6000 Series GeoXH^{TM} handheld differential GPS (dGPS) to record the location of the ground point above which the scanner and targets were placed. This GPS unit has an integrated satellite-based augmentation system which locks onto the most power satellite signal and does real-time correction using the mobile network. The closest base station is McGhee Tyson ANGB (35.81°N, 84.00°W), about 28.47 km away from our study site. At each scan location, the GPS measurement was taken once for 20 mins for the carrier to constrain the horizontal accuracy to 10 cm + 2 parts per million(ppm) and vertical accuracy to 20 cm + 2 ppm. The level of accuracy of this GPS unit is not sufficient to georeference the data collected by the scanner, we used it to roughly place the scans to their geographic locations, and then manually transformed the scan in three dimensions (x, y, and z) and used recognizable features, such as the targets and yacht facility, to register different scans and surveys.

We started each survey with a panoramic scan, which was performed with a 360° horizontal (H) by 307° vertical (V) at a coarse resolution (5 cm point spacing at 50 m radius), followed by 3 scans from 3 fixed positions at 15-m away from the foot of the hillslope at finer resolution (1 cm spacing at 50 m radius). Multiple scan locations help reduce the influence of occlusion caused by rugged terrain, and also improve the density of points at further distance. We selected days with mild temperature and clear weather condition and at least two days after any prior precipitation event to conduct the surveys.

2.2.3 Data processing and DEM generation

We used the FARO SCENE software's (http://www.faro.com/en-us/products/faro-software/scene/overview) target-based method to register the 3 scans in a survey. The location of all scans and reference targets recorded by the dGPS were input to an Iterative Closest Point algorithm (Chetverikov et al., 2002) to help register the scans on a target-to-target basis. Scans were visually checked in correspondence view to make sure the location of identical targets in each scan were well-aligned. The 2014 survey had a root-mean-square error (RMSE) of 3.46 mm, and the 2015 survey had a RMSE of 3.51 mm. For the registration error between the 2014 and 2015 survey, we used permanent artificial features in our scan datasets, such as the walls of the yacht facility, to assess the horizontal offset. The matching sections of wall (composed of $\sim$ 31000 points) in the two datasets showed good agreement, with an RMSE of 0.8 mm, with 95% of the point-to-point offset within 2.91 mm. The ground was used for registration between different scans of the same field survey. However, as the surrounding environment is susceptible to dynamic erosion and deposition events, it is not suitable to use the ground surface to register the two scans. We used the gravel road (composed of $\sim$ 24000 points) adjacent to the site to assess the vertical offset between different surveys. The vertical offset between two surveys in our case is 2.08 mm, with 95% of the point-to-point offset within 5.66 mm.

The two registered surveys were exported as two point cloud files, which were then converted to two raster DEMs of 1-cm grid size using the bilinear interpolation method in the Quick Terrain Modeler (http://appliedimagery.com/). Both DEMs were then projected

to a local Cartesian projection because the point cloud datasets used in this study only cover a small area ($\sim$ 20 m by 20 m). A local Cartesian projection is designed for large-scale mapping purposes, with minimal consideration of the Earth curvature (Kennedy and Kopp, 2002). The 2014 and 2015 DEMs at the 1-cm resolution were resampled using a bilinear interpolation to resolutions of 2-cm, 5-cm, 8-cm, 10-cm, 15-cm, 20-cm, and 30-cm.

2.2.4 DEM of difference

One widely employed method in topographic and geomorphologic research is a change detection technique called DEM of difference (DoD, see Williams 2012). DEMs from different periods are subtracted from each other to produce a raster of differences in elevation:

$$\Delta DEM = DEM_{t_1} - DEM_{t_0} \pm \varepsilon \tag{2.1}$$

Where t_0 is the initial time that elevation data were collected and t_1 is the subsequent time of data collection, and ε is the error term. DoD is a method widely used for comparison between temporal/sequential DEMs and is suitable for elevation change detection in dynamic landforms. This method uses pre-registered time series of DEMs to spatially quantify the volume of eroded and deposited sediment.

We used the DoD method to calculate the change between the 2014 and 2015 datasets and quantify the areas of erosion and deposition. The DoD accounts for not only the elevation changes between these two periods, but also potential errors (ε) caused by noise, registration errors, as well as the vertical or ranging errors of the instrument ($\pm$ 2-mm for the FARO 3-D). One method to quantify the error is to aggregate of the possible errors of various sources, and produce a single value for the maximum potential level of uncertainty (Lane et al., 2003). However, the assumption to apply a maximum level of uncertainty uniformly to an entire surface likely overestimates the uncertainty, thus underestimates the overall changes. The use of a uniformly distributed uncertainty value is especially problematic for areas with high geomorphic complexity but comparably small changes (Brasington et al., 2003; Brasington and Smart, 2003; Westoby et al., 2012; Wheaton et al., 2013, 2010a,b).

Studies have suggested that the uncertainty is associated with the geometries of the terrain surface, and should be considered as spatially varied and calculated on a cell-by-cell basis (Lane et al., 2003; Wheaton, 2008; Wheaton et al., 2010b).

We used the Geometric Change Detection 6.0 (GCD) software to compute the difference between the DEMs that account for the spatially-varied uncertainty (Wheaton et al., 2010b). The GCD using the Fuzzy Inference System tool that combines a set of inputs (e.g. point density, slope, and surface roughness) through a set of fuzzy membership functions to generate an output function for the uncertainty on a cell to cell basis (Wheaton et al., 2010b). The cell-based uncertainty is propagated with the uncertainty of other sources (e.g. registration error, uncertainty of the scanner unit), and produce the level of uncertainty (minimum level of detection) for each cell, and any elevation change at a certain pixel that is less than the level of detection is considered insignificant. A more detailed explanation of this method and the toolset can be found in Wheaton et al. (2010b). In this paper, we designed presumed scenarios in which the same area of interest is surveyed at different point spacing. The input used in the GCD (point density, slope, roughness) are all calculated using the DEM of the corresponding resolution, instead of the DEM of the finest resolution. For the change detection, only the change that is statistically significant at the 95% level is considered, and the cells with changes below the threshold are treated as no change. This treatment may underestimate the elevation changes between these two periods.

2.2.5 Rill network delineation

Various methods and geomorphometric indicators have been used to delineate channel/rill networks from a DEM, such as the use of maximum landform curvature (Passalacqua et al., 2010; Pirotti and Tarolli, 2010; Tarolli and Dalla Fontana, 2009; Tarolli et al., 2012), moving window detection of convex (ridge) and concave (streams) features (Band, 1986; Peucker and Douglas, 1975), and the drop analysis using a pixel-based flow direction determination method (Broscoe, 1959; Tarboton et al., 1992; Tarboton, 2001). In this study, we used the drop analysis method to determine the critical contributing area that allows for the initiation of rills (Broscoe, 1959; Tarboton, 2001). This method selects the weighted contributing area

based upon the assumption that the mean stream drop, or elevation difference between the beginning and the end of stream segments of the same Strahler order should not be statistically different from those of higher orders (Tarboton et al., 1992; Tarboton, 2001). Previous studies showed that the drop analysis method and alternative geomorphometry-based methods produced results that are in good agreement (Vinci et al., 2015). The drop analysis method starts with the basic flow direction and accumulation processes that are commonly used in channel network delineation, and extracts the rill network using a series of values for the critical contributing area that is necessary to initiate the rills. The rill segments in each rill network are then assigned the Strahler's Order, and a t-test is used to compare the average elevation difference for rill segments of different orders (Tarboton et al., 1991). The null hypothesis of the test is that all of the population distribution functions of the samples (in our case, the elevation drops for streams in different orders) are identical. The value that produces the most "identical" elevation drop is considered the optimal threshold to initiate the rills.

We used the 1-cm 2014 DEM for the drop analysis. We calculated the contributing area using a Deterministic-8 single flow method (O'Callaghan and Mark, 1984), and used the Stream Drop Analysis tool in the Terrain-analysis-using-Digital-Elevation-Models (TauDEM) toolbox in ArcGIS 10.3 to perform the rill network extraction of different grid sizes (Tarboton, 2001). Other methods are not considered in this study, as some of the methods are dependent upon the calculation of localized topographic indices using progressive window size. In such cases, the results are subjective to both the size of single pixel and the processing window (Pirotti and Tarolli, 2010; Tarolli, 2014; Tarolli and Dalla Fontana, 2009).

2.2.6 Rill networks assessment

To assess the effect of DEM grid size on the delineation of rill networks, several metrics of the rills, including the total number of rills, the total length of rills, and the average length of rills, to quantitatively assess the delineated rill networks (Strahler, 1952, 1957). We also used the Revised Automated Proximity and Conformity Analysis (RAPCA) tool

(Li et al., 2008; Napieralski et al., 2006) to quantify the offset between the rills derived from the DEMs with larger grid sizes and the reference. RAPCA was originally designed to assess the level of proximity and parallel conformity between observed and simulated boundaries of ice sheets (Li et al., 2008; Napieralski et al., 2006) and it can be used to calculate the minimum, maximum, mean and standard deviation of offsets between any linear feature to the reference. Previous studies used this method in the comparison of fluvial channels and the boundaries of mountain glaciers (Charrier and Li, 2012; Li and Li, 2014).

2.3 Results and Discussion

2.3.1 DEM of Difference and Delineation of Rill Networks

Table 2.2 shows the descriptive statistics of the raw data. The result of the DoD between the 1-cm 2014 and 2015 DEMs shows that the elevation changes (both erosion and deposition) that are statistically significant at 95% level mainly occurred within or close to the rills (Figure 2.3). The total area with statistically significant changes is 23.82 m^2, accounting for 11.56% of the entire hillslope. The area with significant erosion covers 18.11 m^2, and that with deposition covers 5.71m^2. The volume that was eroded is 1.55 m^3, greater than the volume deposited (1.01 m^3). The majority of the erosion occurred on the rill sidewalls, while most deposition occurred on the rill floor. The interrill areas were relatively stable without detectable change on the 95% confidence level, although sparse patches of erosion and deposition can be observed (Figure 2.4).

Table 2.3 shows the results of the constant drop theory. The Stream Drop Analysis tool takes a list of numeric values as the number of contributing pixels in a DEM to initiate a rill. Based on the results, the optimal threshold for the contributing area is about 1500 cm^2. We used this value for the threshold to determine the rill networks for all different grid sizes, and assigned the Strahler stream order to each rill segment.

The deposition was observed mostly along the rill floor and also in the form of sparse clusters in interrill areas. A potential factor controlling deposition is surface armoring, the

exposure of pebbles both in the rill channels and in interrill areas as a result of the selective mechanism of detachment processes. Compared to the coarser particles and pebbles, the finer sediment particles (mainly clay and silt) are relatively easier to get detached and transported. This selective mechanism exposes pebbles on hillslope surface (Figure 2.2), increasing the surface roughness and preventing the rills from being further entrenched and interrill areas from getting detached by rainfall splash or surface sheet flow. As we observed on the slope, the rill bottoms were generally either armored with pebbles or already cut down to the less erodible bedrock (shale) (Figure 2.2). Instead of further entrenching, rill channels tend to widen, creating a larger cross-sectional area to allow for efficient sediment transport until reaching a equilibrium. This model, initially proposed by Foster and Lane (1983), implies that once the down-cut of channel bottom reaches a non-erodible layer, the expansion of channels starts to occur in the form of sidewall sloughing. Although it was originally proposed for ephemeral gully erosions, previous studies also found that this model is suitable for the explanation of rill development (e.g. Lewis et al. 1994.

In some parts of the interrill areas, we also observed surface crusting (a thin layer of dense and tough materials on the surface) in the field. Under this circumstance, soil particles on the surface are less likely to be affected by raindrop impact (McIntyre, 1958). The overland flow in interrill areas is usually not yet concentrated, thus the ability to detach soil particles is not comparable to the shear stress of the concentrated flow within rill channels. The majority of the erosion occurred on the rill sidewalls, due to the higher steepness and relatively looser material compared to interrill areas that are already crusted, and rill floors which are armored. In the field, we observed signs of failure on the rill sidewalls (Figure 2.2), and in the result of DoD, such failures are likely to be represented as a sharp decrease in elevation on rill sidewalls; the sediment collapsed from the sidewalls will feed into the rills, and deposit on the floors until being removed in the future storms.

2.3.2 Effect of grid size on DoD results

Table 2.4 and Figure 2.5 show the effect of grid size on erosion and deposition quantified using DoD. As the grid size progressively increases, the observed total area of change decreases,

as some of the changes that are detectable at a finer scale are smoothed out. The total area of erosion at the finest 1-cm resolution is 18.11 m^2, and it gradually decreases as the grid size increases. The total area of deposition at the finest 1-cm resolution is 5.71 m^2, and it decreases to 1.08 m^2 as grid size increases to 30-cm. When calculating using the 2-cm DEM, the area with the detectable change drop to 67.63% of the reference DEM (1-cm). The decreasing trend slows down and becomes relatively stable when the resolution is greater than 15-cm, but only 46.39% of the area is detectable with change at 95% confidence interval. In addition, the erosion/deposition spots across the hillslope are continuous at the finer scales, but as the grid size increases, the continuity reduces, and areas with smaller vertical changes are smoothed out, leaving gaps between the pixels (Figure 2.5). Compared to the erosion and deposition areas calculated using the reference DEMs, the percentage of erosion area in a sequence of 2-cm, 5-cm, 8-cm, 10-cm, 15-cm, 20-cm, and 30-cm drop first and then become stable around 50%, while the percentage of deposition area drastically decreases to around 10% when the grid size reaches 20 cm.

The volume of erosion and deposition also tend to decrease with the increased grid size (Table 2.5). The total volume of sediment eroded is 0.81 $\pm$ 0.53 m^3 and the total volume of sediment deposited is 0.23 $\pm$ 0.15 m^3 at 1-cm grid size. For the grid size of 30-cm, the volume of erosion decreases to 0.40 $\pm$ 0.27 m^3 (49.38% compared to the reference) and the volume of deposition decreases to 0.05 $\pm$ 0.04 m^3 (49.38% compared to the reference). The volume of erosion does not show a sharp change as the grid size progressively increases, and the 2-cm DEM still produces the volume of erosion that accounted for 82.72% of the reference DEM. The trend becomes flatter after the grid size of 15-cm, and eventually drops below 50% of the reference DEM at the 30-cm grid size. The volume of deposition shows a sharp drop for the grid size of 2-cm, to 0.11$\pm$ 0.09 m^3 (47.83% of the reference). After the grid size increases to and beyond 5-cm, the volume of deposition becomes relatively stationary, and accounts for 13.04% – 34.78% of the volume from the 1-cm DEM.

Our results indicate that erosion tends to be less sensitive to grid size compared to deposition from both areal and volumetric perspectives. As the grid size progressively increases, the area and volume of deposition show faster decreasing rates compared to those

of erosion. The net change volume (the difference between erosion and deposition) tends to decrease at a flat rate with increasing grid sizes. Compared to the reference DEM pair (1-cm), the net change volume accounts for 91.80% of the reference for the 2-cm grid size, and 81.97% of the reference for the 10-cm grid size. The net change volume keeps decreasing to 57.38% of the reference at the 30-cm grid size. The hotspots of change tend to be more sensitive to the smoothing effect at the margins of such hotspots, as the resampling window tends to include more cells with less change into calculation.

Our results indicate different grid size effects on erosion and deposition, possibly due to the overall shapes of the observed phenomenon. Deposition mainly occurred at the rill floor following the thalweg, and the common shape of the depositional areas is more elongated. Compared to the deposition, the erosion mainly occurred at the sidewall of the rills, which are relatively larger compared to the depositional areas (Figure 2.4 & 2.5). Usually, features that are more linear tend to be more sensitive to reduced mapping accuracy/increased grid size (Lechner et al., 2008, 2009; Woodcock and Strahler, 1987). Also, erosion tends to occur at locations where slope gradient is high, whereas deposition occurs where the slope is more gentle. In a grid system, such difference is represented as the magnitude of changes on a vertical dimension, where the value of erosion at pixels with high slope gradient is more pronounced and less likely to be smoothed out. In our case, the resampling process incorporates more areas with no detectable change for deposition, making it more sensitive to the reduction of resolution.

The detection and quantification of both erosion and deposition showed dependency on the scale (grid size), and a possible explanation is that the increased sampling interval resulted in loss of information when terrain is complex (Mark and Aronson, 1984). McNelis (2016) suggested a $10 - 30$ points/m^2 to be optimal density when using TLS to detect gully erosion, that a finer resolution won't bring improve the quantified erosion/deposition amount, whereas a coarser resolution leads to loss of information. However, in our case, no such effect was observed, which suggests that a similar "optimal" scale to study rill/interrill erosion is yet to be determined using sensors with higher accuracy and finer spatial resolution.

2.3.3 Effect of Grid Resolution on Rill Networks

The total number of rill segments shows an overall decreasing pattern as the grid size increases (Table 2.6). Only 292 rill segments are extracted at the grid size of 30-cm, compared to 327 at 1-cm. The total length of the rills also decreases, from 443.98 m (1-cm grid size) to 420.60 m (30-cm grid size). The average length of each rill increases from 1.36 m to 1.44 m. As the rills in our research are extracted based on the DEM, once the spatial resolution of the data reduces, some rills showing zig-zag or meandering at a higher resolution are replaced by a straight line at a coarser resolution. Also, some of the rill segments detected at a fine resolution are no longer detectable at coarse resolutions.

The RAPCA analysis quantified the offsets of the rill networks delineated from various resolution DEMs compared to the 1-cm DEM (Table 2.6). The minimum offset is not included in the table, as in our case, the value is always zero where rills produced from higher grid sizes intersect with those produced using the reference DEM. The results show that the maximum, mean, and standard deviation of the offset increases as DEM grid size increases. The mean offset of rills shows a linear increasing trend with the increased grid size ($R^2 = 0.90$). Compared to the absolute offset, the increase in the relative offset of the rill network is not significant, and the relative offset is always less than one cell size of the DEMs. The offset of delineated rill networks introduced by increased grid size shows limited sensitivity to the larger grid size. However, once the grid size becomes greater than 5-cm, the maximum offset becomes larger than 0.27 cm, which is comparable to the common width of rills (Knighton, 1998). Therefore, it becomes very difficult to represent the rills at the accurate location once the grid size is larger than 5-cm.

2.3.4 Other limitation factors

Our results reflect the nature of scale-dependency in the study of geomorphology. Bishop et al. (2012) emphasized the importance of various facets of scale, including geographic, cartographic, measurement, operational, and computational scales, in the application of high-resolution data for geomorphological mapping. The measurement scale is limited to the size

of the object of interest and the technology used for the measurement; the operational scale is dependent upon the physical processes, feedback mechanism, and how the natural system behaves. The analyses can only be reasonably performed when the measurement scale is in agreement with the operational scale. In our study, the measurement scale is governed by the hillslope area, the morphology of the channeled slope surface, the accuracy and spatial resolution we used for the TLS unit, and the quality of the registration within-survey and between survey. The coarsest resolution necessary to reflect the geometry of a gentle hillslope and a hillslope that is incised with channels is apparently different. In our case, the rills are well-defined and can be as deep as tens of centimeters. However, the spacing, depth, width, and/or sinuosity of the rills are varied for different landscapes. The operational scale of the erosion/deposition processes, on the other hand, is heterogeneous across the hillslope since processes are of different magnitudes and spatial extents. This is also affected by the choice of time intervals between repeated field surveys, as the magnitude of geomorphic changes would be more prominent over longer period, making it easier to be detected. Other factors such as the grain size of the soil, the type of parent material, the climate conditions, the existence or the absence of vegetation, are likely to affect the development of channels and the morphology of the landforms. Thus, our results are likely site-specific and how well the results can be translated to other environmental conditions and technological availabilities is yet to be examined.

2.4 Conclusions

The temporal DEMs produced using TLS exhibited capability in capturing continuous erosional and depositional patterns at the finest resolution. The erosion mainly occurred on rill sidewalls with some patches in interrill areas; the deposition occurred on some rill floors and also on some patch interrill areas. As the DEM resolution progressively reduces, the spatial variations of elevation change at a finer scale become averaged across larger pixels, making it difficult to visually represent the continuous pattern of sediment redistribution along the rills. The absolute values of the area and volume of sediment change tend to decrease as the grid size increases, due to the smoothing effect introduced by larger grid size.

Such results reflect the critical role of scale in geomorphology and the fractal nature of the Earth surface (Mark and Aronson, 1984).

A grid size equal to, or finer than 1-cm is recommended for mapping erosion and deposition in a rilled hillslope. The overall area of detectable change reduces to less than 50% of the 1-cm DEM when the grid size increased to 2-cm. As the grid size increases, the raster cells are no longer showing continuous patterns. Both area and volume of erosion in our study are less sensitive to resolution reduction compared to deposition, presumably due to the different spatial patterns. The deposition mainly occurred at the rill floors, as a narrow band following the thalweg; while rill erosion occurred on the sidewalls of rills, and the erosional areas are relatively less elongated in shape compared to depositional areas. The resampling process incorporates fewer pixels of no data (detectable change) when calculating erosion compared to deposition.

A grid size equal to, or finer than 1-cm is recommended for monitoring sediment delivery of rill/interrill erosions, although a grid size of 5-cm is sufficient if an estimation of 85% for the volume is acceptable. In our case, the relative value of sediment change (shown as the percent compared to the reference) is the least sensitive, and 81.97% of the sediment change is observed at the 10 cm grid size. From an areal perspective, however, the area of detectable change reduces to 67.63% when using a grid size of 2 cm, and 44.58% when using a grid size of 10 cm. In our study area, the total volume of deposited sediment was $0.23 \pm 0.15\ m^3$, which is much less compared to the volume of the sediment that was eroded ($0.81 \pm 0.53\ m^3$). Although the deposition is more sensitive to the increased grid size, the net difference between the volume of deposition and erosion is decreasing at a slower rate, and even at the grid size of 5-cm, we are able to obtain 86.89% of the net sediment volume change.

The total length and the total number of rill segments show a decreasing trend, while the average length of rills increases with greater DEM grid size. As the spatial resolution gets coarser, the detailed shape information of rills can be smoothed by the generalization. The RAPCA method was used to compare the offset between rill networks delineated using the resampled DEMs (with grid size larger than 1-cm) and the reference DEM (1-cm). The results show that although the mean and maximum offset increases as the grid size get larger,

the relative offset is always within one pixel. Therefore, using a larger grid size might reduce the accuracy of the mapped rill networks in the slope, but the effect is always within one pixel.

Our results suggest that while the temporal DEMs produced using TLS are suitable for rill erosion studies, they fail to capture the majority of the change in interrill areas. More accurate scanner units and better control over the errors are necessary to improve the precision and accuracy, possibly enabling the detection of change in interrill areas. We recommend that future research on rill/interrill erosion uses the finest grid size possible to minimize the possible loss of information. In our case, for net sediment change estimation, a grid size finer than 5-cm is sufficient to obtain more than 85% of the information compared to the 1-cm DEM. However, it should be noted that the effect of spatial resolution is likely to differ from site to site, and factors such as rill geometry, grain size, and temporal resolution may also affect the result and should be taken into account.

Acknowledgements

This research was supported by the Geomorphology Specialty Group of the American Association of Geographers and the Stewart K. McCroskey Memorial Fund. Jack McNelis, Rebecca Potter, Gene Bailey, Martin Walker, Robert Friedrichs, and Joseph Robinson helped the field surveys. We want to thank Dr. Tingwu Lei for editing and coordinating the review of the paper, and the three anonymous reviewers who provided valuable comments and suggestions.

References

Band, L. E. (1986). Topographic partition of watersheds with digital elevation models. *Water Resources Research*, 22(1):15–24.

Bishop, M. P., James, L. A., Shroder, J. F., and Walsh, S. J. (2012). Geospatial technologies and digital geomorphological mapping: Concepts, issues and research. *Geomorphology*, 137(1):5–26.

Boardman, J. (2006). Soil erosion science: Reflections on the limitations of current approaches. *Catena*, 68(23):73–86.

Brasington, J., Langham, J., and Rumsby, B. (2003). Methodological sensitivity of morphometric estimates of coarse fluvial sediment transport. *Geomorphology*, 53(3):299–316.

Brasington, J. and Smart, R. M. A. (2003). Close range digital photogrammetric analysis of experimental drainage basin evolution. *Earth Surface Processes and Landforms*, 28(3):231–247.

Broscoe, A. (1959). Quantitative analysis of longitudinal stream profiles of small watersheds. Technical Report 389–402, U.S. Geological Survey, New York.

Cavalli, M., Trevisani, S., Comiti, F., and Marchi, L. (2013). Geomorphometric assessment of spatial sediment connectivity in small Alpine catchments. *Geomorphology*, 188:31–41.

Charrier, R. and Li, Y. (2012). Assessing resolution and source effects of digital elevation models on automated floodplain delineation: A case study from the Camp Creek Watershed, Missouri. *Applied Geography*, 34:38–46.

Chetverikov, D., Svirko, D., Stepanov, D., and Krsek, P. (2002). The trimmed iterative closest point algorithm. In *16th International Conference on Pattern Recognition*, volume 3, pages 545–548, Quebec City, Canada. IEEE.

Eitel, J. U. H., Williams, C. J., Vierling, L. A., Al-Hamdan, O. Z., and Pierson, F. B. (2011). Suitability of terrestrial laser scanning for studying surface roughness effects on concentrated flow erosion processes in rangelands. *Catena*, 87(3):398–407.

Eltner, A. and Baumgart, P. (2015). Accuracy constraints of terrestrial Lidar data for soil erosion measurement: Application to a Mediterranean field plot. *Geomorphology*, 245:243–254.

Eltner, A., Mulsow, C., and Maas, H. G. (2013). Quantitative measurement of soil erosion from TLS and UAV data. *ISPRS-International Archives of the Photogrammetry, Remote Sensing and Spatial Information Sciences*, 1(2):119–124.

Foster, G. R. and Lane, L. (1983). Erosion by concentrated flow in farm fields. In *Proceedings of the DB Simons symposium on erosion and sedimentation*, pages 9.65–9.82. Colorado State University. Fort Collins, CO.

Gao, P. (2013). Rill and Gully Development Processes. In Shroder, J. F., editor, *Treatise on Geomorphology*, volume 7, pages 122–131. Academic Press, San Diego.

García-Quijano, M. J., Jensen, J., Hodgson, M. E., Hadley, B. C., Gladden, J. B., and Lapine, L. A. (2008). Significance of altitude and posting density on LiDAR-derived elevation accuracy on hazardous waste sites. *Photogrammetric Engineering & Remote Sensing*, 74(9):1137–1146.

Haan, C. T., Barfield, B. J., and Hayes, J. C. (1994). *Design Hydrology and Sedimentology for Small Catchments*. Academic Press, London.

Hancock, G. R., Crawter, D., Fityus, S. G., Chandler, J., and Wells, T. (2008). The measurement and modelling of rill erosion at angle of repose slopes in mine spoil. *Earth Surface Processes and Landforms*, 33(7):1006–1020.

Heritage, G. and Hetherington, D. (2007). Towards a protocol for laser scanning in fluvial geomorphology. *Earth Surface Processes and Landforms*, 32(1):66–74.

Horton, R. E. (1945). Erosional development of streams and their drainage basins; hydrophysical approach to quantitative morphology. *Geological society of America bulletin*, 56(3):275–370.

Kennedy, M. and Kopp, S. (2002). *Understanding map projections*. ESRI.

Knighton, D. (1998). *Fluvial Forms and Processes: A New Perspective*. Number Ed. 2. Edward Arnold, London, UK.

Lane, S. N., Westaway, R. M., and Murray Hicks, D. (2003). Estimation of erosion and deposition volumes in a large, gravelbed, braided river using synoptic remote sensing. *Earth Surface Processes and Landforms*, 28(3):249–271.

Lechner, A. M., Jones, S. D., and Bekessy, S. A. (2008). A study on the impact of scale-dependent factors on the classification of landcover maps. In Stein, A., Shi, J., and Wietske, B., editors, *Quality Aspects in Spatial Data Mining*, pages 315–328. CRC Press, Chapman and Hall.

Lechner, A. M., Stein, A., Jones, S. D., and Ferwerda, J. G. (2009). Remote sensing of small and linear features: quantifying the effects of patch size and length, grid position and detectability on land cover mapping. *Remote Sensing of Environment*, 113(10):2194–2204.

Lewis, S. M., Storm, D. E., Barfield, B. J., Ormsbee, L. E., Storm, D. E., and Ormsbee, L. E. (1994). PRORILan erosion model using probability distributions for rill flow and density II. Model validation. *Transactions of the ASAE*, 37(1):115–123.

Li, Y. and Li, Y. (2014). Topographic and geometric controls on glacier changes in the central Tien Shan, China, since the Little Ice Age. *Annals of Glaciology*, 55(66):177–186.

Li, Y., Napieralski, J., and Harbor, J. (2008). A revised automated proximity and conformity analysis method to compare predicted and observed spatial boundaries of geologic phenomena. *Computers & Geosciences*, 34(12):1806–1814.

Mark, D. M. and Aronson, P. B. (1984). Scale-dependent fractal dimensions of topographic surfaces: an empirical investigation, with applications in geomorphology and computer mapping. *Journal of the International Association for Mathematical Geology*, 16(7):671–683.

McIntyre, D. S. (1958). Soil splash and the formation of surface crusts by raindrop impact. *Soil Science*, 85(5):261–266.

McNelis, J. J. (2016). Quantifying Gully Erosion in West Tennessee using High Resolution LiDAR Data. Master's thesis, Knoxville, Tennessee.

Moore, I. D., Grayson, R. B., and Ladson, A. R. (1991). Digital terrain modelling: a review of hydrological, geomorphological, and biological applications. *Hydrological Processes*, 5(1):3–30.

Napieralski, J., Li, Y., and Harbor, J. (2006). Comparing predicted and observed spatial boundaries of geologic phenomena: Automated Proximity and Conformity Analysis applied to ice sheet reconstructions. *Computers & Geosciences*, 32(1):124–134.

Nearing, M. A., Norton, L. D., Bulgakov, D. A., Larionov, G. A., West, L. T., and Dontsova, K. M. (1997). Hydraulics and erosion in eroding rills. *Water Resources Research*, 33(4):865–876.

O'Callaghan, J. F. and Mark, D. M. (1984). The extraction of drainage networks from digital elevation data. *Computer vision, graphics, and image processing*, 28(3):323–344.

Passalacqua, P., Tarolli, P., and FoufoulaGeorgiou, E. (2010). Testing spacescale methodologies for automatic geomorphic feature extraction from lidar in a complex mountainous landscape. *Water Resources Research*, 46(11):W11535.

Pesci, A., Teza, G., and Bonali, E. (2011). Terrestrial laser scanner resolution: Numerical simulations and experiments on spatial sampling optimization. *Remote Sensing*, 3(1):167–184.

Peucker, T. K. and Douglas, D. H. (1975). Detection of surface-specific points by local parallel processing of discrete terrain elevation data. *Computer graphics and Image processing*, 4(4):375–387.

Pike, R. J. (2002). A bibliography of terrain modeling (geomorphometry), the quantitative representation of topography: Supplement 4.0. Technical report.

Pike, R. J., Evans, I. S., and Hengl, T. (2009). Geomorphometry: a brief guide. *Developments in Soil Science*, 33:3–30.

Pirotti, F. and Tarolli, P. (2010). Suitability of LiDAR point density and derived landform curvature maps for channel network extraction. *Hydrological Processes*, 24(9):1187–1197.

Schmid, T., Schack-Kirchner, H., and Hildebrand, E. (2004). A case study of terrestrial laser scanning in erosion research: calculation of roughness and volume balance at a logged forest site. In *Proceedings of the ISPRS Working Group VIII/2: Laser-Scanners for Forest and Landscape Assessment*, pages 3–6. Citeseer.

Smith, M. W. (2015). Section 2.1.5. Direct acquisition of elevation data: Terrestrial Laser Scanning. In Cook, S. J., Clarke, L. E., and Nield, J. M., editors, *Geomorphological Techniques (Online Edition)*. British Society for Geomorphology, London, UK.

Starek, M. J., Mitásová, H., Wegmann, K. W., and Lyons, N. (2013). Space-time cube representation of stream bank evolution mapped by terrestrial laser scanning. *IEEE Geoscience and Remote Sensing Letters*, 10(6):1369–1373.

Strahler, A. N. (1952). Hypsometric (area-altitude) analysis of erosional topology. *Bull. Geol. Soc. America*, 63:1117–1142.

Strahler, A. N. (1957). Quantitative analysis of watershed geomorphology. *Civ. Eng*, 101:1258–1262.

Stroosnijder, L. (2005). Measurement of erosion: Is it possible? *Catena*, 64(23):162–173.

Tarboton, D. G. (2001). TauDEM, terrain analysis using digital elevation models. *ArcGIS Extension. Versão*, 5.

Tarboton, D. G., Bras, R. L., and Rodriguez-Iturbe, I. (1992). A physical basis for drainage density. *Geomorphology*, 5(1):59–76.

Tarboton, D. G., Bras, R. L., and RodriguezIturbe, I. (1991). On the extraction of channel networks from digital elevation data. *Hydrological Processes*, 5(1):81–100.

Tarolli, P. (2014). High-resolution topography for understanding Earth surface processes: opportunities and challenges. *Geomorphology*, 216:295–312.

Tarolli, P. and Dalla Fontana, G. (2009). Hillslope-to-valley transition morphology: new opportunities from high resolution DTMs. *Geomorphology*, 113(1):47–56.

Tarolli, P., Sofia, G., Calligaro, S., Prosdocimi, M., Preti, F., and Dalla Fontana, G. (2015). Vineyards in terraced landscapes: new opportunities from lidar data. *Land Degradation & Development*, 26(1):92–102.

Tarolli, P., Sofia, G., and Dalla Fontana, G. (2012). Geomorphic features extraction from high-resolution topography: landslide crowns and bank erosion. *Natural hazards*, 61(1):65–83.

Vinci, A., Brigante, R., Todisco, F., Mannocchi, F., and Radicioni, F. (2015). Measuring rill erosion by laser scanning. *Catena*, 124:97–108.

Vinci, A., Todisco, F., and Mannocchi, F. (2016). Calibration of manual measurements of rills using Terrestrial Laser Scanning. *Catena*, 140:164–168.

Westoby, M. J., Brasington, J., Glasser, N. F., Hambrey, M. J., and Reynolds, J. M. (2012). Structure-from-Motion'photogrammetry: A low-cost, effective tool for geoscience applications. *Geomorphology*, 179:300–314.

Wheaton, J. M. (2008). *Uncertainty in morphological sediment budgeting of rivers*. PhD thesis, UK.

Wheaton, J. M., Brasington, J., Darby, S. E., Kasprak, A., Sear, D., and Vericat, D. (2013). Morphodynamic signatures of braiding mechanisms as expressed through change in sediment storage in a gravelbed river. *Journal of Geophysical Research: Earth Surface*, 118(2):759–779.

Wheaton, J. M., Brasington, J., Darby, S. E., Merz, J., Pasternack, G. B., Sear, D., and Vericat, D. (2010a). Linking geomorphic changes to salmonid habitat at a scale relevant to fish. *River Research and Applications*, 26(4):469–486.

Wheaton, J. M., Brasington, J., Darby, S. E., and Sear, D. A. (2010b). Accounting for uncertainty in DEMs from repeat topographic surveys: improved sediment budgets. *Earth Surface Processes and Landforms*, 35(2):136–156.

Williams, R. D. (2012). DEMs of difference. In Clarke, L. E. and Nield, J. M., editors, *Geomorphological Techniques (Online Edition)*, number 3.2, chapter Topographi. British Society for Geomorphology, London, UK, 2 edition.

Woodcock, C. E. and Strahler, A. H. (1987). The factor of scale in remote sensing. *Remote Sensing of Environment*, 21(3):311–332.

Woolard, J. W. and Colby, J. D. (2002). Spatial characterization, resolution, and volumetric change of coastal dunes using airborne LIDAR: Cape Hatteras, North Carolina. *Geomorphology*, 48(1):269–287.

Yang, P., Ames, D. P., Fonseca, A., Anderson, D., Shrestha, R., Glenn, N. F., and Cao, Y. (2014). What is the effect of LiDAR-derived DEM resolution on large-scale watershed model results? *Environmental Modelling & Software*, 58:48–57.

Zhang, J. X., Chang, K., and Wu, J. Q. (2008). Effects of DEM resolution and source on soil erosion modelling: a case study using the WEPP model. *International Journal of Geographical Information Science*, 22(8):925–942.

Zhang, P., Tang, H., Yao, W., Zhang, N., and Xizhi, L. V. (2016). Experimental investigation of morphological characteristics of rill evolution on loess slope. *Catena*, 137:536–544.

Appendix for Chapter 2

Table 2.1: Application of TLS for rill/interrill erosion studies

DEM grid size	Study site	Soil Type	Experimental setting [width (m)× length (m)]	Reference
20 cm	Rix's Creek Coal Mine, Australia	mudstone spoil	Engineered slope (100 × 20)	(Hancock et al., 2008)
5 cm	St. Märgen, Germany	dystric cambisol	Virtual field plots (4 × 7)	(Schmid et al., 2004)
2 cm	Perugia, Italy	Calcaric Cambisol	field experiment plot (2 × 11, 4× 11, and 8 × 22)	(Vinci et al., 2016)
2 cm	Andalusia, Spain	colluvium soil	field experiment plot (∼ 20 × 50)	(Eltner and Baumgart, 2015)*
1 cm	Andalusia, Spain	colluvium soil	field experiment plot (∼ 20 × 50)	(Eltner and Baumgart, 2015)*
1 cm	Perugia, Italy	Calcaric Cambisol	field experiment plot (8 × 2)	(Vinci et al., 2015)
1 cm	China	Loess, undisturbed	soil pan (5 × 1)	(Zhang et al., 2016)
1cm	Boise Front Range, US	Andisol	field experiment plot (2 × 4.25)	(Eitel et al., 2011)

* Authors divided the experimental plot into the eastern and western sections, with different grid sizes of 1 cm and 2 cm, respectively.

Table 2.2: The descriptive statistics for each of the point clouds compared in this study

Dataset	Number of points	Average point density (pts/cm^2)	Registration RMSE (mm)
2014	4458176	1.11	3.46 ± 1.13
2015	4791057	1.20	3.51 ± 1.28

Table 2.3: T-statistics for drop analysis with different threshold values

Number of pixels initiating a rill *	*P-Value*
100	0.015
300	0.022
600	0.041
900	0.035
1200	0.476
1500	0.871
1800	0.667
2000	0.385

* The drop analysis is done using the 1-cm DEM.

Table 2.4: The descriptive statistics of the DEMs with incremental grid size derived from the point clouds

	Grid size	1	2	5	8	10	15	20	30
14	Rows	1737	868	347	217	174	116	87	58
	Columns	1878	939	376	235	188	125	94	63
	Min	255.25	255.25	255.25	255.26	255.26	255.31	255.35	255.26
	Max	262.28	262.28	262.28	262.28	262.27	262.25	262.25	262.20
	Mean	258.96	258.96	258.96	258.96	258.95	258.96	258.96	258.95
	STD.ev	1.85	1.85	1.85	1.85	1.85	1.85	1.85	1.85
15	Rows	1737	868	347	217	174	116	87	58
	Columns	1878	939	376	235	188	125	94	63
	Min	255.40	255.41	255.42	255.43	255.26	255.31	255.44	255.56
	Max	262.28	262.27	262.25	262.26	262.27	262.24	262.24	262.24
	Mean	258.96	258.96	258.96	258.96	258.95	258.96	258.96	258.96
	STD.ev	1.85	1.85	1.85	1.85	1.85	1.85	1.85	1.85

Table 2.5: The result of differencing the 2014 and 2015 DEMs at different cell resolutions of the hillslope in Loudon, TN

Cell size(cm)	1	2	5	8	10	15	20	30
Areal								
Total area of erosion (m^2)	18.11	13.4	12.59	11.55	11.88	10.26	9.88	9.54
Percent area of erosion compared to reference	100.00%	73.99%	69.52%	63.78%	65.60%	56.65%	54.56%	52.68%
Total area of deposition (m^2)	5.71	2.71	1.89	1.16	1.64	0.79	0.6	1.08
Percent area of deposition compared to reference	100.00%	47.46%	33.10%	20.32%	28.72%	13.84%	10.51%	18.91%
Total area of detectable change (m^2)	23.82	16.11	14.48	12.71	13.52	11.05	10.48	10.62
Percent area of change compared to reference	100.00%	67.63%	60.79%	53.36%	56.76%	46.39%	44.00%	44.58%
Volumetric								
Total volume of erosion (m^3)	0.81 ± 0.53	0.67 ± 0.45	0.61± 0.41	0.55 ± 0.37	0.57 ± 0.38	0.45 ± 0.30	0.44 ± 0.30	0.40 ± 0.27
Percent volume of erosion compared to reference	100.00%	82.72%	75.31%	67.90%	70.37%	55.56%	54.32%	49.38%
Total volume of deposition (m^3)	0.23 ± 0.15	0.11 ± 0.09	0.08 ± 0.06	0.05 ± 0.04	0.07± 0.06	0.03 ± 0.02	0.03 ± 0.02	0.05 ± 0.04
Percent volume of deposition compared to reference	100.00%	47.83%	34.78%	21.74%	30.43%	13.04%	13.04%	21.74%
Total Net Volume Difference (m^3)	0.58 ± 0.46	0.56 ± 0.42	0.53 ± 0.39	0.50 ± 0.38	0.44 ± 0.35	0.42 ± 0.32	0.41 ± 0.32	0.35 ± 0.27
Percent volume of change compared to reference	100.00%	91.80%	86.89%	81.97%	75.86%	68.85%	67.21%	57.38%

Table 2.6: Morphometric and Revised-automated-proximity-and-conformity-analysis results for rill network delineated using different grid sizes

Grid size (cm)	1	2	5	8	10	15	20	30
Total number of rills	327	312	310	303	301	302	299	292
Total length (m)	443.98	435.70	435.69	433.91	429.46	427.45	426.80	420.60
Average length (m)	1.36	1.40	1.41	1.43	1.43	1.42	1.43	1.44
Maximum offset (m)	NA	0.06	0.27	0.32	0.25	0.44	0.61	1.20
Mean offset (m)	NA	0.01	0.03	0.05	0.04	0.07	0.09	0.25
Standard deviation (m)	NA	0.01	0.04	0.05	0.04	0.07	0.12	0.28
Relative mean offset *	NA	0.40	0.62	0.56	0.43	0.47	0.47	0.82

* Relative mean offset = Mean offset/Grid size

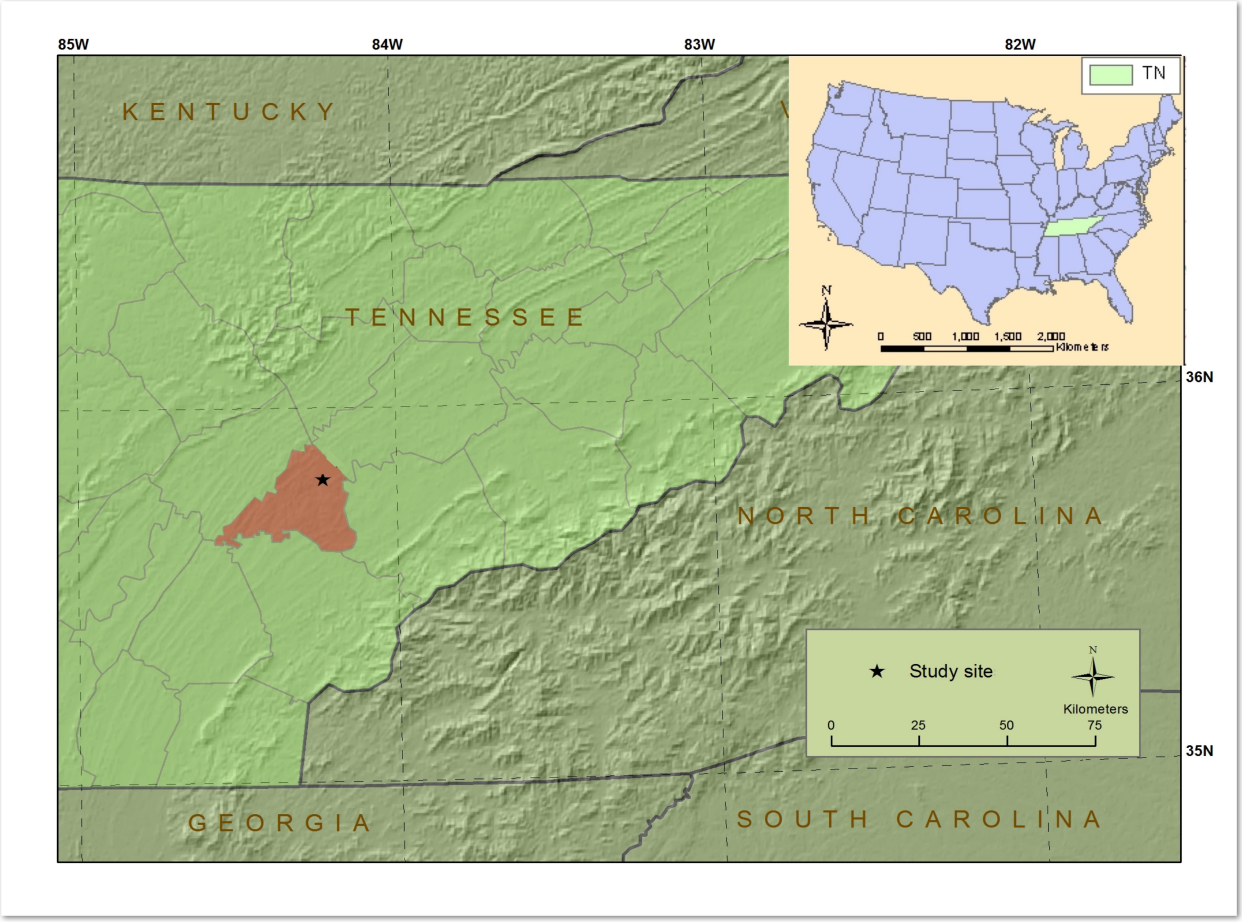

Figure 2.1: Study site

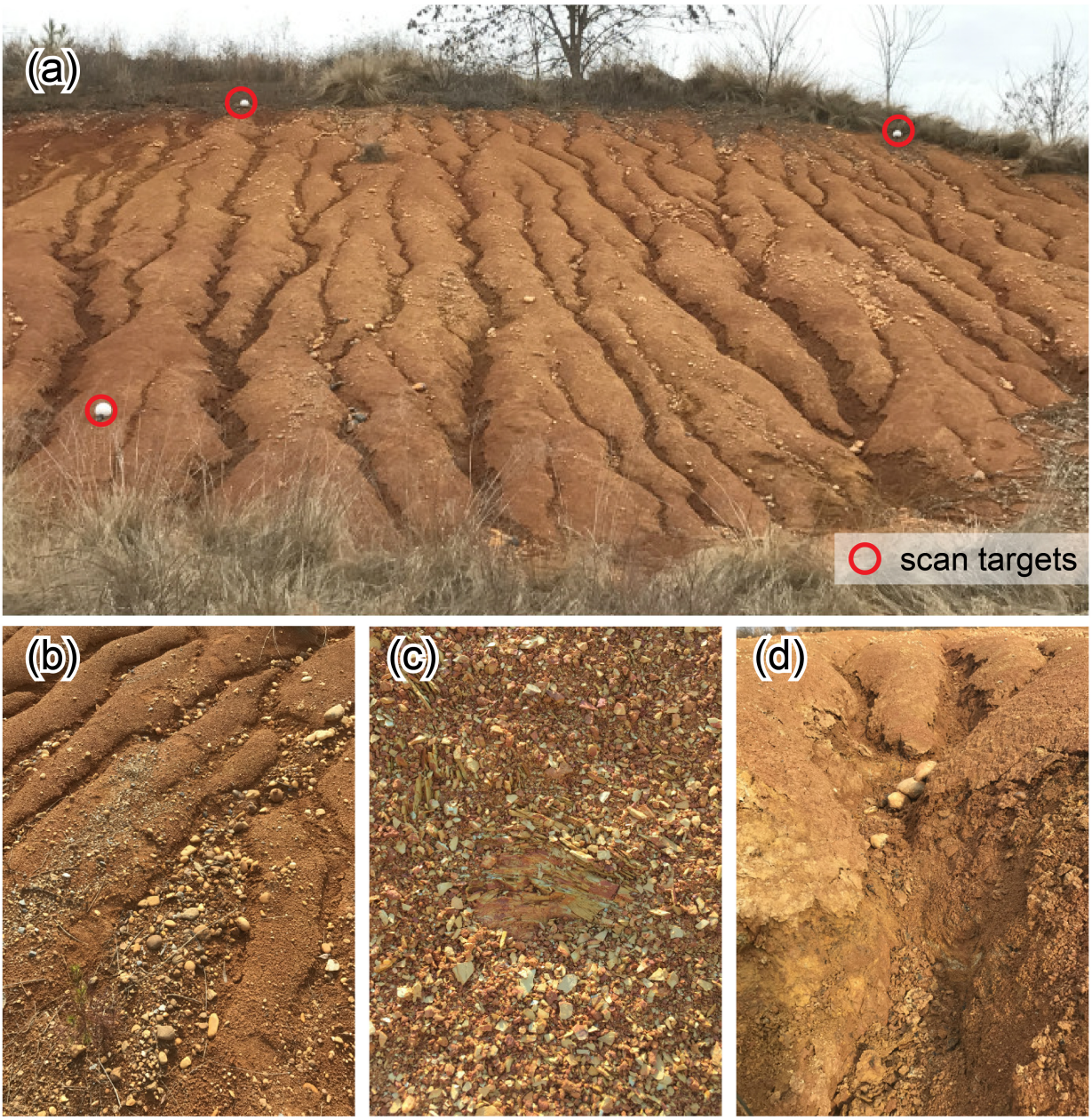

Figure 2.2: The hillslope with well-developed rill networks: a) rills and scan targets; b) surface armoring within rills and in interrill areas; c) bedrock exposed in some rill channels; d) evidence of failure on rill sidewalls.

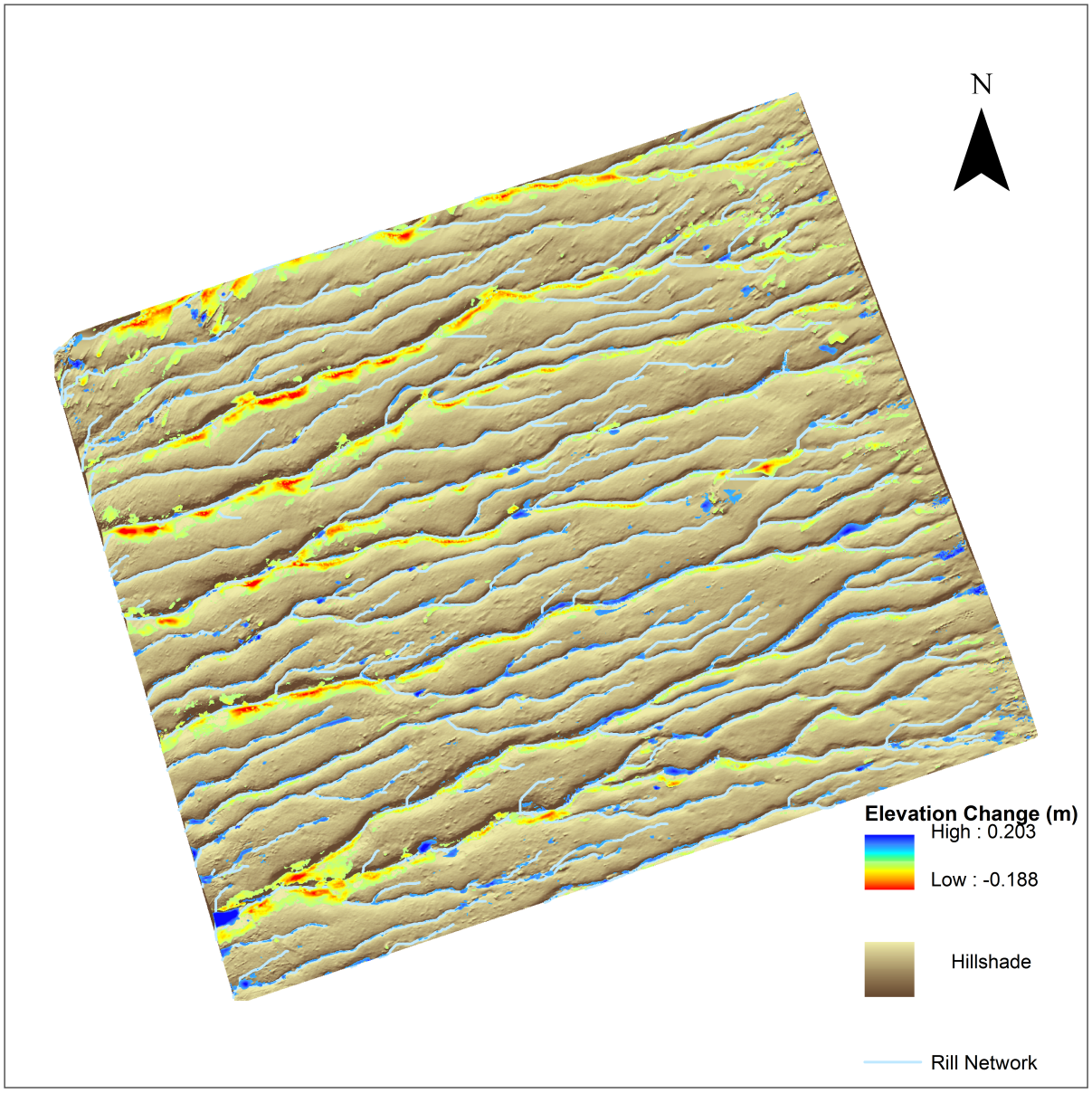

Figure 2.3: The difference between 2015 DEM and 2014 DEM; cold colors imply deposition and warm colors imply erosion.

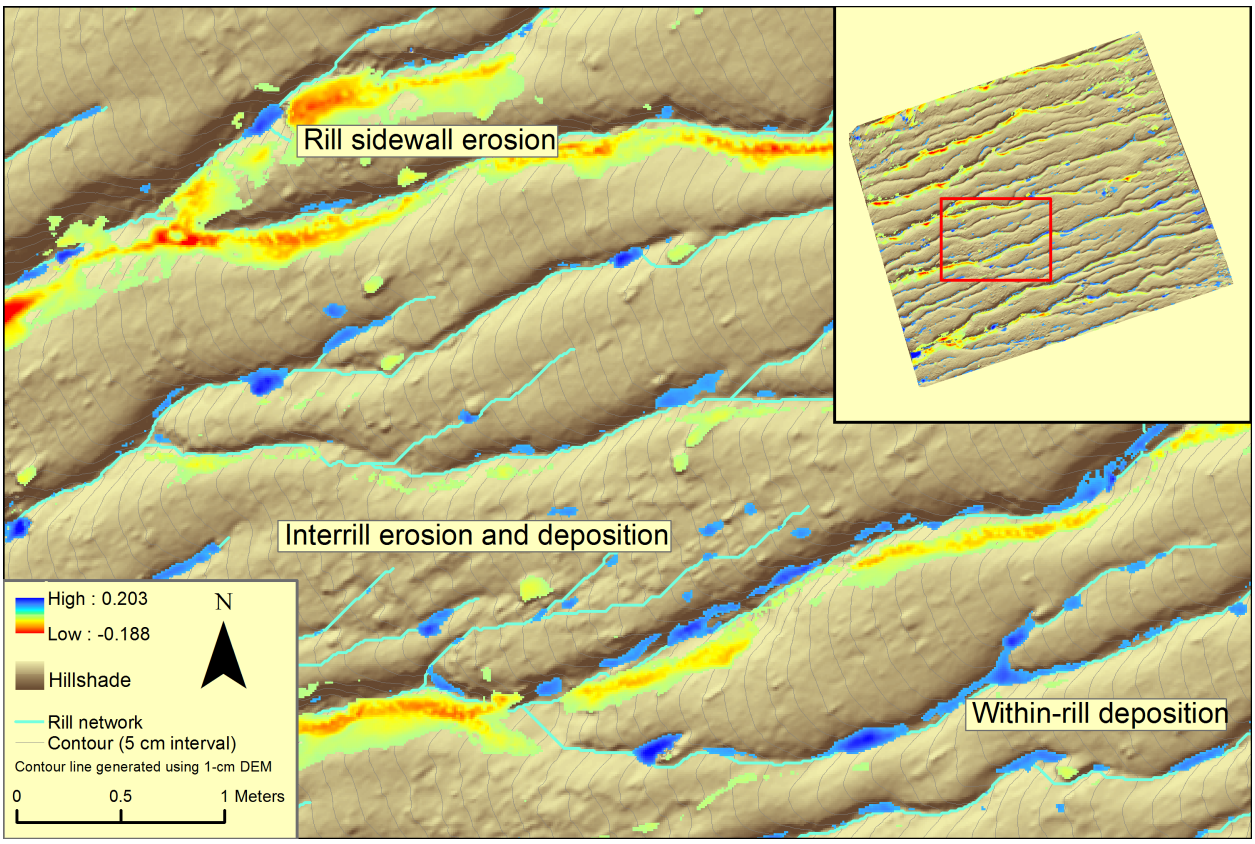

Figure 2.4: Some erosion features observed in a section of our dataset; cold colors imply deposition and warm colors imply erosion.

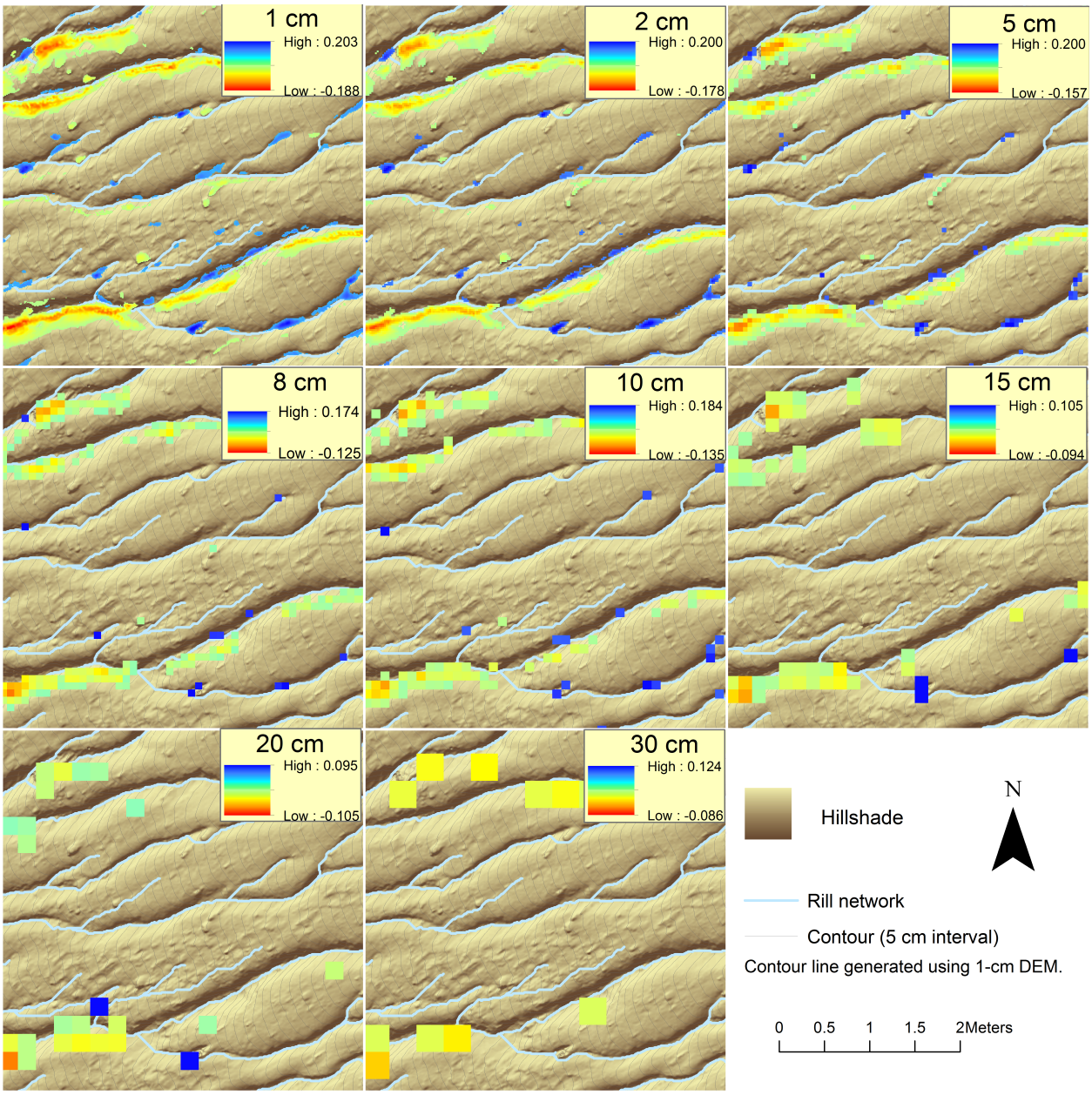

Figure 2.5: The erosion/deposition patterns become more discrete and not as proximate to rills; cold colors imply deposition and warm colors imply erosion.

Chapter 3

Micro-topographic controls on erosion and deposition on a rilled hillslope

This chapter is a manuscript that is prepared for *Earth Surface Processes and Landforms*. The use of "we" in this chapter refers to all co-authors on the manuscript to be submitted. My primary contribution to this work include (i) forming the research idea; (ii) collecting, processing, and analyzing the data; (iii) gathering and organizing the literature; (iv) producing the necessary tables and figures; (v) writing the manuscript.

Abstract

Topography imposes control on the magnitude and spatial pattern of sediment movement by directly governing the path of surface runoff, and is associated with variations of soil properties, including soil texture, moisture, organic matter and others. Previous research has investigated the importance of topography at basin scales, while the influence of topography on surface processes at hillslope scales (micro-topography) has not been systematically examined. The variations of slope, roughness, aspect, and other factors at a micro-topographic scale are likely to affect the erosion and deposition in a rilled hillslope. This research used quantile regression (QR) to investigate the micro-topographic variation and its influence on the sediment movement on a rilled hillslope in Loudon, TN. The elevation data and its derivatives, including slope, aspect, roughness index (RI), terrain wetness index (TWI), drainage density, channel depth, contributing area (CA), and the slope length-gradient (LS) factor were taken into consideration. Our results suggest that CA is the most important variable for both erosion and deposition. A larger rill basin tends to have higher erosion and deposition, although the magnitude of erosion is higher than that of deposition. The slope is positively related to erosion and negatively related to deposition, and the roughness is positively related to deposition and negative to erosion. Areas that are more north-facing are likely to have higher erosion and lower deposition, possibly because the north-facing areas receive less solar insolation in the Northern Hemisphere and usually have higher soil moisture content, resulting in faster generation of surface runoff. Larger TWI and LS lead to more erosion possibly due to higher soil moisture content. Generally, the relationships between topographic variation and erosion/deposition on a hillslope are consistent with the erosion/deposition studies at basin scales. Future research is necessary to further translate the conclusions to assist land management practices.

3.1 Introduction

Topography imposes critical impact on the magnitude and spatial distribution of water-induced soil erosion and deposition. Topography governs the pattern of surface flow and influences the flow velocity and subsequently the erosive power. Terrain characteristics are also associated with variations of soil properties (e.g. soil moisture, organic matter, and particle size), which affect a variety of hydrological processes including infiltration, runoff generation, and ponding (Schneiderman et al., 2007). Soil erosion models including the Universal Soil Loss Equation (USLE, Wischmeier and Smith 1978), Revised Universal Soil Loss Equation (RUSLE, Renard et al. 1997), and Water Erosion Prediction Project (WEPP, Nearing et al. 1989) incorporated factors including slope and curvature to represent the characteristics of topography. However, the majority of the models use a single parameter to represent the topography of a hillslope/experiment plot, without accounting for the spatially varied terrain characteristics on the hillslope surface (Liu et al., 2000; McCool et al., 1997). These single factors denoting the topography mainly emphasize the slope length, gradient, or concavity/convexity (Liu et al., 2000; Nearing et al., 1989; Wischmeier and Smith, 1978), while the micro-scale topographic variation (e.g. roughness) is often incorporated as a non-topographic parameter (e.g. as the cover factor in USLE). Although it is generally accepted that the topography influences the spatial patterns of erosion and deposition, much emphasis has been given to this topic at a watershed scale (Desmet and Govers, 1995; Montgomery and Brandon, 2002; Tarolli et al., 2012), with a few attempts at a plot scale (Eltner and Baumgart, 2015; Eltner et al., 2013; Vinci et al., 2015), possibly due to a lack of means to obtain elevation data of high resolution and accuracy. The majority of the publicly available digital elevation models (DEMs) are at the scale of meters, making them not ideal for the erosion/deposition quantification and assessment within a hillslope.

Recent development in remote sensing technologies (e.g. airborne/terrestrial laser scanning and unmanned aerial systems) allows for the high-resolution mapping of the terrain features and the detection of geomorphic changes (Brubaker et al., 2013; Eitel et al., 2011; Eltner and Baumgart, 2015; Hancock et al., 2008; Lucieer et al., 2014; Vinci et al., 2015).

Subsequently, a wide range of successful applications of those high-resolution DEMs has been executed in the field of hillslope processes over the past decades. Hancock et al. (2008) used a terrestrial laser scanner (TLS) to generate a DEM at the cm scale that was used as the input for landform evolution modeling. Eitel et al. (2011) examined the impact of surface roughness on concentrated flow processes of experimental plots, and cm-level DEM pairs were used to detect the surface change due to rill erosion. Vinci et al. (2015) found TLS advantageous compared to the manual survey when measuring rill length and eroded volume. Despite the emerging success of TLS in the micro-scale (cm or sub-cm) geomorphic studies, no research has been conducted to systematically evaluate the influence of micro-topographic variations on the erosion and deposition at the hillslope extent.

This research aims to examine the impact of micro-topographic variations on erosion and deposition by identifying representative topographic factors that best predict erosion and deposition on the hillslope. Although the term "micro-topography" was conventionally used to represent the surface roughness, we hereby broadly define it as a variety of topographic indices (e.g. slope, aspect, roughness, and others) derived from high-resolution (cm or sub-cm) DEMs. The research questions include:

i What is the spatial pattern of erosion and deposition on a rilled hillslope?

ii What are the most important micro-topographic factors that influence erosion and deposition, respectively?

iii How do the most significant micro-topographic factors influence erosion and deposition?

3.2 Study area

Our study site is a non-vegetated hillslope located in Loudon County, Tennessee (35°37'32.52"N, 84°12'59.69"W, Figure 3.1). This area is dominated by the Humid Subtropical climate (Cfa in Köppen climate classification). Located in East Tennessee, this region is featured with perennial precipitation and strong seasonality with hot summers and mild winters. The precipitation events are frequent and sometimes featured with high intensity. With

the local soil and topographic conditions that are prone to intense water-induced erosion, soil loss in this area has been impairing the agricultural productivity and fragmenting the landscape (Harden and Mathews, 2000; Matmon et al., 2003; Turnage et al., 1997). Once occupied by hardwood forests, this area was subsequently cleared for cultivation, grazing, and construction. Currently, this area is dominated by croplands and grassland, with successional forests dominated by mesophytic species. Chestnut oak (*Quercus montana*) and eastern white pine (*Pinus strobus*) mixed-forests are typical for the higher elevation ridges, while areas with lower elevations are occupied with white oak (*Quercus alba*), tulip poplar (*Liriodendron tulipifera*), and other species. The change of land use also led to a much higher erosion rate that is approximately greater compared to the natural background erosion rate by an order of magnitude (Leigh and Webb, 2006).

The annual total precipitation in this area is 1300 mm, and the annual mean temperature is 15°C. This hillslope is situated on the terrace of the Little Tennessee River, which originated from the Blue Ridge Province of the southern Appalachian Mountains and meanders westward into the Ridge and Valley physiographic province, constantly eroding the carbonate and silicate sedimentary rock layers formed during the Cambrian and Ordovician age (Chapman et al., 1982; Delcourt et al., 1986). The site is located within the Southern Dissected Ridges and Knobs sub-ecoregion, and the dominant parent material at our site is shale. The parent materials gradually weather to silty and clayey Ultisols, a type of fine-grained soil that is susceptible to rilling and gullying (Luffman et al., 2015). Particle size analyses on 6 soil samples collected at the site show that the texture of the soil is mainly clay (70.00%) with a limited amount of silt (14.67%) and sand (15.33%).

The engineered hillslope was created during the construction of the Christensen Yacht facility in 2007 according to Google Earth historical images. The construction created an almost non-vegetated hillslope that has undergone intense erosion since then. Bluestem grass (*Schizachyrium scoparium*) was planted on the terrace above the hillslope and also as a strip at the bottom of the slope to control erosion. Despite such efforts, rills emerged on the surface of the hillslope with 20 m in length from the top to the foot and 27° in slope gradient, detaching and transporting sediment that was subsequently deposited at the foot

of the hillslope. The southwest-facing slope is 257° clockwise from north, and the attitude of the slope ranges from approximately 255 m to 263 m a.s.l.. This study focuses on a vegetation-free section of the hillslope that extends about 20 m in length by 20 m in width of the hillslope. Since no man-made boundaries (earthen berms, metal sheets, etc.) were constructed there, the hydrology at the site is not disturbed, and the erodible materials are abundant, making it ideal for long-term erosion monitoring and observation (Boix-Fayos et al., 2006).

3.3 Materials and methods

3.3.1 Data acquisition

We conducted 5 field surveys at the study site on December 10th, 2014, March 7th, 2015, June 11th, 2015, September 13th, 2015, and December 16th, 2015, respectively. Elevation data of the slope surface were collected using a FARO Focus3D X 330 TLS, a scanner unit with a shortwave infrared laser (wavelength 1550 nm). We used an elevator tripod on which the scanner was mounted, and set the height of the scanner at approximately 2 m above ground with dual-axis compensation function activated. This scanner unit can scan the surrounding environment at a 360° horizontal and 307° vertical view with a scan radius of 330 m, and the ranging accuracy of the scanner is ± 2 mm at 50 m distance. During one scan, the scanner emits up to 976000 laser pulses per second. The size of a laser spot is 2.25 mm at the exit, and as it gets further away from the scanner, the laser beam diverges at 0.19 mrad (0.011°). In our case, the ranging distance between the scanner and the slope varies from approximately 10 to 20 m, and the corresponding size of the laser spot ranges from 4.15 to 6.05 mm, based on the calculation method introduced by Pesci et al. (2011). Before each survey, we placed 5 identical spherical reference targets (ATS Scan Reference System with a diameter of 139 mm) around the slope. The targets are important to intra-survey registration, and we tried to distribute these targets in a uniform fashion while avoiding any potential disturbance on the slope. We did not install permanent targets for concerns of

theft or vandalism. Since the scan targets are placed differently for each survey, we only used the targets for registering intra-survey scans.

A Trimble GeoExplorer 6000 Series GeoXH^{TM} handheld differential GPS (dGPS) was used to record the location where the scanner and targets were placed. This dGPS unit has a built-in satellite-based augmentation system, and a real-time correction on the coordinates can be performed once the system locks onto the strongest satellite signal. The nearest GPS base station is the McGhee Tyson ANGB (35.81°N, 84.00°W), which is approximately 28 km away from our study site. At each location, we performed the dGPS measurement for at least 20 mins, and this allows the carrier to update the horizontal accuracy to 10 cm ± 2 parts per million (ppm) and the vertical accuracy to 20 cm ± 2 ppm. Since such level of accuracy is not sufficient for cm level geo-referencing, the coordinates collected are used only to coarsely place the scans at their relative locations in the 3-D virtual environment before manual registration was performed. Further details of intra-survey registration and between-survey geo-referencing are given in sub-section Pre-processing and DEM generation.

Surveys were performed on days with mild temperature and clear sky condition, and at least two days after any prior precipitation event. Each survey starts with a coarse resolution (approximately 5 cm point spacing at 50 m radius) panoramic scan at the maximum viewing angle of the scanner unit (360° horizontal by 307° vertical) about 10 m away from the foot of the hillslope. At least 3 scans were performed subsequently from 3 different locations at a similar distance from the slope. The subsequent scans were parameterized so only the section of slope that we are interested was captured at a much finer resolution (approximately 1-cm spacing at a 50-m distance). We conducted multiple scans to minimize the occlusion caused by the roughness of the terrain, and by merging the multiple scans together, a relatively uniform density of points can be obtained. For each field survey, we also tried to re-occupy the same scanning locations to achieve comparable geometry of occlusion (Lague et al., 2013), but returning to the exact identical scan locations is difficult, as the environment is undergoing dynamic erosion and deposition processes (Girardeau-Montaut et al., 2005).

3.3.2 Pre-processing and DEM generation

The registration and geo-referencing were performed in the FARO SCENE^{TM} software. This software has a target-based registration function that allows for intra-survey registration between different scans. An Iterative Closest Point algorithm (Chetverikov et al., 2002) is incorporated in this software to help align the scans on a target-to-target basis. At last, we visually checked the results of the registration/geo-referencing in a correspondence view and manually placed the different scans using the scan targets and other features in our scan with regular geometry (e.g. the wall of the yacht facility) to further improve the results.

The panoramic scan performed at a relatively coarser resolution is used as the reference for intra-survey registration. Once the scans within the same survey are registered, they are considered a cluster. Any transformation in the between-survey geo-referencing is performed based on the entire cluster while the relative locations of scans in the same cluster stay fixed. The reference cluster for geo-referencing was the December 2014 survey. We used the root-mean-square error (RMSE) between control points in each survey to assess the quality of the registration and geo-referencing. The RMSE is calculated in a three-dimensional space (x, y, and z). The intra-survey RMSE is calculated based on the offset of the 5 spherical targets in three-dimensions, while the geo-referencing RMSE is calculated based on the permanent artificial features captured in our survey with regular geometry (e.g. walls of the yacht facility). The RMSE for intra-survey registration and the between-survey geo-referencing are listed in Table 3.1.

We then exported the 5 surveys as 5 separate point cloud files, with each point stored as a single data entry with attributes (x, y, and z) defining their location in the three-dimensional space. The section of the slope we surveyed is free of vegetation, so no vegetation removal is necessary in data processing. We then converted the point cloud files to 5 DEMs of 1 cm resolution using a bilinear interpolation method and projected all DEMs to a local Cartesian projection. The bilinear interpolation algorithm determines the value of a grid cell using the linear combination of four nearby neighbors while the value on each dimension (x or y) in the linear function is determined while the other is held fixed. A more detailed instruction

of the calculating method can be found in Kidner et al. (1999). The method is suitable for continuous spatial datasets that don't exhibit distinct boundaries and is widely accepted in converting LiDAR datasets to raster DEMs (Cobby et al., 2001; Rees, 2000; Smith et al., 2004). The local Cartesian projection focuses on the center point of the area of interest and defines a plane that is tangent to the spheroid at the center point, without accounting for the differences in z between corresponding points on the plane and the spheroid (Kennedy and Kopp, 2002). In our case, since the scanner stores each point in a Cartesian space, the use of the local Cartesian projection best preserves the original quality of the data since the distortion of the z is negligible due to the small extent of our study area.

3.3.3 DEM of difference

We used the DEM of Difference (DoD) method to calculate the erosion and deposition in our study area. The DoD method is a widely used for geomorphic change detection based on temporal DEMs of the same study area (Williams, 2012). The differences between two DEMs obtained at time t_1 and time t_0 are quantified based on the equation:

$$\Delta DEM = DEM_{t_1} - DEM_{t_0} + \varepsilon \tag{3.1}$$

where t_0 is the initial time when the DEM was collected, t_1 is the subsequent time of data collection, and ε is the error. The calculation is performed on a cell-to-cell basis, and the result is a raster with cells of positive values representing deposition and negative values representing erosion. The error (ε) in the equation is propagated using the ranging error associated with the scanner (2 mm), the registration and geo-referencing error (see Table 3.1), the noise created by local elevation variation, and the error associated with environmental factors (e.g. atmospheric conditions, soil moistures, etc.).

The Geometric Change Detection 6.0 (GCD) software allows for the DoD calculation while accounting for the spatially varied uncertainties (Wheaton et al., 2010). The GCD uses the Fuzzy Inference System that applies the fuzzy membership function to assign the uncertainties of each individual cell based on a set of input variables including point density,

roughness, and slope. For example, cells of high point density, low roughness, and low slope gradient are considered with low uncertainty and vice versa. When performing the DoD calculation, the output uncertainty is propagated along with uncertainties from other sources (e.g. registration, survey method). A more detailed instruction on the method is available through Wheaton et al. (2010). We repeated the DoD analysis between each adjacent surveys, and produced 4 DoD raster files from the 5 temporal DEMs, and only considered the change that is statistically significant at the 95% confidence level. The output raster of the DoD allows for the estimate of the volume of erosion and that of deposition.

3.3.4 Micro-topographic indices considered in this study

A number of micro-topographic factors are associated with erosion and deposition. The following subsections briefly review each factor and summarize the relationships between individual index and erosion/deposition. Most of the indices are derived based on DEMs with the resolution of meters, or tens of meters, and have been commonly used for watershed-scale research purposes in previous literature. To what degree that the findings at a watershed scale are translatable to a smaller hillslope scale is to be determined in our study.

Contributing Area

The contributing area denotes the entire area that contributes to the generation of runoff to a certain location. Contributing area has been widely used for channel network modeling (O'Callaghan and Mark, 1984; Tarboton et al., 1991), soil moisture mapping (Beven and Kirkby, 1979; Moore et al., 1991), and soil erosion prediction (Desmet and Govers, 1995, Montgomery and Brandon, 2002). The contributing area is considered positively related to rill erosion: for Hortonian overland flow, the contributing area affects rill discharge thus indirectly influences rill hydraulics (Beven and Kirkby, 1979; Desmet and Govers, 1996). Contributing area is also found to be correlated to the frequency of rill occurrence (Ludwig, et al., 1995) and a correlation between the rill cross-sectional area and a power function of the contributing area has been observed (Desmet and Govers, 1997; Ludwig et al., 1995).

Roughness

Terrain Roughness describes the variation and irregularities of soil surface created due to grains, micro-aggregates, soil clodiness, and farming implements (Allmaras et al., 1966; Linden and Van Doren, 1986; Riley, 1999; Römkens and Wang, 1986; Saleh, 1993, 1994). The recent use of digital photogrammetry, laser profile meters, or TLS provides more efficient and accurate alternatives compared to traditional techniques (Aguilar et al., 2009; Eitel et al., 2011). A higher roughness reduces soil erosion by increasing hydraulic resistance and dissipating the flow energy (Abrahams and Parsons, 1991; Römkens and Wang, 1986). Roughness also delays runoff generation by increasing depression storage and infiltration (Cogo et al., 1984; Darboux and Huang, 2005; Gómez and Nearing, 2005).

Elevation

Elevation in this research is included as a approximation of the effective slope length, which describes the distance from the drainage divide to a certain location (Liu et al., 2000; McCool et al., 1997, 1989). Moore and Burch (1986) suggested that the sediment yield per unit area is proportional to the length of the slope if the erosion is governed by the steady-state discharge per unit width. The slope length has been widely incorporated in the USLE (Wischmeier and Smith, 1978) and RUSLE (Renard et al., 1997) based on a power function between normalized soil loss and slope length. Some studies found that the slope length is also related to the ratio of rill to interrill erosion (Foster et al., 1977; McCool et al., 1997, 1989). Other studies found increased deposition rates with increased slope length and suggested that the relationship between the sediment yield and slope length is scale-dependent (Yair and Raz-Yassif, 2004).

Slope gradient

The slope gradient refers to the steepness of a certain area, and on a plot scale, it is positively related to both interrill and rill erosion (Abrahams et al., 1996; Fox and Bryan, 2000; Meyer et al., 1975). Some studies established a power function between erosion and

slope steepness (Desmet and Govers, 1997; Fu et al., 2011; Mah et al., 1992). Soil erosion models including RUSLE commonly incorporate the slope gradient and the slope length as one single factor (Desmet and Govers, 1996; Morgan et al., 1984; Renard et al., 1997). At finer scales, it is shown that slope positively affects the within-channel erosion by increasing the within-channel detachment through higher shear stress on the channel bed or more frequent occurrences of tension crack on sidewalls (Haan et al., 1994; Martínez-Casasnovas et al., 2009; Nearing et al., 1989).

Rill density

The rill density is defined as the number of rills per unit width (rill spacing) or the total length of rills per unit area (Tucker and Bras, 1998). Rill density varies for different slope steepness, slope length, runoff condition, soil texture, erodibility, and variation in precipitation (Fang et al., 2015; Gilley et al., 1990; Meyer and Monke, 1965; Shen et al., 2015). Soil erosion models, such as the KYERMO (Hirschi and Barfield, 1988a) and WEPP (Nearing et al., 1989), incorporated parameters denoting rill density in the prediction of erosion. The KYERMO model suggested that the rill density controls sediment yield mainly by affecting rill detachment and boundary shear stress, and the testing of model showed that higher rill density leads to reduced sediment yield, as the surface runoff is of lower flow rates while distributed over more rills (Hirschi and Barfield, 1988a,b). Olsen (2016) assessed rill networks and sediment yields during the post-wildfire erosion in the Coastal Ranges of California, and found rill density highly correlated to sediment yields ($R^2 = 0.97$). The rill density changes over time with the development of rill networks, and so far no consensus exists as for how to parameterize rill density for erosion prediction.

Aspect

The aspect influences soil properties, including the soil depth, moisture, pH, organic matter, and other soil nutrients (Agassi et al., 1990; Cerdà et al., 1995; Kutiel and Lavee, 1999; Qiu et al., 2001; Rech et al., 2001; Reid, 1973). The aspect affects the soil moisture on the surface layer, and usually the north-facing slopes have higher soil moisture compared

to the south-facing slopes in the Northern Hemisphere (Hanna et al., 1982; Reid, 1973). Since soil moisture is directly related to the infiltration and runoff generation, erosion rates differ between north- and south-facing slopes (Torri, 1996). No consensus exists regarding the effect of aspect on soil erosion, as the relationship between aspect and erosion is often obfuscated by complex interactions between environmental and experimental factors, such as microclimate (Marque and Mora, 1992), vegetation cover (Cerdà, 1998; Marque and Mora, 1992; Notario del Pino and Ruiz-Gallardo, 2015) and other experiment treatments (Agassi and Ben-Hur, 1991).

Topographic wetness index

The Topographic Wetness Index (TWI) was originally proposed by Beven and Kirkby (1979) to quantify the topographic control on hydrological processes. TWI is derived based on contributing area and the slope (calculation detailed in Table 3.2), and is related to soil depth, infiltration rate, runoff generation, soil texture, and soil aggregates (Barling et al., 1994; Burt and Butcher, 1985; Hancock et al., 2015; Western et al., 2004). Studies have found positive relationships between TWI and sediment yield through hillslope channel erosion (Daba et al., 2003; Kheir et al., 2007; Pike et al., 2009).

LS factor

The Slope length-gradient (LS) factor incorporates information regarding the slope length and gradient to predict soil erosion (McCool et al., 1997; Renard et al., 1997; Wischmeier and Smith, 1978). The LS factor is positively related to erosion and is a sensitive parameter in RUSLE/USLE (McCool et al., 1997). Although the original LS factor was introduced at the plot scale and defined as the proportion to the standard plot of a given slope length, many new methods have developed to derive this factor in GIS using DEMs, based on the contributing area and the slope gradient (Oliveira et al., 2013; Tetzlaff and Wendland, 2012; Desmet and Govers, 1995). Molnár and Julien (1998) used LS factor calculated at various resolutions to estimate soil erosion and concluded that the detailed slope gradient can be smoothed out with increased cell size thus affecting the calculation result. The LS factor

was almost universally used as a plot-wise parameter, but the efficacy of using the LS factor to predict erosion on the micro-scale has not been investigated. We used the DEM-based method proposed by Desmet and Govers (1995) to extract the LS factor.

Channel depth

Channel depth, or the measure of elevation difference for any pixel and the dividing ridge, reflects the location of a certain pixel along the cross-section of the basins: lower values of channel depth represent interfluve areas, while higher values represent channels. The spatial pattern of the channel depth is dependent upon the general terrain characteristics; in relatively flat regions, the channel depth values should be stable; while in regions with high variation in elevation, the index has larger variances. The channel depth is useful in soil classification, soil organic carbon mapping, and geomorphic feature analyses (Abdel-Kader, 2013; Adhikari et al., 2014; Feuillet et al., 2012; Yang et al., 2016).

3.3.5 Calculation of the factors

We derived the above-mentioned 9 factors in ArcGIS 10.4 and SAGA GIS using 4 DEMs (December 2014, March 2015, June 2015, and September 2015). These 4 DEMs are considered the initial stages, and the elevation changes occurred until the next survey are produced by the DoD analyses. We used rill basins to derive summary statistics of each variable, defining the median, sum, or percentage value within each basin. The basins were derived using the watershed tool in TauDEM (Tarboton, 2001). We then generated points at 0.5 m interval along the rills to segment the rill basins into a series of non-overlapping polygons at equal intervals.

All geomorphic indices are calculated based on the 1-cm DEMs, and subsequently summarized for the rill basin segments. The information of the independent variables is detailed in Table 3.2. The aspect (surface facing) extends clockwise from 0° (north) to full 360° (again north), and we used the first harmonic of the Fourier transformation to convert the aspect to the cosine and sine components. The Fourier transformation is widely

accepted in statistical models for terrain analysis to differentiate influence of aspect into the north-south and west-east variations, meanwhile maintaining the circular and continuous nature of the aspect (Evans, 2006; Li et al., 2016). For factors including the contributing area (Erskine et al., 2006), LS (Desmet and Govers, 1996), RI (Mukherjee et al., 2013), and TWI (Sörensen et al., 2006), a variety of calculation methods are available. To date, no specific calculation methods have been proven especially advantageous, and the merits of various methods are dependent upon the explicit research topic, scale of the area, data source, and data resolution. We selected calculation methods that are less computationally intense and prioritized methods that produce unitless indices so the findings are possibly more translatable.

3.3.6 Quantile regression

We used the quantile regression (QR) models to examine the relationship between erosion/deposition and the independent variables listed in Table 3.2. The QR was developed based on the modification of classical Ordinary Least Squares (OLS) regression.

Classical OLS regression which is based on the estimation of regression coefficient using the unconditional mean by solving

$$\hat{\beta} = \underset{\beta \in \mathbb{R}^{\rho}}{\arg\min} \sum (y_i - x_i^{'}\beta)^2. \tag{3.2}$$

QR is originally developed by Koenker and Hallock (2001). The quantile regression estimates the coefficient using the conditional quantile τ as,

$$\hat{\beta}(\tau) = \underset{\beta \in \mathbb{R}^{\rho}}{\arg\min} \sum \rho_{\tau}(y_i - x_i^{'}\beta) \tag{3.3}$$

where τ is the τ_{th} quantile $(0 < \tau < 1)$ that is defined as,

$$Q(\tau) = \inf\{y : F(y) \geq \tau\} \tag{3.4}$$

which satisfies

$$F(y) = Prob(Y \leq y) \tag{3.5}$$

The QR is considered more suitable for this research because 1) QR is more robust for potential outliers; 2) QR provides better performance when variables are non-Gaussian; 3) QR is more robust when the variables do not exhibit homoscedasticity (similar variance for all x).

Spatial autocorrelation among variables violates the assumption of independence for common statistical practices (Legendre, 1993). In our case, a variety of sources might contribute to the spatial autocorrelation from the variables, through hydrological and other physical processes associated with the movement of sediment. Spatial autocorrelation might also be affected by the spatial structure imposed through the choice of spatial areal units, the segments at the 0.5 m interval, to summarize the data.

We used a group k-fold cross-validation method to minimize the influence of spatial autocorrelation while achieving the optimal quantile τ without overfitting. The group k-fold cross-validation method divides data into k groups based on a categorical variable; the cross-validation is repeated for k times, and for each iteration, $k-1$ groups are used to train the model and the one group that is left out is then used to validate the model. The k results from the iterations are eventually averaged to yield an estimation. There are 19 rill drainage points at the foot of the slope, and to reduce the spatial autocorrelation, we divided the entire dataset into 19 groups based on the 19 outlets to which the basin segments drain. Therefore, the segments within a rill basin cannot be included in both the training and testing sets.

Since we included various terrain derivatives that may or may not share redundant information, it is possible for our model to produce biased estimation unless variables are selected in an objective fashion. We used the Recursive Feature Elimination (RFE) with external validation to select the fewest possible variables that preserve the best predictive ability (Kuhn, 2008). Sometimes a backward feature selection approach is used for statistical

models: the model loads all the variables in the beginning and the least important variable is dropped at each iteration, until the model performance converges at an optimal set of variables. However, such approach is susceptible to over-fitting to the training data but the variables of selection may be uninformative when predicting on new datasets (Ambroise and McLachlan, 2002). The RFE approach accounts for such issues by enclosing the backward feature selection within a resampling procedure, that for each iteration, the data are partitioned into different training and testing subsets, and the performance of the model is evaluated using the MSE of the testing subset. The variables included in the final model are determined based on a consensus ranking from all the iterations (Kuhn, 2012).

3.4 Results

3.4.1 DEM of Difference

Table 3.3 summarizes the areal and volumetric changes in the study area during the 4 periods in the 1 year cycle. In all situations, both erosion and deposition were observed in the study area and our study area underwent intensive erosion, with a total of $1.19 \pm 0.46\ m^3$ sediment eroded and $0.17 \pm 0.08\ m^3$ sediment deposited from December 2014 to December 2015. The total net volume of sediment delivery is $1.02 \pm 0.54\ m^3$. The March – June period witnessed the largest volume of erosion ($0.38 \pm 0.16\ m^3$) followed by the September – December period ($0.36 \pm 0.13\ m^3$); the December 2014 – March 2015 and the September – December periods underwent the largest volume of deposition ($0.05 \pm 0.03\ m^3$ and $0.05 \pm 0.02\ m^3$, separately).

Figure 3.2 shows the spatial pattern of erosion and deposition in the study area during the 4 periods from December 2014 to December 2015. Generally, the rills are more dynamic compared to interrill areas, with the majority of the detectable changes having occurred either within or in proximity to the rills. The majority of the interrill areas are relatively stable, that only a few "hotspots" of erosion or deposition can be observed in interrill areas.

3.4.2 Variable selection

Table 3.4 shows the results of the Pearson's correlation analyses between the dependent variables and independent variables. Both erosion and deposition are correlated with several independent variables, and many independent variables are correlated with one another. High correlation is observed between some of the variables. For example, the correlation coefficient between the slope and the LS is 0.83, and the correlation between the slope and RI is 0.97. The LS factor is highly correlated with CA (0.73) and RI (0.84). The correlations might lead to biased estimation of coefficients and affect the efficacy of OLS regression.

We used the RFE to select the fewest variables that could achieve the minimal MSE. Table 3.5 shows the results of the RFE. The erosion model and the deposition model achieved the least MSEs with 8 and 9 variables, respectively. The variables in Table 3.5 are ranked in correspondence to their importance to the model (reflected in the % change in MSE).The % change in MSE can also be viewed as a measurement of the relative importance of each variable in the model. In the erosion model, the CA is the most important factor and the model with only the CA has a high MSE of 0.28600. With more variables included in the model, the MSE gradually decreases until it increases again. The second most important factor is the slope, followed by the CosA, Depth, RI, TWI, LS and Elevation. For the deposition model, the CA is also of the highest importance, followed by Elevation, Depth, CosA, TWI, LS, Slope, RD, and RI. The RD was only included in the deposition model, and the SinA is the only variable not included in either the erosion or the deposition model. This suggest that the variation of the aspect on the west-east direction in our study area did not have significant influence on the erosion and deposition.

3.4.3 Quantile regression for erosion/deposition modeling

Figure 3.3 shows the comparison between the observed and predicted erosion/deposition using OLS regression and QR models. The OLS regression models produced R^2 values of 0.19 and 0.31 for erosion and deposition, respectively; the QR models produce R^2 values of 0.29 and 0.34, respectively. The QR model has stronger explanatory ability compared

to the OLS regression model, possibly because the amount of erosion and deposition in our study area do not follow a uniform distribution. The QR models also produced less biased prediction at the extreme values when the optimal quantile parameter was adopted. The predictions made by the QR showed a better agreement with the observed values compared to those of the OLS regression models (the black and red dashed lines are closer in QR models).

Table 3.6 – 3.9 show the coefficients of individual variables in the QR models. We examined the erosion and the deposition models for the 4 periods and for each model, the quantile (τ) that produces the smallest cross-validation MSE were used. Generally, CA is associated with higher erosion and deposition, although the absolute value of the coefficient for CA is relatively higher in the erosion model, although during the Jun. 2015 – Sep. 2015 period, the coefficient for CA (0.015) in the deposition model is slightly higher than the absolute value of CA coefficient (0.011) in the Erosion model. As is shown in Table 3.6 – 3.9, the steepness of the slope is also associated with higher erosion and lower deposition. In our study area, the slope has been incised with well-developed rills, and rill sidewalls are steeper compared to interrill areas and rill floors. During rainfall events, the flow in the rills would slough the sidewalls and failure events would occur when the stability reaches a certain threshold. The coefficient of slope represents the influence of steepness change on the magnitude of erosion/deposition. For example, the coefficient of slope in the Dec. 2014 - Mar. 2015 model is -0.332 for erosion and -0.025 for deposition, and this suggests that one degree of slope change will have an effect of -0.357 cm on the average elevation change. This effect of slope is the greatest during the Mar. 2015 - Jun. 2015 period, when the combined coefficient from the erosion model (-0.356) and the deposition model (-0.227) is -0.583 cm. This is possibly because the materials are relatively loose at the beginning of this period following the diurnal freeze-thaw cycles in the past winter, and the sidewalls of the rills are more vulnerable when exposed to the sloughing of the concentrated flow.

A higher roughness is associated with higher deposition and lower erosion, since more rugged terrain surface tends to dissipate the flow power therefore reduces the transport capacity. In our study site, the roughness is introduced by the surface armoring created by

the selective processes from the rill flows. During the four periods, higher elevation generally leads to lower erosion and lower deposition, which is reflected by the field observation that the areas closer to the top of the hillslope are generally more inactive compared to the foot area. A larger depth leads to less erosion and more deposition. Areas with the largest depth are usually where the rills are most deeply incised, such as the rill floors; the deeper the rills grow, the more compact and less erodible the materials will be.

Moreover, several factors that are generally considered to be related to soil moisture affect erosion and deposition. Our results suggest that a larger CosA leads to higher erosion and lower deposition. The CosA represents the facing of an area in a north-south direction, and a larger CosA is closer to due north. North-facing areas are more likely to have higher soil moisture in the Northern Hemisphere, thus during the rainfall events, more likely to be saturated and generating runoff more quickly. The effect of soil moisture is more pronounced in frequent consecutive rainfall events, as the moisture present in the soil has not been fully evaporated. A larger TWI leads to higher erosion and lower deposition. One possible reason is that areas with higher TWI values are more likely to have higher soil moisture, and during an rainfall event, or consecutive rainfall events, locations with higher soil moisture would have more rapid runoff generation and concentration.

3.5 Discussion

3.5.1 Seasonal variation of erosion and deposition

Different precipitation and temperature conditions during the 4 scan periods likely to contribute to variations in erosion and deposition. The December 2014 to March 2015 period witnessed less erosion and more deposition compared to the other 3 periods. A possible explanation is that the transport capacity of the flows during this period was relatively limited. During most days of this period, the low temperature in our study area was below the freezing point and the observed change might be driven by the freeze-thaw mechanism. Historical daily meteorological data are available at U.S. climate data (www.usclimatedata.com). Figure 3.4 illustrates the variation of daily high temperature, low

temperature, precipitation, and snow at Lenoir City, TN, USA (35.79°N, 84.26°W), which is approximately 18 km from the study area. The daily low temperature dropped below 0°C starting late October, and for most days of November, December, and January, the daily temperature fluctuates above and below 0°C. Meanwhile, occasional precipitation events may keep the soil moist, allowing for intense freeze-thaw cycles with the diurnal variation of the temperature. Barnes et al. (2016) found that a thin soil layer on the surface can be heaved by ice crystals formed during freezing seasons, and these crystals leads to failures and within-channel deposition during thawing. The mass failures along the sidewalls created by freeze-thaw cycle lead to wider cross-sections that reduced the flow velocities within the rills (Gatto, 2000). The DoD result during the first period suggests that the limited transport capacity created more within-channel deposition in the first period, leading to higher sediment supply in the subsequent period which resulted in high erosion rates between the 03/2015 and the 06/2015 surveys.

3.5.2 Factors controlling erosion and deposition

Factors show different importance regarding their impact on erosion and deposition, and their influences also differ at different scales. CA is the most important variables in all models, suggesting the importance of relative location on the slope and the relative location within a rill basin. The coefficients of the QR models show that a larger TWI value leads to more erosion and less deposition, and the closer the facing is to the due north (larger CosA), the more erosion and less deposition are observed. Both TWI and aspect are indirect indicators of soil moisture content. In an area with lower TWI, or more south-facing, the soil moisture level is likely to be lower, and vice versa. During a rainfall event, the drier soil is able to absorb more precipitation and postponing the generation and concentration of surface runoff. Depth is another important factor in most of our models, and this variable denotes the importance of relative location along the cross-section of a rill. A larger depth suggests less erosion and more deposition in our study area. The rills in our study area have been well developed, and the deeper rills have reached to a compact layer when they get to $\sim$ 25 cm deep, where the bed materials are not completely decomposed. These materials

are less-erodible compared to the loose materials at the surface layer. The failure events will provide higher sediment supply into the rills, and these materials are likely to deposit, even temporarily, at the rill floors where the depth is the greatest.

3.5.3 Limitations of this work

The complex nature of the erosion and deposition processes introduces challenges to modeling the sediment redistribution at a hillslope scale using grid-based approaches (Gessesse et al., 2010; Nouwakpo et al., 2017). Although the use of modern remote-sensing technologies (e.g. terrestrial and airborne laser scanning, unmanned aerial systems) allows for accurate detection and reconstruction of the details of terrain surface, various tools are designed for their respective purposes with different levels of accuracy. The choice of method should be in correspondence with the extent of the study area, the size of the feature to be monitored, the acceptable level of error, and other factors, such as temporal intervals of data acquisition and logistic availabilities. TLS is useful in our study by allowing for rapid mass sampling of the terrain surface with no direct interference, and the high-resolution dataset enabled the differentiation and quantification of the spatially varied erosion and deposition. However, limited to the errors from various sources, we could not detect most of the changes in the interrill areas.

A closer field examination shows that the redistribution of sediment in our study area is further complicated by other factors, including surface armoring and crusting (Figure 3.5). The erosive power gradually exhausts the relatively finer particles (e.g. clay and silt) that are more easily to be detached and transported, leaving behind coarser materials including some pebbles. Our model also did not take into account the heterogeneity of soil properties, including particle size, organic matter, and soil moisture. The spatially heterogeneous properties of soil particles, if included, would possibly improve the performance of our model. However, a mass sampling of the entire slope at such fine resolution can be both expensive and time-consuming, and causing some damaging interferences to the plot. Other factors such as the existence of the pebbles within our study area are also likely to change the erosion/deposition patterns by altering surface hydrology. We observed the exposure of

pebbles in both rill channels and the interrill areas. The pebbles help prevent raindrop splash and sheet erosion on interrill areas by reducing the impact of raindrops and dissipating flow energy with an increased surface roughness; they also protect the floors of the rills from further entrenchment. The sudden increase in roughness may cause the transport capacity of flow to decrease, leading to depositions within the rills. We also observed surface crusting in our study area, with a thin layer of dense and tough materials forming on the soil surface. This layer can offset the impact of raindrop in interrill areas (Mah et al., 1992).

3.6 Conclusions

This research used statistical models to examine the micro-topographic factors and its influence on sediment movement across a rilled hillslope. Generally, the quantile regression model (QR) showed stronger predictive ability compared to the classical GLM, with 29% of the variability for erosion and 34% for deposition explained by the micro-topographic variables. The coefficients of 9 factors (contributing area, roughness, slope length, gradient, rill density, aspect, wetness, LS, and channel depth) reflect the level of their influence on the prediction of erosion or deposition in the QR models. A larger CA leads to higher erosion and deposition, although the absolute value of the coefficient for CA in the erosion model is relatively higher. A steeper slope increases the amount of erosion and reduces deposition. Roughness is positively related to deposition and negatively related to erosion. Rill floors with larger depth value tend to have less erosion and more deposition. The cosine component of the aspect is associated with higher erosion and lower deposition, possibly due to higher soil moisture on the north-facing slopes with limited solar insolation. The Topographic Wetness Index (TWI), another index that is positively associated with the soil moisture, also leads to higher erosion and lower deposition. Through all period, the coefficients of individual variable showed consistent influence on erosion and deposition.

Acknowledgements

This research received financial support from the Geomorphology Specialty Group of the American Association of Geographers, the Stewart K. McCroskey Memorial Fund from the Department of Geography at the University of Tennessee Knoxville, and the Newton W. and Wilma C. Thomas Fellowship from the University of Tennessee Knoxville. Jack McNelis, Rebecca Potter, Gene Bailey, Martin Walker, Robert Friedrichs, Joseph Robinson, and Yasin Wahid Rabby helped in the field surveys.

References

Abdel-Kader, F. H. (2013). Digital Soil Mapping Using Spectral and Terrain Parameters and Statistical Modelling Integrated into GIS-Northwestern Coastal Region of Egypt. In *Developments in Soil Classification, Land Use Planning and Policy Implications*, pages 353–371. Springer.

Abrahams, A. D., Li, G., and Parsons, A. J. (1996). Rill hydraulics on a semiarid hillslope, southern Arizona. *Earth Surface Processes and Landforms*, 21(1):35–47.

Abrahams, A. D. and Parsons, A. J. (1991). Resistance to overland flow on desert pavement and its implications for sediment transport modeling. *Water Resources Research*, 27(8):1827–1836.

Adhikari, K., Hartemink, A. E., Minasny, B., Kheir, R. B., Greve, M. B., and Greve, M. H. (2014). Digital mapping of soil organic carbon contents and stocks in Denmark. *PloS one*, 9(8):e105519.

Agassi, M. and Ben-Hur, M. (1991). Effect of slope length, aspect and phosphogypsum on runoff and erosion from steep slopes. *Soil Research*, 29(2):197–207.

Agassi, M., Morin, J., and Shainberg, I. (1990). Slope, aspect, and phosphogypsum effects on runoff and erosion. *Soil Science Society of America Journal*, 54(4):1102–1106.

Aguilar, M. A., Aguilar, F. J., and Negreiros, J. (2009). Off-the-shelf laser scanning and close-range digital photogrammetry for measuring agricultural soils microrelief. *Biosystems engineering*, 103(4):504–517.

Allmaras, R. R., Burwell, R. E., Larson, W. E., and Holt, R. F. (1966). Total porosity and random roughness of the interrow zone as influenced by tillage. Technical report, U.S. Department of Agriculture.

Ambroise, C. and McLachlan, G. J. (2002). Selection bias in gene extraction on the basis of microarray gene-expression data. *Proceedings of the national academy of sciences*, 99(10):6562–6566.

Barling, R. D., Moore, I. D., and Grayson, R. B. (1994). A quasi-dynamic wetness index for characterizing the spatial distribution of zones of surface saturation and soil water content. *Water Resources Research*, 30(4):1029–1044.

Barnes, N., Luffman, I., and Nandi, A. (2016). Gully erosion and freeze-thaw processes in clay-rich soils, northeast Tennessee, USA. *GeoResJ*, 9:67–76.

Beven, K. J. and Kirkby, M. J. (1979). A physically based, variable contributing area model of basin hydrology. *Hydrological Sciences Journal*, 24(1):43–69.

Boix-Fayos, C., Martínez-Mena, M., Arnau-Rosalén, E., Calvo-Cases, A., Castillo, V., and Albaladejo, J. (2006). Measuring soil erosion by field plots: Understanding the sources of variation. *Earth-Science Reviews*, 78(3–4):267–285.

Brubaker, K. M., Myers, W. L., Drohan, P. J., Miller, D. A., and Boyer, E. W. (2013). The use of LiDAR terrain data in characterizing surface roughness and microtopography. *Applied and Environmental Soil Science*, 2013.

Burt, T. P. and Butcher, D. P. (1985). Topographic controls of soil moisture distributions. *European Journal of Soil Science*, 36(3):469–486.

Cerdà, A. (1998). The influence of aspect and vegetation on seasonal changes in erosion under rainfall simulation on a clay soil in Spain. *Canadian journal of soil science*, 78(2):321–330.

Cerdà, A., Imeson, A. C., and Calvo, A. (1995). Fire and aspect induced differences on the erodibility and hydrology of soils at La Costera, Valencia, southeast Spain. *Catena*, 24(4):289–304.

Chapman, J., Delcourt, P. A., Cridlebaugh, P. A., Shea, A. B., and Delcourt, H. R. (1982). Man-land interaction: 10,000 years of American Indian impact on native ecosystems in the lower Little Tennessee River Valley, eastern Tennessee. *Southeastern Archaeology*, pages 115–121.

Chetverikov, D., Svirko, D., Stepanov, D., and Krsek, P. (2002). The trimmed iterative closest point algorithm. In *16th International Conference on Pattern Recognition*, volume 3, pages 545–548, Quebec City, Canada. IEEE.

Cobby, D. M., Mason, D. C., and Davenport, I. J. (2001). Image processing of airborne scanning laser altimetry data for improved river flood modelling. *ISPRS Journal of Photogrammetry and Remote Sensing*, 56(2):121–138.

Cogo, N. P., Moldenhauer, W. C., and Foster, G. R. (1984). Soil loss reductions from conservation tillage practices. *Soil Science Society of America Journal*, 48(2):368–373.

Daba, S., Rieger, W., and Strauss, P. (2003). Assessment of gully erosion in eastern Ethiopia using photogrammetric techniques. *Catena*, 50(2):273–291.

Darboux, F. and Huang, C.-h. (2005). Does soil surface roughness increase or decrease water and particle transfers? *Soil Science Society of America Journal*, 69(3):748–756.

Delcourt, P. A., Delcourt, H. R., Cridlebaugh, P. A., and Chapman, J. (1986). Holocene ethnobotanical and paleoecological record of human impact on vegetation in the Little Tennessee River Valley, Tennessee. *Quaternary Research*, 25(3):330–349.

Desmet, P. J. J. and Govers, G. (1995). GIS-based simulation of erosion and deposition patterns in an agricultural landscape: a comparison of model results with soil map information. *Catena*, 25(1-4):389–401.

Desmet, P. J. J. and Govers, G. (1996). A GIS procedure for automatically calculating the USLE LS factor on topographically complex landscape units. *Journal of Soil and Water Conservation*, 51(5):427–433.

Desmet, P. J. J. and Govers, G. (1997). Two-dimensional modelling of the within-field variation in rill and gully geometry and location related to topography. *Catena*, 29(3):283–306.

Eitel, J. U. H., Williams, C. J., Vierling, L. A., Al-Hamdan, O. Z., and Pierson, F. B. (2011). Suitability of terrestrial laser scanning for studying surface roughness effects on concentrated flow erosion processes in rangelands. *Catena*, 87(3):398–407.

Eltner, A. and Baumgart, P. (2015). Accuracy constraints of terrestrial Lidar data for soil erosion measurement: Application to a Mediterranean field plot. *Geomorphology*, 245:243–254.

Eltner, A., Mulsow, C., and Maas, H. G. (2013). Quantitative measurement of soil erosion from TLS and UAV data. *ISPRS-International Archives of the Photogrammetry, Remote Sensing and Spatial Information Sciences*, 1(2):119–124.

Erskine, R. H., Green, T. R., Ramirez, J. A., and MacDonald, L. H. (2006). Comparison of grid-based algorithms for computing upslope contributing area. *Water Resources Research*, 42(9).

Evans, I. S. (2006). Glacier distribution in the Alps: statistical modelling of altitude and aspect. *Geografiska Annaler: Series A, Physical Geography*, 88(2):115–133.

Fang, H., Sun, L., and Tang, Z. (2015). Effects of rainfall and slope on runoff, soil erosion and rill development: an experimental study using two loess soils. *Hydrological Processes*, 29(11):2649–2658.

Feuillet, T., Mercier, D., Decaulne, A., and Cossart, E. (2012). Classification of sorted patterned ground areas based on their environmental characteristics (Skagafjörur, Northern Iceland). *Geomorphology*, 139:577–587.

Foster, G. R., Meyer, L. D., and Onstad, C. A. (1977). A runoff erosivity factor and variable slope length exponents for soil loss estimates. *Trans. ASAE*, 20(4):683–687.

Fox, D. M. and Bryan, R. B. (2000). The relationship of soil loss by interrill erosion to slope gradient. *Catena*, 38(3):211–222.

Fu, S., Liu, B., Liu, H., and Xu, L. (2011). The effect of slope on interrill erosion at short slopes. *Catena*, 84(1):29–34.

Gatto, L. W. (2000). Soil freeze-thaw-induced changes to a simulated rill: Potential impacts on soil erosion. *Geomorphology*, 32(1):147–160.

Gessesse, G. D., Fuchs, H., Mansberger, R., Klik, A., and Rieke-Zapp, D. H. (2010). Assessment of erosion, deposition and rill development on irregular soil surfaces using close range digital photogrammetry. *The Photogrammetric Record*, 25(131):299–318.

Gilley, J. E., Kottwitz, E., and Simanton, J. R. (1990). Hydraulic characteristics of rills. *Transactions of the ASAE*, 33(6):1900–1906.

Girardeau-Montaut, D., Roux, M., Marc, R., and Thibault, G. (2005). Change detection on points cloud data acquired with a ground laser scanner. *International Archives of Photogrammetry, Remote Sensing and Spatial Information Sciences*, 36(part 3):W19.

Gómez, J. A. and Nearing, M. A. (2005). Runoff and sediment losses from rough and smooth soil surfaces in a laboratory experiment. *Catena*, 59(3):253–266.

Haan, C. T., Barfield, B. J., and Hayes, J. C. (1994). *Design Hydrology and Sedimentology for Small Catchments*. Academic Press, London.

Hancock, G. R., Crawter, D., Fityus, S. G., Chandler, J., and Wells, T. (2008). The measurement and modelling of rill erosion at angle of repose slopes in mine spoil. *Earth Surface Processes and Landforms*, 33(7):1006–1020.

Hancock, G. R., Wells, T., Martinez, C., and Dever, C. (2015). Soil erosion and tolerable soil loss: Insights into erosion rates for a well-managed grassland catchment. *Geoderma*, 237:256–265.

Hanna, A. Y., Harlan, P. W., and Lewis, D. (1982). Soil available water as influenced by landscape position and aspect. *Agronomy Journal*, 74(6):999–1004.

Harden, C. P. and Mathews, L. (2000). Rainfall response of degraded soil following reforestation in the Copper Basin, Tennessee, USA. *Environmental Management*, 26(2):163–174.

Hirschi, M. C. and Barfield, B. J. (1988a). KYERMO – A Physically Based Research Erosion Model Part I. Model Development. *Transactions of the ASAE*, 31(3):804–813.

Hirschi, M. C. and Barfield, B. J. (1988b). KYERMO – A physically based research erosion model Part II. Model sensitivity analysis and testing. *Transactions of the ASAE*, 31(3):814–820.

Kennedy, M. and Kopp, S. (2002). *Understanding map projections*. ESRI.

Kheir, R. B., Wilson, J., and Deng, Y. (2007). Use of terrain variables for mapping gully erosion susceptibility in Lebanon. *Earth Surface Processes and Landforms*, 32(12):1770–1782.

Kidner, D., Dorey, M., and Smith, D. (1999). What's the point? Interpolation and extrapolation with a regular grid DEM. In *Fourth International Conference on GeoComputation, Fredericksburg, VA, USA*.

Koenker, R. and Hallock, K. F. (2001). Quantile regression. *Journal of economic perspectives*, 15(4):143–156.

Kuhn, M. (2008). Caret package. *Journal of Statistical Software*, 28(5):1–26.

Kuhn, M. (2012). Variable selection using the caret package.

Kutiel, P. and Lavee, H. (1999). Effect of slope aspect on soil and vegetation properties along an aridity transect. *Israel Journal of Plant Sciences*, 47(3):169–178.

Lague, D., Brodu, N., and Leroux, J. (2013). Accurate 3D comparison of complex topography with terrestrial laser scanner: Application to the Rangitikei canyon (N-Z). *ISPRS Journal of Photogrammetry and Remote Sensing*, 82:10–26.

Legendre, P. (1993). Spatial autocorrelation: trouble or new paradigm? *Ecology*, 74(6):1659–1673.

Leigh, D. S. and Webb, P. A. (2006). Holocene erosion, sedimentation, and stratigraphy at Raven Fork, southern Blue Ridge Mountains, USA. *Geomorphology*, 78(1):161–177.

Li, Y., Li, Y., Lu, X., and Harbor, J. (2016). Geomorphometric Controls on Mountain Glacier Changes Since the Little Ice Age in the Eastern Tien Shan, Central Asia. *Annals of the American Association of Geographers*, pages 1–15.

Linden, D. R. and Van Doren, D. M. (1986). Parameters for characterizing tillage-induced soil surface roughness. *Soil Science Society of America Journal*, 50(6):1560–1565.

Liu, B. Y., Nearing, M. A., Shi, P. J., and Jia, Z. W. (2000). Slope length effects on soil loss for steep slopes. *Soil Science Society of America Journal*, 64(5):1759–1763.

Lucieer, A., Turner, D., King, D. H., and Robinson, S. A. (2014). Using an Unmanned Aerial Vehicle (UAV) to capture micro-topography of Antarctic moss beds. *International Journal of Applied Earth Observation and Geoinformation*, 27:53–62.

Ludwig, B., Boiffin, J., Chad, J., and Auzet, A.-V. (1995). Hydrological structure and erosion damage caused by concentrated flow in cultivated catchments. *Catena*, 25(1):227–252.

Luffman, I. E., Nandi, A., and Spiegel, T. (2015). Gully morphology, hillslope erosion, and precipitation characteristics in the Appalachian Valley and Ridge province, southeastern USA. *Catena*, 133:221–232.

Mah, M. G. C., Douglas, L. A., and Ringrose-Voase, A. J. (1992). Effects of crust development and surface slope on erosion by rainfall. *Soil Science*, 154(1):37–43.

Marque, M. A. and Mora, E. (1992). The influence of aspect on runoff and soil loss in a Mediterranean burnt forest (Spain). *Catena*, 19(3–4):333–344.

Martínez-Casasnovas, J. A., Ramos, M. C., and García-Hernández, D. (2009). Effects of land-use changes in vegetation cover and sidewall erosion in a gully head of the Penedès region (northeast Spain). *Earth Surface Processes and Landforms*, 34(14):1927–1937.

Matmon, A., Bierman, P. R., Larsen, J., Southworth, S., Pavich, M., Finkel, R., and Caffee, M. (2003). Erosion of an ancient mountain range, the Great Smoky Mountains, North Carolina and Tennessee. *American Journal of Science*, 303(9):817–855.

McCool, D. K., Foster, G. R., Mutchler, C. K., and Meyer, L. D. (1989). Revised slope length factor for the Universal Soil Loss Equation. *Transactions of the ASAE*, 32(5):1571–1576.

McCool, D. K., Foster, G. R., and Weesies, G. A. (1997). Slope length and steepness factor. In et al. Renard, editor, *Predicting soil erosion by water – A guide to conservation planning with Revised Universal Soil Loss Equation (RUSLE)*. USDA-ARS Special Publication, Washington, D.C.

Meyer, L. D., Foster, G. R., and Romkens, M. J. M. (1975). Source of soil eroded by water from upland slopes. *Present and prospective technology for predicting sediment yields and sources*, 177(ARS-S-40):189.

Meyer, L. D. and Monke, E. J. (1965). Mechanics of soil erosion by rainfall and overland flow. *Trans. ASAE*, 8(4):572–577.

Molnár, D. K. and Julien, P. Y. (1998). Estimation of upland erosion using GIS. *Computers & Geosciences*, 24(2):183–192.

Montgomery, D. R. and Brandon, M. T. (2002). Topographic controls on erosion rates in tectonically active mountain ranges. *Earth and Planetary Science Letters*, 201(3–4):481–489.

Moore, I. D. and Burch, G. J. (1986). Modelling erosion and deposition: topographic effects. *Transactions of the ASAE*, 29(6):1624–1630.

Moore, I. D., Grayson, R. B., and Ladson, A. R. (1991). Digital terrain modelling: a review of hydrological, geomorphological, and biological applications. *Hydrological Processes*, 5(1):3–30.

Morgan, R. P. C., Morgan, D. D. V., and Finney, H. J. (1984). A predictive model for the assessment of soil erosion risk. *Journal of agricultural engineering research*, 30:245–253.

Mukherjee, S., Mukherjee, S., Garg, R. D., Bhardwaj, A., and Raju, P. L. N. (2013). Evaluation of topographic index in relation to terrain roughness and DEM grid spacing. *Journal of Earth System Science*, 122(3):869–886.

Nearing, M. A., Foster, G. R., Lane, L. J., and Finkner, S. C. (1989). A process-based soil erosion model for USDA-Water Erosion Prediction Project technology. *Transactions of ASAE*, 32(5):1587–1593.

Notario del Pino, J. S. N. and Ruiz-Gallardo, J.-R. (2015). Modelling post-fire soil erosion hazard using ordinal logistic regression: a case study in South-eastern Spain. *Geomorphology*, 232:117–124.

Nouwakpo, S. K., Weltz, M. A., McGwire, K. C., Williams, J. C., Osama, A. H., and Green, C. H. (2017). Insight into sediment transport processes on saline rangeland hillslopes using three-dimensional soil microtopography changes. *Earth Surface Processes and Landforms*, 42(4):681–696.

O'Callaghan, J. F. and Mark, D. M. (1984). The extraction of drainage networks from digital elevation data. *Computer vision, graphics, and image processing*, 28(3):323–344.

Oliveira, A. H., da Silva, M. A., Silva, M. L. N., Curi, N., Neto, G. K., and de Freitas, D. A. F. (2013). Development of topographic factor modeling for application in soil erosion models. In *Soil processes and current trends in quality assessment*. InTech.

Olsen, W. (2016). *Effects of Wildfire And Post-Fire Salvage Logging on Rill Networks and Sediment Delivery in California Forests*. PhD thesis.

Pesci, A., Teza, G., and Bonali, E. (2011). Terrestrial laser scanner resolution: Numerical simulations and experiments on spatial sampling optimization. *Remote Sensing*, 3(1):167–184.

Pike, A. C., Mueller, T. G., Schörgendorfer, A., Shearer, S. A., and Karathanasis, A. D. (2009). Erosion index derived from terrain attributes using logistic regression and neural networks. *Agronomy Journal*, 101(5):1068–1079.

Qiu, Y., Fu, B., Wang, J., and Chen, L. (2001). Soil moisture variation in relation to topography and land use in a hillslope catchment of the Loess Plateau, China. *Journal of hydrology*, 240(3):243–263.

Rech, J. A., Reeves, R. W., and Hendricks, D. M. (2001). The influence of slope aspect on soil weathering processes in the Springerville volcanic field, Arizona. *Catena*, 43(1):49–62.

Rees, W. G. (2000). The accuracy of digital elevation models interpolated to higher resolutions. *International Journal of Remote Sensing*, 21(1):7–20.

Reid, I. (1973). The influence of slope orientation upon the soil moisture regime, and its hydrogeomorphological significance. *Journal of hydrology*, 19(4):309–321.

Renard, K. G., Foster, G. R., Weesies, G. A., McCool, D. K., and Yoder, D. C. (1997). Predicting soil erosion by water: a guide to conservation planning with the Revised Universal Soil Loss Equation (RUSLE). Technical report, U.S. Department of Agriculture, Washington DC.

Riley, S. J. (1999). A Terrain Ruggedness Index that Quantifies Topographic Heterogeneity. *intermountain Journal of sciences*, 5(1–4):23–27.

Römkens, M. J. M. and Wang, J. Y. (1986). Effect of tillage on surface roughness. *Trans. ASAE*, 29(2):429–433.

Saleh, A. (1993). Soil roughness measurement: chain method. *Journal of Soil and Water Conservation*, 48(6):527–529.

Saleh, A. (1994). Measuring and predicting ridge-orientation effect on soil surface roughness. *Soil Science Society of America Journal*, 58(4):1228–1230.

Schneiderman, E. M., Steenhuis, T. S., Thongs, D. J., Easton, Z. M., Zion, M. S., Neal, A. L., Mendoza, G. F., and Todd Walter, M. (2007). Incorporating variable source area hydrology into a curve-number-based watershed model. *Hydrological Processes*, 21(25):3420–3430.

Shen, H., Zheng, F., Wen, L., Lu, J., and Jiang, Y. (2015). An experimental study of rill erosion and morphology. *Geomorphology*, 231:193–201.

Smith, S. L., Holland, D. A., and Longley, P. A. (2004). The importance of understanding error in lidar digital elevation models. *International Archives of the Photogrammetry, Remote Sensing and Spatial Information Sciences*, 35:996–1001.

Sörensen, R., Zinko, U., and Seibert, J. (2006). On the calculation of the topographic wetness index: evaluation of different methods based on field observations. *Hydrology and Earth System Sciences Discussions*, 10(1):101–112.

Tarboton, D. G. (2001). TauDEM, terrain analysis using digital elevation models. *ArcGIS Extension. Versão*, 5.

Tarboton, D. G., Bras, R. L., and Rodriguez-Iturbe, I. (1991). On the extraction of channel networks from digital elevation data. *Hydrological Processes*, 5(1):81–100.

Tarolli, P., Sofia, G., and Dalla Fontana, G. (2012). Geomorphic features extraction from high-resolution topography: landslide crowns and bank erosion. *Natural hazards*, 61(1):65–83.

Tetzlaff, B. and Wendland, F. (2012). Modelling sediment input to surface waters for German states with MEPhos: methodology, sensitivity and uncertainty. *Water resources management*, 26(1):165–184.

Torri, D. (1996). Slope, aspect and surface storage. In Agassi, M., editor, *Soil erosion, conservation and rehabilitation*, pages 77–106. Marcel Dekker, New York.

Tucker, G. E. and Bras, R. L. (1998). Hillslope processes, drainage density, and landscape morphology. *Water Resources Research*, 34(10):2751–2764.

Turnage, K. M., Lee, S. Y., Foss, J. E., Kim, K. H., and Larsen, I. L. (1997). Comparison of soil erosion and deposition rates using radiocesium, RUSLE, and buried soils in dolines in East Tennessee. *Environmental Geology*, 29(1):1–10.

Vinci, A., Brigante, R., Todisco, F., Mannocchi, F., and Radicioni, F. (2015). Measuring rill erosion by laser scanning. *Catena*, 124:97–108.

Western, A. W., Zhou, S.-L., Grayson, R. B., McMahon, T. A., Blöschl, G., and Wilson, D. J. (2004). Spatial correlation of soil moisture in small catchments and its relationship to dominant spatial hydrological processes. *Journal of hydrology*, 286(1):113–134.

Wheaton, J. M., Brasington, J., Darby, S. E., and Sear, D. A. (2010). Accounting for uncertainty in DEMs from repeat topographic surveys: improved sediment budgets. *Earth Surface Processes and Landforms*, 35(2):136–156.

Williams, R. D. (2012). DEMs of difference. In Clarke, L. E. and Nield, J. M., editors, *Geomorphological Techniques (Online Edition)*, number 3.2, chapter Topographi. British Society for Geomorphology, London, UK, 2 edition.

Wischmeier, W. H. and Smith, D. D. (1978). Predicting rainfall erosion losses-A guide to conservation planning. (20782).

Yair, A. and Raz-Yassif, N. (2004). Hydrological processes in a small arid catchment: scale effects of rainfall and slope length. *Geomorphology*, 61(1):155–169.

Yang, R.-M., Zhang, G.-L., Yang, F., Zhi, J.-J., Yang, F., Liu, F., Zhao, Y.-G., and Li, D.-C. (2016). Precise estimation of soil organic carbon stocks in the northeast Tibetan Plateau. *Scientific reports*, 6:21842.

Appendix for Chapter 3

Table 3.1: The descriptive statistics of surveys and registration/geo-referencing quality

Dataset	Number of points	Avg. point density (pts/cm^2)	RMSE (cm)*	
			Intra-survey	Between-survey
12/2014	7671276	1.91	0.35 ± 0.11	0 (reference)
03/2015	8983232	2.25	0.35 ± 0.13	0.53 ± 0.08
06/2015	8223775	2.06	0.34 ± 0.11	0.41 ± 0.08
09/2015	8059708	2.02	0.33 ± 0.12	0.44 ± 0.05
12/2015	7931839	1.99	0.35 ± 0.14	0.40 ± 0.07

* mean ± standard error

Table 3.2: Variables included as inputs to the statistical analyses

Factor	Variable name	Unit	Summary Statistics	Calculation method
Contributing area	CA	m^2	median	D8 method
Slope length	Elevation	m	median	–
Slope gradient	Slope	°	median	Derived using DEM
Surface facing	Aspect	°	median	Derived using DEM. Transformed to cosine and sine components to represent north-south and east-west trend separately
Rill density	Drainage	m/m^2	median	L/A, where L is the total length of rill and A is the area
Roughness	RI	m	median	$RI = \sqrt{\sum (x_{ij} - x_{00})^2}$, where x_{00} is the elevation of the central cell, and x_{ij} is the elevation of each neighboring cell in a 3 × 3 kernel
Topographic Wetness Index	TWI	unitless	median	$TWI = \ln(\alpha / \tan\beta)$, where α is the contributing area, and β is the slope
LS factor	LS	unitless	median	$LS = (\frac{(A_{i,j-in}+D^2)^{m+1}-A_{i,j-in}^{m+1}}{D^{m+2}\times x_{i,j}^{m}\times 22.13^{m}}) \times \sqrt{G_x^2 + G_y^2}$,where m is the slope length exponent, $A_{i,j-in}$ is the contributing area at the inlet of grid cell with coordinates (i, j), α is the aspect of the cell, D is the grid cell size, and G_x and G_y represents gradient on x and y directions.

Table 3.3: The areal and volumetric changes within our study area during the 4 scans

Date	12/2014 – 03/2015	03/2015 – 06/2015	06/2015 – 09/2015	09/2015 – 12/2015	Total
Areal					
Area w. Detectable Change (m^2)	5.83	8.73	6.86	8.75	–
Area of Erosion (m^2)	3.80	8.59	6.35	7.37	–
Area of Deposition (m^2)	2.03	0.14	0.52	1.38	–
Percent of Area w. Detectable Change	3.76%	5.63%	4.42%	5.65%	–
Volumetric					
Volume of Erosion (m^3)	0.18 ± 0.07	0.38 ± 0.16	0.27 ± 0.10	0.36 ± 0.13	1.19 ± 0.46
Volume of Deposition (m^3)	0.07 ± 0.03	0.03 ± 0.01	0.04 ± 0.02	0.05 ± 0.02	0.17 ± 0.08
Net sediment change (m^3)	0.13 ± 0.10	0.35 ± 0.17	0.23 ± 0.12	0.31 ± 0.15	1.02 ± 0.54

Table 3.4: Results of Pearson's correlation analysis

	erosion	deposition	elevation	slope	LS	CA	Depth	aspect	RD	RI
deposition	-0.11									
elevation	0.38**	-0.17***								
slope	-0.30***	0.23***	-0.36***							
LS	-0.37***	0.25	-0.50**	0.83***						
CA	-0.43***	0.31**	-0.55***	0.53***	0.73***					
Depth	0.27**	-0.12	-0.10*	-0.01	0.03	0.15**				
aspect	0.04	-0.09*	0.01	-0.06	-0.07	-0.01	0.07			
RD	-0.01	0.04	0.06	0.04***	0.25**	0.15	-0.07**	-0.11***		
RI	-0.31***	0.24***	-0.37***	0.97***	0.84***	0.58***	-0.02**	-0.09	0.04**	
TWI	0.02**	0.01	-0.07***	-0.52***	-0.05	0.00	0.10	0.00	0.31	-0.50***

* significant at the 0.1 level ($p < 0.1$);
** significant at the 0.05 level ($p < 0.05$);
*** significant at the 0.01 level ($p < 0.01$).

Table 3.5: Change of MSE as more variables are included in the final models

	Erosion		**Deposition**	
No. of variables	Variable*	MSE**	Variable*	MSE**
1	CA	0.28600	CA	0.22500
2	Slope	0.22090	Elevation	0.17898
3	CosA	0.20833	Depth	0.16456
4	Depth	0.19665	CosA	0.15949
5	RI	0.19082	TWI	0.15715
6	TWI	0.17694	LS	0.15247
7	LS	0.17349	Slope	0.14779
8	**Elevation**	**0.17151**	RD	0.14223
9	RD	0.17241	**RI**	**0.14077**
10	SinA	0.17286	SinA	0.14155

* The variables are ranked according to their importance in each model in descending order.
** The minimal MSE produced with the fewest variables is in bold.

Table 3.6: Coefficients of the QR models: Dec. 2014 – Mar. 2015

Erosion model* ($\tau = 0.56$)				**Deposition model** ($\tau = 0.53$)			
$n = 322$	Coefficients	std. error	*P-value*	$n = 297$	Coefficients	std.error	*P-value*
constant	-2.235	1.186	0.060	constant	16.454	2.903	0.000
CA	-0.011	0.005	0.042	CA	0.010	0.002	0.000
Slope	-0.322	0.090	0.000	Slope	-0.025	0.013	0.065
CosA	-0.367	0.116	0.002	CosA	-0.726	0.213	0.001
RI	81.325	43.617	0.000	RI	95.151	12.201	0.000
Depth	1.199	0.669	0.074	RD	0.036	0.027	0.185
TWI	-0.115	0.055	0.035	Depth	0.425	1.164	0.715
LS	-0.012	0.005	0.021	TWI	-0.056	0.042	0.188
Elevation	0.009	0.004	0.000	LS	0.068	0.228	0.767
				Elevation	-0.058	0.011	0.000

* Erosion values are shown as negative elevation change.

Table 3.7: Coefficients of the QR models: Mar. 2015 – Jun. 2015

Erosion model* ($\tau = 0.66$)				**Deposition model** ($\tau = 0.59$)			
$n = 285$	Coefficients	std. error	*P-value*	$n = 302$	Coefficients	std.error	*P-value*
constant	6.454	2.525	0.011	constant	3.098	1.328	0.019
CA	-0.127	0.007	0.000	CA	0.011	0.002	0.000
Slope	-0.356	0.160	0.000	Slope	-0.227	0.085	0.000
CosA	-0.798	0.337	0.019	CosA	-0.142	0.115	0.143
RI	68.499	19.014	0.000	RI	68.773	56.161	0.216
Depth	1.727	0.353	0.001	RD	-0.099	0.022	0.000
TWI	-0.967	0.451	0.033	Depth	0.085	0.081	0.299
LS	1.956	1.018	0.056	TWI	-2.020	0.239	0.000
Elevation	0.085	0.028	0.003	LS	-3.699	0.447	0.000
				Elevation	-0.019	0.007	0.002

* Erosion values are shown as negative elevation change.

Table 3.8: Coefficients of the QR models: Jun. 2015 – Sep. 2015

Erosion model* ($\tau = 0.63$)				**Deposition model** ($\tau = 0.52$)			
$n = 341$	Coefficients	std. error	*P-value*	$n = 169$	Coefficients	std.error	*P-value*
constant	-0.647	2.078	0.755	constant	-1.816	4.472	0.685
CA	-0.011	0.004	0.008	CA	0.015	0.006	0.000
Slope	-0.012	0.007	0.113	Slope	-0.210	0.059	0.000
CosA	-0.124	0.049	0.012	CosA	-0.705	0.091	0.000
RI	88.795	38.530	0.022	RI	17.169	14.803	0.256
Depth	1.409	1.302	0.280	RD	-0.057	0.041	0.162
TWI	-0.039	0.016	0.015	Depth	1.553	1.065	0.147
LS	-0.305	0.027	0.000	TWI	-0.759	0.237	0.002
Elevation	0.004	0.006	0.481	LS	1.565	0.408	0.000
				Elevation	-0.144	0.044	0.000

* Erosion values are shown as negative elevation change.

Table 3.9: Coefficients of the QR models: Sep. 2015 – Dec. 2015

Erosion model* ($\tau = 0.58$)				**Deposition model** ($\tau = 0.66$)			
$n = 290$	Coefficients	std. error	*P-value*	$n = 149$	Coefficients	std.error	*P-value*
constant	-5.791	1.452	0.000	constant	-11.040	4.232	0.010
CA	-0.015	0.002	0.000	CA	0.021	0.003	0.000
Slope	-0.049	0.012	0.000	Slope	-0.017	0.033	0.607
CosA	-0.177	0.102	0.083	CosA	-0.265	0.147	0.073
RI	95.925	26.975	0.000	RI	42.273	40.107	0.300
Depth	0.034	0.014	0.012	RD	-0.009	0.022	0.680
TWI	-0.042	0.083	0.017	Depth	1.553	1.065	0.147
LS	-0.429	0.189	0.022	TWI	-0.092	0.093	0.322
Elevation	0.020	0.006	0.000	LS	0.408	3.910	0.917
				Elevation	0.047	0.018	0.009

* Erosion values are shown as negative elevation change.

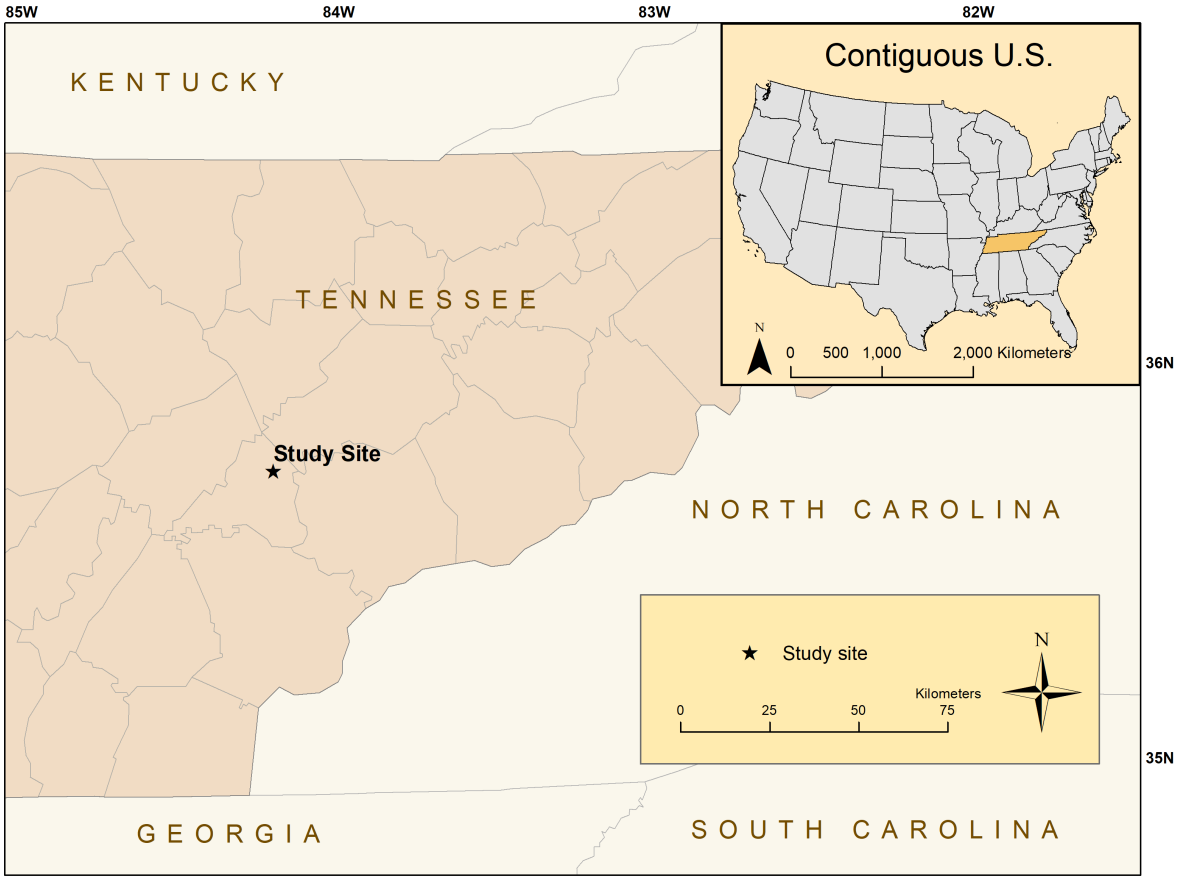

Figure 3.1: Study area of this research

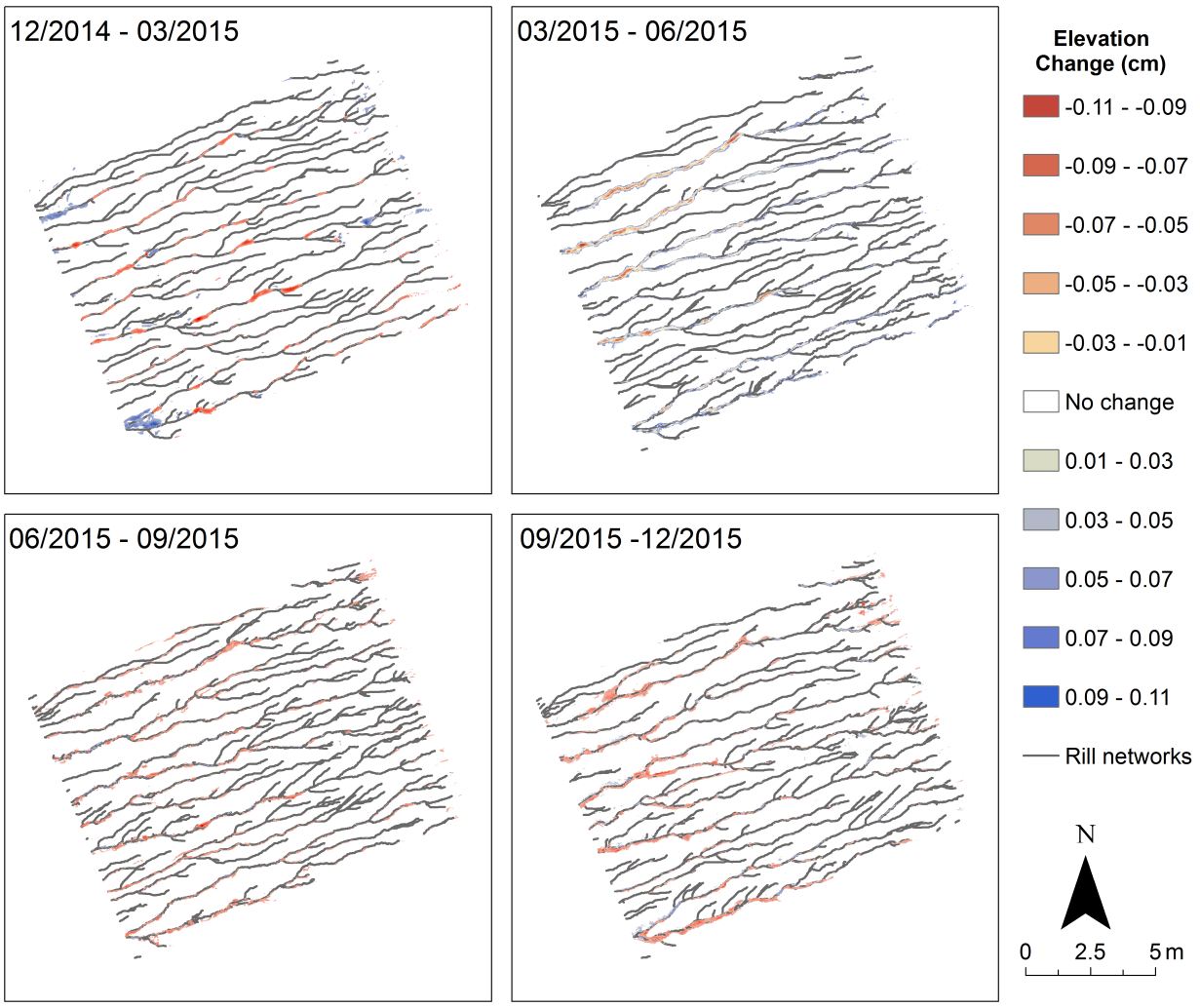

Figure 3.2: the DoD results show the spatial pattern of sediment redistribution in our study area.

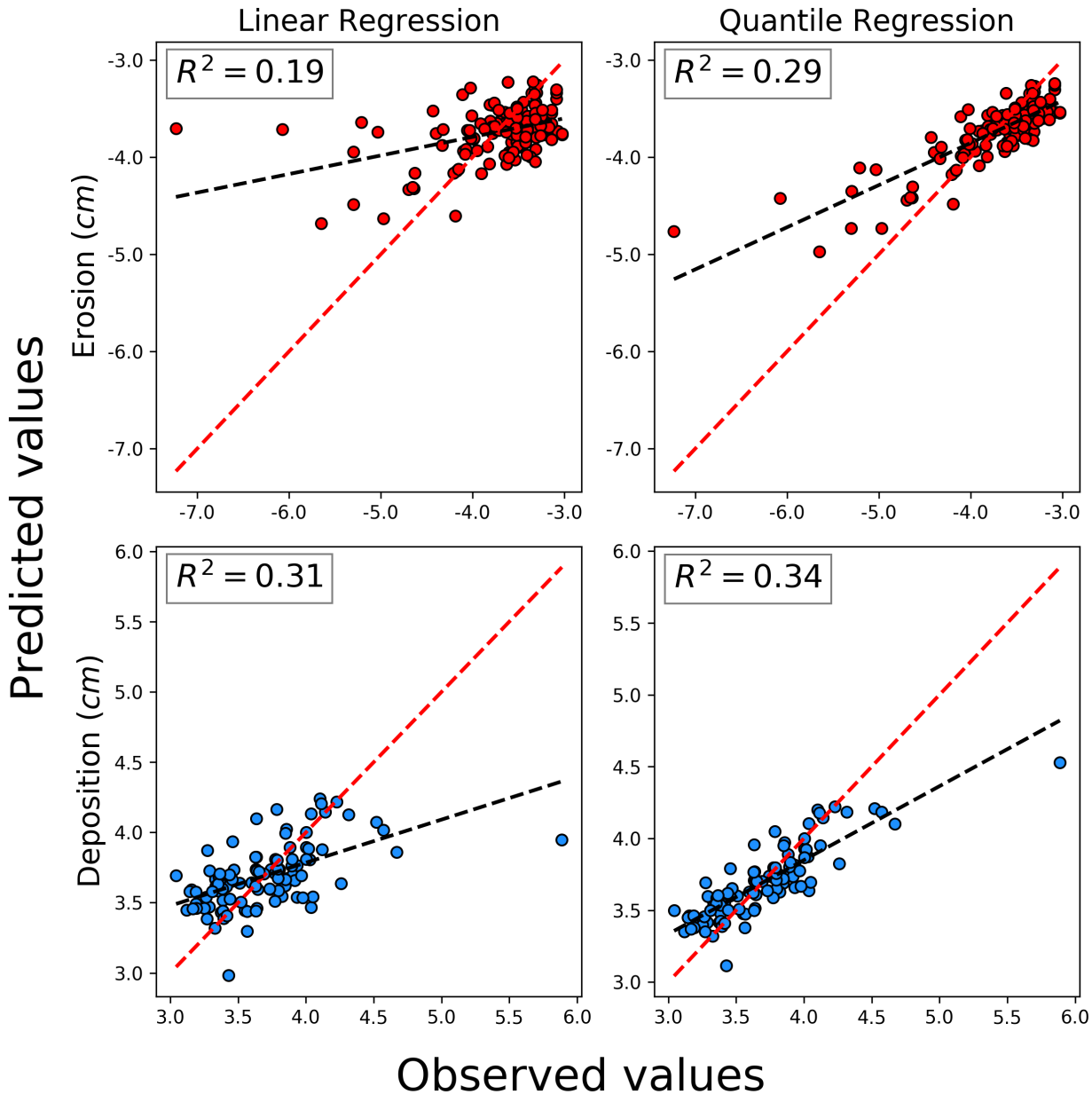

Figure 3.3: Predicted vs. observed erosion and deposition using LR and QR models. The regression between predicted and observed values is shown in black dashed lines; the red dashed line represents $y = x$ (perfect agreement).

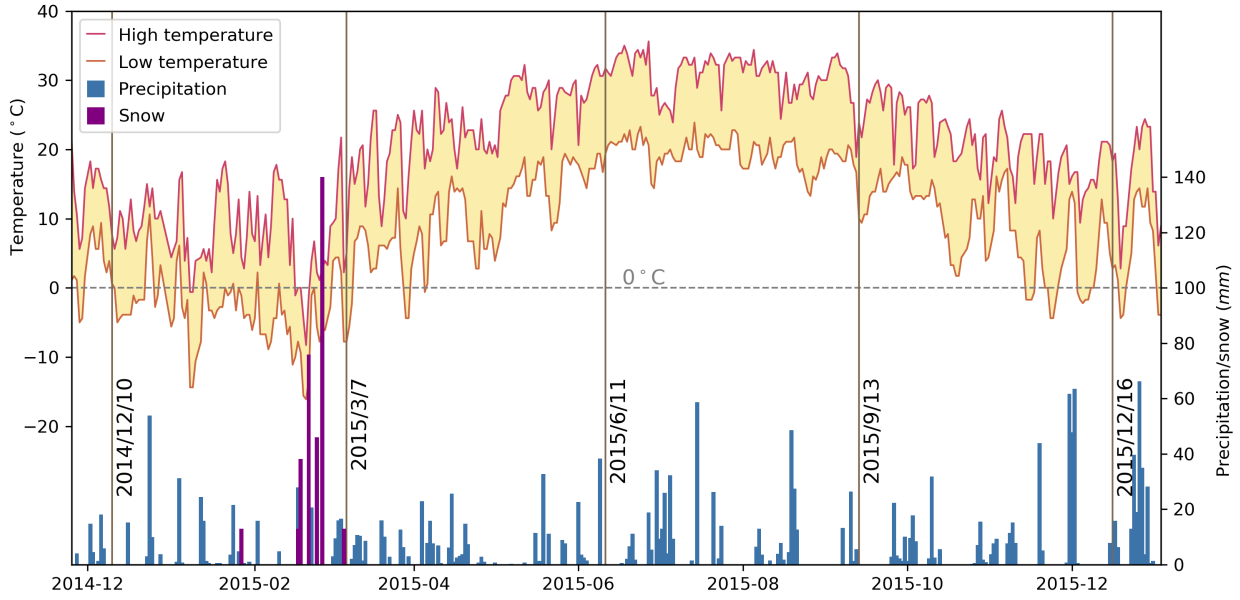

Figure 3.4: The variation of high temperature, low temperature, precipitation, and snow in our study area during the span of this research. The data is obtained from U.S. climate data (http://www.usclimatedata.com/climate/lenoir-city/tennessee/united-states/ustn0284). Vertical brown lines represent five days on which the field surveys were undertaken.

(a) surface armoring with pebbles covering the floor of a rill **(b)** surface crusting in the interrill areas

Figure 3.5: Field photos

Chapter 4

Structural and sedimentological connectivity on a rilled hillslope

This chapter is a manuscript that is prepared for *Science of the Total Environment*. The use of "we" in this chapter refers to all co-authors to be on the manuscript to be submitted. My primary contribution to this work include (i) forming the research idea; (ii) collecting, processing, and analyzing the data; (iii) gathering and organizing the literature; (iv) producing the necessary tables and figures; (v) writing the manuscript.

Abstract

Sedimentological connectivity within channels is governed by the balance between the sediment load and the transport capacity of the flow. Such balance is influenced by the longitudinal (dis)continuity of the channels associated with local depressions and channel confluences. Most studies have focused on the (de)coupling of structural and sedimentological connectivity on a basin scale, with only few examining this phenomenon on a hillslope. Important questions are yet to be asked, including how barriers and confluence affect the flow/sediment balance, and the spatial extent at which these influences take place. This study investigates the relationship between structural and sedimentological connectivity within a rill network on a hillslope in Loudon, Tennessee. We used a time-series of digital elevation models (DEMs) to quantify the temporal erosion/deposition on the hillslope from December 2014 to December 2016, and rill basins were segmented at an interval of 0.05 m to summarize the changes along the profile. Our results show that both longitudinal erosion and deposition exhibit an exponential trend along the profile. The magnitude of the erosion is dominant on the hillslope with a higher coefficient (2.86) than that of the deposition (2.06). The rill length accounts for 46% of the variability for erosion and 24% for deposition. The depressions are correlated with higher erosion at approximately $\sim$ 10 cm at the downslope direction. The correlations between the erosion and the confluence are significant from approximately 20 cm upslope through 25 cm downslope with the peak at 5 cm. The correlation between the deposition and the depression is significant from 20 cm to 5 cm upstream with the peak at 10 cm. These results reveal various spatial extents of events that compromise the structural connectivity and how it influences the sedimentological connectivity.

4.1 Introduction

Channels are critical venues to transport eroded sediments across different landscapes. One measure for the efficiency of sediment transport is the sediment delivery ratio, the proportion of sediment reaching the basin outlet to the total amount of sediment eroded. This ratio is often less than one as the capacity of the sediment transport is influenced by various geomorphological, environmental, and biological factors (Croke and Hairsine, 2006; Ferro and Minacapilli, 1995; Fryirs, 2013; Richards, 2002; Walling, 1983). The sediment delivery ratio is also conceptualized as the sedimentological connectivity to denote how efficient sediment can travel between different compartments of the landscape (Fryirs, 2013; Wester et al., 2014). Originally introduced by Chorley and Kennedy (1971), connectivity describes how material and energy travel across different components of a system. This concept has been extended to describe the within-basin sediment transport and the physical linkage between compartments of landform units (Brierley et al., 2006; Fryirs et al., 2007; Wester et al., 2014). Fryirs (2013) proposed three types of connectivity, including the longitudinal, lateral, and vertical linkages, based on the spatial context of various processes including hillslope reworking/development, channel incision/expansion, and slope denudation and erosion via mass movement, creep, wash, etc. The longitudinal connectivity examines the linkage along an upstream-downstream direction, the lateral connectivity describes the relationship between the slope/channels networks/floodplains, and the vertical connectivity characterizes the interactions between surface and subsurface components.

Previous research has extensively examined the relationship between the topographic/ structural connectivity and the sedimentological/functional connectivity that has been characterized based on different geomorphic behaviors, environmental responses, and geomorphometric characteristics (Brierley and Fryirs, 2013; Cavalli et al., 2013; Cohen et al., 2008; Fryirs, 2013; Harvey, 2001; Ijjasz-Vasquez and Bras, 1995; Montgomery, 1994; Tarolli and Dalla Fontana, 2009; Wethered et al., 2015). The structural (dis)connectivity takes two forms: the depressions (broken linkage) and the confluence of channels (merged linkage). The depressions are formed either by natural processes (e.g. karst processes) or artificial

barriers (e.g. check dams). Once the precipitation rate exceeds the infiltration rate, the surface runoff accumulates within such depressions, and can only escape through evaporation, infiltration, or overspill. Ponding in such depressions dissipates the impact of raindrops and reduces the flow velocity, leading to increased deposition if the transport capacity is exceeded by the sediment load. The confluences are junctions where different channels merge together. The flow dynamics and mixing at these junctions are complicated with spatially varied factors on sediment routing (Best, 1988; Boyer et al., 2006; De Serres et al., 1999). The sediment movement and the distribution of shear layer at the confluences are mainly governed by the momentum ratio between confluence flows, the confluence angles, and bed morphology (Rhoads and Sukhodolov, 2001; Sukhodolov and Rhoads, 2001). Research has shown that the discordance of channel bed at the confluence tend to increase the vertical mixing within the channel, and therefore the location of confluence is likely to experience massive scouring that is able to create increased channel depth (Biron et al., 2004; Ullah et al., 2015). The implications of confluences on structural connectivity is usually reflected in changes in network geometry and the channel cross-sections (Benda et al., 2003; Grant and Swanson, 1995; Wohl and Pearthree, 1991).

At a basin scale, the connectivity is conceptualized as the linkage between different components including hillslopes, fluvial channels, and valleys. The (dis)connectivity — or sediment delivery ratio — between hillslopes and valleys are controlled by the slope gradient, slope convexity/concavity, bed material, vegetation, and other factors (Brierley et al., 2006; de Vente and Poesen, 2005; de Vente et al., 2007; Ferro and Minacapilli, 1995; Walling, 1983). The sediment movement on the hillslope is driven by weathering, mass wasting, and erosion (Selby, 1982), while the sediment transport from hillslopes to channels are often constrained by the lateral linkage (Fryirs, 2013) which is governed by the stability of hillslopes (e.g. landslide) and episodic flooding events (floodplain inundation). The spatially varied particle size along a hillslope-valley gradient also imposes influence on the transfer of sediment (Tarolli and Dalla Fontana, 2009; Tucker and Bras, 1998).

At the hillslope scale, the general trend of sediment movement varies regarding different length of the rill channel. Such relationship is driven by the increased flow power as

more runoff becomes concentrated at downslope direction (Auzet et al., 1995; Foster and Lane, 1983). It is generally accepted that the longitudinal connectivity within a hillslope is governed by the shape of the catchment, drainage pattern, drainage density, channel geometry, and the existence of barriers (Brierley et al., 2006). The connectivity within hillslopes is likely to change over space and time at different stages of rill formation and development (Darboux et al., 2002; Darboux and Huang, 2005; Gessesse et al., 2010). Researchers have established some quantitative relationships between rill length and erosion volume; one widely accepted model is a power relationship between the rill length and the eroded volume ($V = aL^b$, where L is the length of the rill, and a and b are both coefficients (Di Stefano et al., 2017). The relationship between the flow power and erosion is further complicated by factors, including variations of rainfall duration and intensity, bed material, particle size, vegetation, and micro-topography (Eitel et al., 2011; Knapen et al., 2007a,b; McCarroll and Nesje, 1996; Richards, 1973; Römkens and Wang, 1986). The presence of rock fragments, grass strips, walls, and terraces have further influences on the coupling of structural and sedimentological connectivity. Over time, rills on steep hillslope connect to a network that exhibits paralleled patterns of higher spacing at lower slopes, forming master rills (Horton, 1945; Knighton, 1998; Selby, 1982). The connected structures of the rill network increase the transport capacity and facilitate the surface runoff concentration. As the rills get deeper and wider at lower slopes, the magnitude of erosion increases. Some master rills may eventually connect to larger channels including gullies or ephemeral streams (Haan et al., 1994; Ritter et al., 2011).

The hillslopes are a major source of sediment influx contributing to the fluvial system, and in-depth research on the structural and sedimentological connectivity is necessary to strengthen our understanding in sediment routing and erosion control (Detty and McGuire, 2010). Recently, there has been an increased interest in studying the longitudinal (dis)connectivity within a hillslope (Bracken and Croke, 2007; Kirkby and Bracken, 2009; Lesschen et al., 2009; Penuela Fernandez et al., 2014; Wester et al., 2014). Wester et al. (2014) investigated the post-wildfire hillslopes in California and concluded that erosional events are dominant when the contributing area is less than 10 m^2, but such phenomenon

is also influenced by different durations and intensity of rainfall and whether the erosion occurred in rills or interrill areas.

Research has shown that the (de)coupling of structural and sediment connectivity is subjective to spatial and temporal scales (de Vente and Poesen, 2005; Fryirs et al., 2007; López-Vicente et al., 2015; Masselink et al., 2016; Nardi and Rinaldi, 2015). The existing literatures exhibited stronger interest in the connectivity at a basin scale with an emphasis on hillslope-valley coupling (Brunton and Bryan, 2000; Harvey, 2001; Michaelides and Wainwright, 2002; Tarolli and Dalla Fontana, 2009), whereas the connectivity within the hillslopes (upslope-downslope and interrill-rill) is still not well understood. Important questions need to be addressed to improve our understanding in the influences of local barriers/depressions on the flow/sediment properties, such as when and where such influences exist and to what extent these influences take place. This research aims to examine the structural and sedimentological connectivity within rills and attempts to reveal the relationship between the local depressions, rill confluence, and sedimentological connectivity by examining the following questions:

(1) Do the depressions influence the erosion/deposition positively or negatively?

(2) Do the confluences affect the erosion/deposition positively or negatively?

(3) What is the spatial extent of such influences?

4.2 Study area

This research focuses on an engineered, vegetation-free hillslope in Loudon County, Tennessee, United States (35°37'32.52"N, 84°12'59.69"W, Fig. 4.1). The climate of this region is categorized as Cfa (Humid Subtropical) in the Köppen climate Classification that is featured with hot summers and moderate winters, and precipitation is abundant throughout the year. The annual mean temperature is approximately 15 °C and the annual total precipitation is about 1300 mm. The region is currently occupied by agricultural lands, grassland, and successional forests mainly composed of mesophytic species. The intense and

frequent rainfall events, the steep topography in the region, and the human activities such as agriculture and mining, created a scenario that makes the hillslope susceptible to water-induced soil erosion (Harden and Mathews, 2000; Leigh and Webb, 2006; Luffman et al., 2015; Matmon et al., 2003; Nandi and Luffman, 2012; Turnage et al., 1997).

Our studied hillslope is situated on the terrace of the Little Tennessee River, which originates from the Blue Ridge Province of the southern Appalachian Mountains (Delcourt et al., 1986). The parent material of the site is shale that has developed into silty and clayey Ultisols, vulnerable to rilling and gullying (Luffman et al., 2015; Nandi and Luffman, 2012). Historical images of Google Earth reveal that the hillslope was formed with all vegetation removed during the construction of the Christenson Yacht facility sometime in 2007. Although bluestem grass (*Schizachyrium scoparium*) was planted at some locations within the property to control erosion and sediment delivery, the slope of interest was free from vegetation and erosion created rill networks on the hillslope surface. The slope extends about 20m from the top to the bottom with the altitude ranging between approximately 263 m and 255 m a.s.l., and the overall slope gradient is approximately 27°. This study focuses on a vegetation-free section of the slope, and the dimension of the section is about 20 m by 20 m. We did not set up any physical boundaries (e.g. earthen berms or metal sheets), therefore, the hydrology at the site was not disturbed, and the erodible material within the section is likely to be non-exhaustive with sediment feeding into the system from areas above the slope. Such properties make this section of the slope suitable for long-term monitoring and observation of the sediment dynamics (Boix-Fayos et al., 2006).

4.3 Methods

To address the research questions, this research adopted the following workflow (Fig. 4.2):

a. Data collection and pre-processing: to obtain the temporal elevation data in the study area, remove the outliers, and geo-reference raw data;

b. Data processing: to convert the data to raster format, perform error propagation and change detection, and create spatial series of indices denoting the structural and sedimentological connectivity;

c. Data analyses: to extract the signal and the noise from the spatial series, and examine the relationship between the processed series.

4.3.1 Data collection

A total number of 7 field surveys were conducted on 7 different days between December 10th, 2014 and December 14th, 2016, respectively. When choosing the dates for the survey, we only selected days with clear weather condition and no prior precipitation in the past 2 days. We used a FARO Focus3D X330 Laser Scanner to survey our study site. This scanner unit emits shortwave infrared laser (wavelength 1550 nm) and is able to survey the surrounding environment at 360° horizontal and 307° vertical view at a radius of 330 m. The ranging accuracy of the scanner is approximately ± 2 mm at 50 m distance using laser pulses that are emitted at up to 976000 pulses/second. For this scanner unit, the size of a single laser spot is 2.25 mm at the exit, and the beam diverges at 0.19 mrad (0.011°) as it gets further away. The distance between the scanner unit and the intercepting slope surface ranges approximately from 10 m to 20 m in our case, and the size of the laser spot ranges between 4.15 mm and 6.05 mm using the calculation method detailed in Pesci et al. (2011). We started each survey with a panoramic scan (360° horizontal by 307° vertical) at a relatively coarse resolution (a point spacing of about 5 cm at 50 m radius) followed by at 3 – 5 subsequent finer resolution scans that were performed with a point spacing of about 1 cm at 50 m. The scans were conducted at different angles to prevent possible occlusions due to rugged terrain surface. We tried to occupy the same scan locations for surveys on different dates to achieve comparable geometry between surveys, as suggested by Lague et al. (2013).

We used the reference target spheres (diameter of 139 mm) produced by the ATS Scan Reference System for within-survey registration. We placed the target spheres around the slope prior to each survey at locations that are of good visibility, and tried to have the targets

placed as uniform as possible without disturbing the slope surface. Out of concerns about vandalism or theft, no targets were permanently installed at the study site. During the survey, the scanner is mounted on an elevator tripod at approximately 2 m above ground, with dual-axis compensation function activated. We used a Trimble GeoExplorer 6000 Series GeoXH^{TM} handheld differential GPS (dGPS) to store the locations of the scanner and the reference targets. The augmentation function of this dGPS unit allows for a real-time correction of the coordinates based on the satellite signals. The GPS base station closest to our study site is at the McGhee Tyson Air National Guard Base (35.81°N, 84.00°W) approximately 28 km away. Once updated through the satellite network, the dGPS can yield a horizontal accuracy of 10 cm ± 2 parts per million (ppm) and a vertical accuracy of 20 cm ± 2 ppm. The coordinates collected may not be accurate enough for geo-referencing but are useful in placing the scans coarsely in their relatively same location at each survey period. The procedures for intra-survey registration and between-survey geo-referencing are further detailed in the next section.

4.3.2 Data pre-precessing

We used the FARO SCENE^{TM} for the intra-survey registration and between-survey geo-referencing. The intra-survey registration was performed using a target-based method; the SCENE software is able to extract the spherical targets in each scan, and use an Iterative Closest Point algorithm (Chetverikov et al., 2002) to align the scans within the same survey. The minimal root mean squared error (RMSE) between any two scans are calculated using the three-dimensional data (x, y, and z) on a point-to-point basis to evaluate the quality of the registration/geo-referencing. The workflow of pre-processing typically starts with intra-survey registration. The panoramic scan at a coarser resolution was treated as the reference scan based on which other scans within the same survey were aligned. Based on the target spheres the RMSE is calculated, and the software would use the Iterative Closest Point algorithm to re-align the scans until a minimal RMSE is achieved. Once the minimal RMSE for all scans within the same survey is achieved, the scans are now managed as a cluster and

any further transformations would only be performed on the cluster without affecting the relative positions of scans within the cluster.

The between-survey geo-referencing was performed in FARO SCENE^{TM} using manual registration in the corresponding view based on permanent features in the scans that share regular geometry, such as the walls of the yacht facility. When geo-referencing the between-survey scans, the first survey (Dec. 10th 2014) was used as the reference scan based on which the locations of the other surveys were transformed to. The summary statistics of the 7 surveys and the registration results are shown in Table 4.1. After the registration, the 7 surveys are exported as 7 separate files which store the three-dimensional location information (x, y, and z) of all the points. Each point cloud file is then converted to a raster DEM of 1 cm spatial resolution in Quick Terrain Modeler. A bilinear algorithm was used to interpolate the points and the final DEMs are projected to a local Cartesian projection, a projection commonly used for large-scale mapping (Kennedy and Kopp, 2002). The local Cartesian projection does not account for the curvature of the earth, but the distortion introduced by this projection is negligible since our study area is small.

4.3.3 Change calculation

We investigated the geomorphic changes between 7 field surveys using the DEM of Difference (DoD) method. The DoD method is designed for geomorphic change detection and is capable of mapping, detecting, and quantifying the erosion and deposition between temporal DEMs collected over the same study area. The DoD method uses the two temporal DEMs as input and calculates the difference on a pixel-to-pixel basis. The output of DoD is a raster with the value of each pixel representing the elevation change at the location — positive values suggest deposition and negative values suggest erosion. The geomorphic change between any two DEMs is calculated as:

$$\Delta DEM = DEM_{t_1} - DEM_{t_0} + \varepsilon \tag{4.1}$$

where the DEM_{t_0} and DEM_{t_1} denote DEMs collected at time t_0 (prior survey) and the t_1 (subsequent survey), respectively; ε is the error, which is a propagation of uncertainties of various sources, including the error associated with the scanner unit, the within-survey registration, and between-survey geo-reference. We performed 6 DoD analyses between the 7 temporal DEMs using the Fuzzy Inference System-based error propagation in the Geomorphic Change Detection (GCD) tool. The method and the GCD tool are further detailed in Wheaton et al. (2010). In this paper, we only considered the elevation changes that are significant at the $p < 0.05$ level. The output of the DoD was a raster file that allows for the estimation of the net volume of sediment change:

$$V_{net} = A \times \sum_{i=1}^{N} \Delta Z_i \tag{4.2}$$

where V_{net} is the net volume of sediment change, A is the pixel size, N is the total number of pixels, and ΔZ_i is the change in elevation for pixel i. The volume of erosion or deposition can be quantified separately using equation 4.2 by only considering negative/positive values in the output DEM.

4.3.4 Rill networks delineation

The rill networks within our study area were delineated in the TauDEM plug-in in ArcGIS (Tarboton, 2001). The minimal number of pixels that allow for the initiation of the channel was determined using the Drop Analysis method (Broscoe, 1959). This method is based upon the assumption that the mean stream drop, or the range of elevation between the starting and the ending nodes of stream segments of the same Strahler order should not be statistically different from those of other orders. The input for the Drop Analysis method includes a DEM and a list of integers denoting different numbers of pixels that allow for the initiation of streams. For each number in the list, the algorithm delineates the rill network based on the Deterministic-8 method, a method that calculates the flow direction for each pixel based on the steepest slope within the nearest 8 neighboring pixels (Tarboton et al., 1992). This method allows for an objective approach of channel delineation that also accounts

for site-specific information. Initially proposed for the delineation of the fluvial channels, this method has also been used in recent research to delineate hillslope channels including rills and gullies; results showed that this method produces output that is in agreement with morphology-based methods (Lu et al., 2017; Vinci et al., 2015).

4.3.5 Structural and functional connectivity

To quantify the structural and the sedimentological connectivity, the choice of the areal units is critical to capture the longitudinal variations. Wester et al. (2014) used a series of rectangles with identical geometry (25 m by 0.05 m) that are perpendicular to the rill/gullies to track the along-channel changes of sedimentological connectivity. This approach has several limitations (Fig. 4.3a). First, the size of the rectangles is universal and arbitrarily defined, but this might create rectangles whose width is too small to capture the change along the transact, or too large to go beyond the drainage divide. Second, overlap and gap between adjacent rectangles would occur where the channel bends. Last, the width of the rills varies over space (Govindaraju and Kavvas, 1992; Torri et al., 2006), and a universal width imposed upon the entire longitudinal direction of the rills may not always be appropriate. All three limitations are difficult to address and tend to create unintended errors of omission and commission that should not be ignored.

Brierley and Fryirs (2013) proposed a method to segment river channels into homogeneous reaches of varying lengths. This method is by definition a point-sampling method that requires the researcher to possess *a priori* expert knowledge regarding the site, since the locations of segmentation have to be representative (Brierley and Fryirs, 2013; Nardi and Rinaldi, 2015). This model does not take into account the changes at the interfluve (Fig. 4.3b). Conceptualized initially to study connectivity within fluvial channels, this method might not be as for hillslope channels, since the flow in hillslope channels is ephemeral and episodic, and going through rapid changes. Also, for a paralleled drainage pattern such as the networks of rills on steep hillslopes, each individual rill may or may not share comparable characteristics, and identification and segmentation based on each individual rill would be challenging and labor intensive.

We employed a method that uses "sub-watersheds" (Fig.4.3c) to summarize the erosion and deposition along the rills. The "sub-watersheds" are non-overlapping polygons created at 0.05 m intervals along the channel with all pixels in the same polygon contributing to the same outlet. These polygons are of various shapes and widths, but a fixed interval guarantees a uniform sampling distance along the rill basin. For the rill networks in each rill basin, the "sub-watersheds" of the longest rill are delineated. The Arc Hydro Tools package (Maidment, 2002) was used to create the polygons in ArcGIS. We only included the longest rills for each network because the inclusion of these secondary rills would bring noise to our longitudinal sequence. For examples, the locations where secondary rills join the major rill may vary and the secondary rills may have varied contributing area, flow property, and/or sediment load. We did not include polygons that intersect with the boundary of our study site to minimize the impact of the edge effect. For the structural connectivity analysis, we used the number of depression pixels (sometimes also referred to as "sinks") and confluences as indicators. The depression pixels are ones that have the lowest elevation among its 8 neighboring cells (local depressions within the DEMs); the confluences are the locations where two separate rill channels join. The percent of pixels that are identified as depressions and the number of nodes where rill segments merge within each polygon were used as the indicator for structural connectivity, and the sedimentological connectivity is represented by the results of DoD. The total upland sediment yield at each location was also calculated as the cumulative deposition and erosion toward the downslope direction.

To examine the relationships between our 4 series (erosion, deposition, depression, and confluence), it is necessary to remove the trends — the overall tendency of the data domain, while keeping the inherent variability of the data (Wu et al., 2007). In most cases, the trend can be represented using an intrinsically-fitted monotonic function. We decomposed the 4 series (erosion, deposition, depressions, and confluence) using the Empirical Mode Decomposition (EMD) method. The EMD extracts different frequencies from the data by repeatedly removing cubic splines of descending frequencies using local extrema through a sifting process. The sifting process only stops when the data series are symmetric regarding zero mean, and the residuals become a monotonic function. The EMD is capable of decomposing the trends into different intrinsic mode functions that are oscillatory functions

that exhibit amplitude and frequency modulations, and is able to adapt to nonlinear, non-stationary data, and the user does not have to define the function form of the trend (Flandrin et al., 2005; Huang et al., 2003; Wu et al., 2007). Another advantage of the EMD is that it does not require any pre-defined wavelet basis, and thus would avoid possible spurious harmonics. A more detailed description of the EMD can be found at Huang et al. (1999, 2003).

Once the 4 series (erosion, deposition, depressions, and confluence) were de-trended, we used the Cross-Correlation Function (CCF) to examine the relationship between the structural connectivity and sedimentological connectivity. The CCF requires that the input series are evenly spaced and share the same length, and is based on the assumption that both series have stationarity, *i.e.* constant mean and variance over time. Originally developed for the analyses of time-series data or the signals, the CCF measures the similarity between two time-series at the same or different times, and it also measures how well one series can be used to explain the other series (Scargle, 1989). The CCF between two series of interest $X(t)$ and $Y(t)$ is calculated as the expectation of the product of the values of X and Y observed at different times separated by the lag l:

$$C_{XY}(l) = \frac{1}{n} \sum_{t=1}^{n-l} x_t y_{t+l} \tag{4.3}$$

where n is the number of consecutive observations of both series (Shumway and Stoffer, 2017). For any value of l, the sample correlation coefficient C_{XY} will be calculated and compared to the 95% significance limits $\pm\ l$, where $l = 1.96/\sqrt{n}$.

4.3.6 Change in channel geometry

We sampled 9 cross-sections along one of the longest rills in the rill network to examine the change of channel cross-section over time (Fig. 4.4). The locations of the cross-sections were manually picked so they are relatively evenly spaced from one another. The profile analyses tool in ArcMap 10.5 was used to extract the elevation information along the profiles.

By comparing the elevation change between two survey dates, we can detect the most sedimentologically active areas along the cross-section, and determine if the channel has been widening or deepening. These changes affect the shear stress of the concentrated flow (τ), by affecting the shape of the cross-sections and the channel slope. The shear stress is calculated as:

$$\tau = \gamma RS \tag{4.4}$$

where γ is the unit weight of water; R is the hydraulic radius; and S is the slope of the channel. The hydraulic radius R is equal to A/P, where A is the cross-sectional area and P is the wetted perimeter.

4.4 Results

4.4.1 Sediment change over time

The DoD results showing the change of sediment in our study area over time are presented in Table 4.2. Our study area underwent more erosion compared to deposition during all 6 periods. The first period (December 2014 – March 2015) had the lowest amount of erosion ($0.18 \pm 0.07\ m^3$). The last two periods (December 2015 – May 2016 and May 2016 – December 2016) both showed a high volume of erosion ($0.53 \pm 0.17\ m^3$ and $0.55 \pm 0.16\ m^3$), as well as the highest volume of net sediment loss ($0.55 \pm 0.20\ m^3$ and $0.55 \pm 0.16\ m^3$). This is possibly due to longer intervals between the scan dates. The first period (December 2014 – March 2015) also witnessed the highest amount of deposition ($0.07 \pm 0.03\ m^3$).

4.4.2 Structural and sedimentological connectivity

Fig. 4.5 shows the structural connectivity (represented by the percent of area that are depressions and the number of confluences) as well as the sedimentological connectivity (erosion and deposition) along the flow paths (rills). The rate of increase for the erosion

is dominantly higher than that of the deposition. The magnitude of both the erosion and deposition tends to increase further down the drainage basin. Approximately 85% of the total sediment loss occurred at the lower 50% of the rills. Generally, depression pixels account for less than 5% of each individual rill basin segment, and there is no apparent trend regarding how depressions and confluence points change along the rills over space.

4.4.3 Sediment dynamics along the profile

The volume of erosion and deposition increases along the profile, and the increasing rates also tend to increase as rills get further down the slope (Fig. 4.5). The log-transformed erosion and deposition values both increase along the distance downslope (Fig. 4.6). However, the coefficient of the erosion function (2.86) is greater than that of the deposition (2.06). The magnitude of erosion increases faster compared to that of deposition as getting closer to the lower end of the rills. The R^2 value of erosion (0.46) is also greater than that of the deposition (0.24). This is possibly due to the differences in the driving mechanisms between erosion and deposition; erosion in the rills are more related to the growing erosive power of the concentrated flow (directly related to the rill length as a power function), while deposition is more driven by local micro-topographic factors including slope and roughness (Giménez and Govers, 2001; Govers, 1992; Govers et al., 2000; Haan et al., 1994; Nearing et al., 1997; Sankey et al., 2010).

We decomposed the erosion, deposition, depressions, and confluence series using the EMD method. Here we only kept the residuals for the cross-correlation analyses. The residuals of erosion, deposition, depressions, and confluence are plotted in Fig. 4.7, and exhibit the overall stationarity along the rill profile.

The results of the cross-correlation function are shown in Fig. 4.8. The cross-correlation function calculates the correlation coefficient at different lags (1 lag = 0.05 m), and we used the 0.95 confidence level to highlight the most significant coefficients in the results of the CCF. The correlations between erosion and depression are mostly insignificant, except the correlation at lag = 2 that is barely above the significance level, suggesting that the

existence of depressions is likely correlated with higher erosion at approximately 10 cm at the downslope direction. The correlations between the erosion and confluence are statistically significant between lag -4 and lag 5. The correlation increases from the lag of -4 and becomes the highest at 1, and then tapers until becoming not significant at the lag of 6. This suggests that the confluence of rills are positively related to higher erosion from 20 cm above to 25 cm below the confluence point. The correlation between deposition and the depressions is significant between lag of -4 and -1, with the peak occurring at lag = -2, indicating positive relationships between deposition and depressions with the greatest at approximately 10 cm above the depression location. The correlation between the deposition and confluence is not significant.

4.4.4 Cross-section analyses

Fig. 4.9 shows the changes to the geometry of the 9 cross-sections over time. It can be observed that rills get deeper and wider as it gets further downslope. The steepness of the rill sidewalls is lower when the cross-section is either close to the top (cross-section 1 – 3) or the foot of the slope (cross-section 6 – 9); whereas in the middle of the slope, the sidewalls are relatively steeper (cross-section 4 – 5). This is possibly a manifestation of cross section changes at different stages of rill incision. Where it is closer to the top of the hillslope, the concentrated flow power is rather limited and rills are relatively shallow; as moving further down the hillslope, the flow power gets stronger and the scouring on the rill floor becomes more pronounced. Once the rills become deep enough, the scouring of the rill bottoms is challenged as the floors eventually reach a non-erodible layer (in our case the shale). Instead, the rills develop horizontally by eroding the sidewalls. The failure of the sidewalls provides sediment supply into the rills and sometimes causes temporary depositions, and this process leads to wider rill cross-sections.

4.5 Discussion

4.5.1 Difference in mechanisms of erosion and deposition

The sediment dynamics leading to the changes on hillslopes are mainly driven by the rainstorms. Once the rills and gullies start to form on the hillslopes, the surface runoff gets concentrated and the flow power becomes the dominant driving force of erosion. The geometry of the channels, including the planar geometry (the structure of the rill networks) and the profile geometry (including concavity/convexity, cross-section shapes and areas) becomes relevant when the connectivity of such channels is directly associated with the transport capacity of the mixture of runoff and sediment. It was generally accepted that the erosion associated with concentrated flow is a governed by a threshold effect, that erosion only occurs when one of the variables including flow shear stress (τ), stream power (ω), or discharge (Q) exceeds certain critical values (Giménez and Govers, 2001; Govers, 1987; Knapen et al., 2007b; Line and Meyer, 1989). Govers (1992) found that the relationship between the flow velocity and the discharge can be predicted by the flow areas, while soil texture or slope gradient has limited influence over the flow characteristics. Our results show that the rill length accounts for 46% of the variability associated with log-transformed erosion (Fig. 4.6), suggesting a strong influence of the concentrated flow power on the magnitude of erosion.

Deposition occurs when the sediment load exceeds the transport capacity. On rilled hillslopes, deposition is found to be negatively correlated with the slope gradient and surface roughness (Brenneman and Laflen, 1982; Cochrane and Flanagan, 2006; Haan et al., 1994). In our study site, the deposition also increases exponentially with the distance downslope; as we get closer to the foot of the hillslope, rill floors are generally wider and we have more roughness created by the pebbles left within channel due to the long-term sorting process. However, the relationship between rill length and deposition is not as pronounced as that between rill length and erosion (Fig. 4.6). This may be a combined effect of wider channel cross-sections, lower slopes, and local bed roughness. Higher roughness is able to dissipate

the flow power and reduce the transport capacity; the higher roughness also introduces local depressions that will facilitate more settling of the particles.

4.5.2 Channel geometry change

The location of the thalweg of the rill network is determined by micro-topography variations, especially when the surface roughness is altered (Gessesse et al., 2010). The first period experienced the lowest volume of net sediment loss, with an average elevation change of -2.2 cm; the last period underwent the highest volume of net sediment loss with an average elevation change of -4.1 cm. The rill underwent both erosion and deposition at different times and different locations. Over time, the cross sections tend to grow deeper due to erosion mainly at the bottom of the rill. The rill cross-sections have yet to become stable by the end of our field survey. The rills in the study site have developed for more than 7 years on the slope, and are sometimes as deep as 30 cm. Nevertheless, these rills keep incising, creating larger cross-sectional areas which are capable of transporting a great amount of flow and sediments. Aside from rill floor incisions (such as profile 4 – 6 during the 1st period and profile 3 during the 2nd period), rill sidewall sloughing also occurred at certain cross-sections, especially the profile 4 through 8 during the 5th period. Such sloughing is most likely to occur when the sidewalls become steep. For example, profile 5 during the 5th period underwent intense sidewall sloughing with increased amount of sediment feeding into the rill segments. Before the sloughing, the sidewalls of the rills were relatively steep, and the failure events created a more stable geometry. Deposition also occurs in the rills, and the majority of the depositions occur at the bottom of the rills (e.g. profile 1 and 2 during the 6th period). Possible sources of such sediment supply include sidewall failures (e.g. profile 9 during the 5th period), and incoming sediment flux from upland areas.

In a side-wall failure event, a large amount of sediment is detached off the sidewall and feeds into the rills. In such cases, the cross-sectional area (A) will remain unchanged (assuming no sediment exchange on the upstream-downstream direction), while the wetted perimeter (P) will be larger because the rill width has increased, leading to a smaller hydraulic radius (R) and thus a smaller shear stress (τ). However, the rills keep expanding

in our study area, since the rills keep transporting the detached sediment throughout the networks, the A will increase as erosion occurs on rill sidewalls and floors. This is observed as long-term rill growth in the form of incision. This incision will not cease until reaching a non-erodible layer, which is the shale layer in our case.

4.5.3 Flow connectivity and sediment movement

On rilled hillslopes, the continuity of the flow hydraulics is complicated by the local topographic variations. The depressions act as local storage for the surface runoff during rainstorms. The storage can dissipate the flow energy, and a reduced flow energy will lead to local deposition Once the transport capacity becomes lower than the sediment load. Our results show that depositions are positively related to the depressions at a distance of 5 – 20 cm on the upstream direction. This shows the spatial extent of the depression's influence of the local depositions. The influence of confluences on the rill hydrology is associated with the turbidity created by the interaction of the flows. Rills are usually developed on hillslopes that are steep, and rill flows are shallow with the depth comparable to bed roughness elements. Sometimes, supercritical flow occurs when confluences exist, forming the confluence hydrodynamic zone (Hager, 1989; Kenworthy and Rhoads, 1995), where depth increases by 20 – 30 times and complex turbidity even extends back into the merging channels. Research has observed both rapid, local, as well as protracted mixing and recovery (Kenworthy and Rhoads, 1995; Mosley, 1976). Results in our study supported the conclusions of these studies, and we are also able to identify the spatial extent of the intensification of erosion as a consequence of the merging flows. Further investigation is necessary to understand how local depressions influence the erosion and deposition regarding different geomorphometric information (size, depth, and other properties). Our study did not take into account the secondary, tertiary and other smaller rills that enter the main rill channel. The influence of confluence is likely to differ regarding the location, angle, and flow properties of the merging channels.

4.6 Conclusions

This research investigates the longitudinal sedimentological connectivity and its relationship with the structural connectivity. The depressions within the rills and the confluences of the rills are closely related to the sedimentological connectivity on a rilled hillslope. Both erosion and deposition increase exponentially along the rills, while the coefficient of erosion (2.86) is greater than that of deposition (2.06), suggesting that erosion tends to be dominant over deposition along the rill profile. The rill length accounts for 46% of the variability for erosion and 24% of the variability for deposition. The depressions are positively correlated with erosion in the downslope direction. The correlations between the erosion and confluence are statistically significant in both the upstream and downstream direction with the peak close to the location of the confluence. The correlation between deposition and the depressions are significant in the upstream direction.

Acknowledgements

We would like to thank the Geomorphology Specialty Group of the American Association of Geographers, the Stewart K. McCroskey Memorial Fund, and the Thomas Fellowship for providing financial support for this research. Jack McNelis, Rebecca Potter, Gene Bailey, Martin Walker, Robert Friedrichs, Joseph Robinson, and Yasin Wahid Rabby helped in the field surveys.

References

Auzet, A. V., Boiffin, J., and Ludwig, B. (1995). Concentrated flow erosion in cultivated catchments: influence of soil surface state. *Earth Surface Processes and Landforms*, 20(8):759–767.

Benda, L., Veldhuisen, C., and Black, J. (2003). Debris flows as agents of morphological heterogeneity at low-order confluences, Olympic Mountains, Washington. *Geological society of America bulletin*, 115(9):1110–1121.

Best, J. L. (1988). Sediment transport and bed morphology at river channel confluences. *Sedimentology*, 35(3):481–498.

Biron, P. M., Ramamurthy, A. S., and Han, S. (2004). Three-dimensional numerical modeling of mixing at river confluences. *Journal of Hydraulic Engineering*, 130(3):243–253.

Boix-Fayos, C., Martínez-Mena, M., Arnau-Rosalén, E., Calvo-Cases, A., Castillo, V., and Albaladejo, J. (2006). Measuring soil erosion by field plots: Understanding the sources of variation. *Earth-Science Reviews*, 78(3–4):267–285.

Boyer, C., Roy, A. G., and Best, J. L. (2006). Dynamics of a river channel confluence with discordant beds: Flow turbulence, bed load sediment transport, and bed morphology. *Journal of Geophysical Research: Earth Surface*, 111(4).

Bracken, L. J. and Croke, J. (2007). The concept of hydrological connectivity and its contribution to understanding runoff-dominated geomorphic systems. *Hydrological Processes*, 21(13):1749–1763.

Brenneman, L. G. and Laflen, J. M. (1982). Modeling sediment deposition behind corn residue. *Transactions of the ASAE*, 25(5):1245–1250.

Brierley, G., Fryirs, K., and Jain, V. (2006). Landscape connectivity: the geographic basis of geomorphic applications. *Area*, 38(2):165–174.

Brierley, G. J. and Fryirs, K. A. (2013). *Geomorphology and river management: applications of the river styles framework*. John Wiley & Sons.

Broscoe, A. (1959). Quantitative analysis of longitudinal stream profiles of small watersheds. Technical Report 389-402, U.S. Geological Survey, New York.

Brunton, D. A. and Bryan, R. B. (2000). Rill network development and sediment budgets. *Earth Surface Processes and Landforms*, 25(7):783–800.

Cavalli, M., Trevisani, S., Comiti, F., and Marchi, L. (2013). Geomorphometric assessment of spatial sediment connectivity in small Alpine catchments. *Geomorphology*, 188:31–41.

Chetverikov, D., Svirko, D., Stepanov, D., and Krsek, P. (2002). The trimmed iterative closest point algorithm. In *16th International Conference on Pattern Recognition*, volume 3, pages 545–548, Quebec City, Canada. IEEE.

Chorley, R. J. and Kennedy, B. A. (1971). *Physical geography: a systems approach*. Prentice Hall.

Cochrane, T. A. and Flanagan, D. C. (2006). Sediment deposition in a simulated rill under shallow flow conditions. *Transactions of the ASABE*, 49(4):893–903.

Cohen, S., Willgoose, G., and Hancock, G. (2008). A methodology for calculating the spatial distribution of the area-slope equation and the hypsometric integral within a catchment. *Journal of Geophysical Research: Earth Surface*, 113(3).

Croke, J. C. and Hairsine, P. B. (2006). Sediment delivery in managed forests: a review. *Environmental Reviews*, 14(1):59–87.

Darboux, F., Davy, P., Gascuel-Odoux, C., and Huang, C. (2002). Evolution of soil surface roughness and flowpath connectivity in overland flow experiments. *Catena*, 46(2–3):125–139.

Darboux, F. and Huang, C. (2005). Does soil surface roughness increase or decrease water and particle transfers? *Soil Science Society of America Journal*, 69(3):748–756.

De Serres, B., Roy, A. G., Biron, P. M., and Best, J. L. (1999). Three-dimensional structure of flow at a confluence of river channels with discordant beds. *Geomorphology*, 26(4):313–335.

de Vente, J. and Poesen, J. (2005). Predicting soil erosion and sediment yield at the basin scale: Scale issues and semi-quantitative models. *Earth-Science Reviews*, 71(1–2):95–125.

de Vente, J., Poesen, J., Arabkhedri, M., and Verstraeten, G. (2007). The sediment delivery problem revisited. *Progress in Physical Geography*, 31(2):155–178.

Delcourt, P. A., Delcourt, H. R., Cridlebaugh, P. A., and Chapman, J. (1986). Holocene ethnobotanical and paleoecological record of human impact on vegetation in the Little Tennessee River Valley, Tennessee. *Quaternary Research*, 25(3):330–349.

Detty, J. M. and McGuire, K. J. (2010). Topographic controls on shallow groundwater dynamics: implications of hydrologic connectivity between hillslopes and riparian zones in a till mantled catchment. *Hydrological Processes*, 24(16):2222–2236.

Di Stefano, C., Ferro, V., Palmeri, V., and Pampalone, V. (2017). Measuring rill erosion using structure from motion: A plot experiment. *Catena*, 156:383–392.

Eitel, J. U. H., Williams, C. J., Vierling, L. A., Al-Hamdan, O. Z., and Pierson, F. B. (2011). Suitability of terrestrial laser scanning for studying surface roughness effects on concentrated flow erosion processes in rangelands. *Catena*, 87(3):398–407.

Ferro, V. and Minacapilli, M. (1995). Sediment delivery processes at basin scale. *Hydrological Sciences Journal*, 40(6):703–717.

Flandrin, P., Gonçalvès, P., and Rilling, G. (2005). Hilbert-Huang Transform: Introduction and Applications. *World ScientIfic: Teaneck, NJ, pp. S7-74 S*, 200.

Foster, G. R. and Lane, L. (1983). Erosion by concentrated flow in farm fields. In *Proceedings of the DB Simons symposium on erosion and sedimentation*, pages 9.65–9.82. Colorado State University. Fort Collins, CO.

Fryirs, K. A. (2013). (Dis) Connectivity in catchment sediment cascades: a fresh look at the sediment delivery problem. *Earth Surface Processes and Landforms*, 38(1):30–46.

Fryirs, K. A., Brierley, G. J., Preston, N. J., and Kasai, M. (2007). Buffers, barriers and blankets: the (dis) connectivity of catchment-scale sediment cascades. *Catena*, 70(1):49–67.

Gessesse, G. D., Fuchs, H., Mansberger, R., Klik, A., and Rieke-Zapp, D. H. (2010). Assessment of erosion, deposition and rill development on irregular soil surfaces using close range digital photogrammetry. *The Photogrammetric Record*, 25(131):299–318.

Giménez, R. and Govers, G. (2001). Interaction between bed roughness and flow hydraulics in eroding rills. *Water Resources Research*, 37(3):791–799.

Govers, G. (1987). Spatial and temporal variability in rill developement processes at the Huldenberg experimental site. In Bryan, R. B., editor, *Rill Erosion :Processes and Significance*, number 8, chapter Catena Ver, pages 17–34.

Govers, G. (1992). Relationship between discharge, velocity and flow area for rills eroding loose, non-layered materials. *Earth Surface Processes and Landforms*, 17(5):515–528.

Govers, G., Takken, I., and Helming, K. (2000). Soil roughness and overland flow. *Agronomie*, 20(2):131–146.

Govindaraju, R. S. and Kavvas, M. L. (1992). Characterization of the rill geometry over straight hillslopes through spatial scales. *Journal of hydrology*, 130(1–4):339–365.

Grant, G. E. and Swanson, F. J. (1995). Morphology and processes of valley floors in mountain streams, western Cascades, Oregon. *Natural and anthropogenic influences in fluvial geomorphology*, pages 83–101.

Haan, C. T., Barfield, B. J., and Hayes, J. C. (1994). *Design Hydrology and Sedimentology for Small Catchments*. Academic Press, London.

Hager, W. H. (1989). Supercritical flow in channel junctions. *Journal of Hydraulic Engineering*, 115(2):243–259.

Harden, C. P. and Mathews, L. (2000). Rainfall response of degraded soil following reforestation in the Copper Basin, Tennessee, USA. *Environmental Management*, 26(2):163–174.

Harvey, A. M. (2001). Coupling between hillslopes and channels in upland fluvial systems: implications for landscape sensitivity, illustrated from the Howgill Fells, northwest England. *Catena*, 42(2):225–250.

Horton, R. E. (1945). Erosional development of streams and their drainage basins; hydrophysical approach to quantitative morphology. *Geological society of America bulletin*, 56(3):275–370.

Huang, Shen, Z., and Steven R. Long, N. E. (1999). A new view of nonlinear water waves: the Hilbert spectrum1. *Annual Review of Fluid Mechanics*.

Huang, N. E., Wu, M.-L. C., Long, S. R., Shen, S. S. P., Qu, W., Gloersen, P., and Fan, K. L. (2003). A confidence limit for the empirical mode decomposition and Hilbert spectral analysis. In *Proceedings of the Royal Society of London A: Mathematical, Physical and Engineering Sciences*, volume 459, pages 2317–2345. The Royal Society.

Ijjasz-Vasquez, E. J. and Bras, R. L. (1995). Scaling regimes of local slope versus contributing area in digital elevation models. *Geomorphology*, 12(4):299–311.

Kennedy, M. and Kopp, S. (2002). *Understanding map projections*. ESRI.

Kenworthy, S. T. and Rhoads, B. L. (1995). Hydrologic control of spatial patterns of suspended sediment concentration at a stream confluence. *Journal of hydrology*, 168(1–4):251–263.

Kirkby, M. J. and Bracken, L. J. (2009). Gully processes and gully dynamics. *Earth Surface Processes and Landforms*, 34(14):1841–1851.

Knapen, A., Poesen, J., and De Baets, S. (2007a). Seasonal variations in soil erosion resistance during concentrated flow for a loess-derived soil under two contrasting tillage practices. *Soil and Tillage Research*, 94(2):425–440.

Knapen, A., Poesen, J., Govers, G., Gyssels, G., and Nachtergaele, J. (2007b). Resistance of soils to concentrated flow erosion: A review. *Earth-Science Reviews*, 80(1–2):75–109.

Knighton, D. (1998). *Fluvial Forms and Processes: A New Perspective*. Number Ed. 2. Edward Arnold, London, UK.

Lague, D., Brodu, N., and Leroux, J. (2013). Accurate 3D comparison of complex topography with terrestrial laser scanner: Application to the Rangitikei canyon (N-Z). *ISPRS Journal of Photogrammetry and Remote Sensing*, 82:10–26.

Leigh, D. S. and Webb, P. A. (2006). Holocene erosion, sedimentation, and stratigraphy at Raven Fork, southern Blue Ridge Mountains, USA. *Geomorphology*, 78(1):161–177.

Lesschen, J. P., Schoorl, J. M., and Cammeraat, L. H. (2009). Modelling runoff and erosion for a semi-arid catchment using a multi-scale approach based on hydrological connectivity. *Geomorphology*, 109(3–4):174–183.

Line, D. E. and Meyer, L. D. (1989). Evaluating interrill and rill erodibilities for soils of different textures. *Transactions of the ASAE*, 32(6):1995–1999.

López-Vicente, M., Quijano, L., Palazón, L., Gaspar, L., and Izquierdo, A. N. (2015). Assessment of soil redistribution at catchment scale by coupling a soil erosion model and a sediment connectivity index (Central Spanish Pre-Pyrenees). *Cuadernos de investigación geográfica*, 41:127–147.

Lu, X., Li, Y., Washington-Allen, R. A., Li, Y., Li, H., and Hu, Q. (2017). The effect of grid size on the quantification of erosion, deposition, and rill network. *International Soil and Water Conservation Research*, 5(3):241–251.

Luffman, I. E., Nandi, A., and Spiegel, T. (2015). Gully morphology, hillslope erosion, and precipitation characteristics in the Appalachian Valley and Ridge province, southeastern USA. *Catena*, 133:221–232.

Maidment, D. R. (2002). *Arc Hydro: GIS for water resources*, volume 1. ESRI, Inc.

Masselink, R. J. H., Keesstra, S. D., Temme, A. J. A. M., Seeger, M., Giménez, R., and Casalí, J. (2016). Modelling discharge and sediment yield at catchment scale using connectivity components. *Land Degradation & Development*, 27(4):933–945.

Matmon, A., Bierman, P. R., Larsen, J., Southworth, S., Pavich, M., Finkel, R., and Caffee, M. (2003). Erosion of an ancient mountain range, the Great Smoky Mountains, North Carolina and Tennessee. *American Journal of Science*, 303(9):817–855.

McCarroll, D. and Nesje, A. (1996). Rock surface roughness as an indicator of degree of rock surface weathering. *Earth Surface Processes and Landforms*, 21(10):963–977.

Michaelides, K. and Wainwright, J. (2002). Modelling the effects of hillslope-channel coupling on catchment hydrological response. *Earth Surface Processes and Landforms*, 27(13):1441–1457.

Montgomery, D. R. (1994). Landscape dissection and drainage area-slope thresholds. *Process models and theoretical geomorphology*.

Mosley, M. P. (1976). An experimental study of channel confluences. *The Journal of Geology*, 84(5):535–562.

Nandi, A. and Luffman, I. (2012). Erosion related changes to physicochemical properties of Ultisols distributed on calcareous sedimentary rocks. *Journal of sustainable development*, 5(8):52–68.

Nardi, L. and Rinaldi, M. (2015). Spatio-temporal patterns of channel changes in response to a major flood event: the case of the Magra River (central-northern Italy). *Earth Surface Processes and Landforms*, 40(3):326–339.

Nearing, M. A., Norton, L. D., Bulgakov, D. A., Larionov, G. A., West, L. T., and Dontsova, K. M. (1997). Hydraulics and erosion in eroding rills. *Water Resources Research*, 33(4):865–876.

Penuela Fernandez, A., Rocio Rodriguez Pleguezuelo, C., Javaux, M., and Bielders, C. L. (2014). Effect of sheet and rill erosion on overland flow connectivity in bare agricultural plots. In *EGU General Assembly Conference Abstracts*, volume 16.

Pesci, A., Teza, G., and Bonali, E. (2011). Terrestrial laser scanner resolution: Numerical simulations and experiments on spatial sampling optimization. *Remote Sensing*, 3(1):167–184.

Rhoads, B. L. and Sukhodolov, A. N. (2001). Field investigation of three-dimensional flow structure at stream confluences: 1. Thermal mixing and time-averaged velocities. *Water Resources Research*, 37(9):2393–2410.

Richards, K. (2002). Drainage basin structure, sediment delivery and the response to environmental change. *Geological Society, London, Special Publications*, 191(1):149–160.

Richards, K. S. (1973). Hydraulic geometry and channel roughness; a non-linear system. *American Journal of Science*, 273(10):877–896.

Ritter, D. F., Kochel, R. C., and Miller, J. R. (2011). *Process geomorphology*. Waveland Press, Long Grove, IL.

Römkens, M. J. M. and Wang, J. Y. (1986). Effect of tillage on surface roughness. *Transactions of the ASAE*, 29(2):429–433.

Sankey, J. B., Glenn, N. F., Germino, M. J., Gironella, A. I. N., and Thackray, G. D. (2010). Relationships of aeolian erosion and deposition with LiDAR-derived landscape surface roughness following wildfire. *Geomorphology*, 119(1–2):135–145.

Scargle, J. D. (1989). Studies in astronomical time series analysis. III-Fourier transforms, autocorrelation functions, and cross-correlation functions of unevenly spaced data. *The Astrophysical Journal*, 343:874–887.

Selby, M. J. (1982). *Hillslope Materials and Processes*. Oxford University Press, New York, NY.

Shumway, R. H. and Stoffer, D. S. (2017). *Time Series Analysis and Its Applications*. Springer International Publishing.

Sukhodolov, A. N. and Rhoads, B. L. (2001). Field investigation of three-dimensional flow structure at stream confluences: 2. Turbulence. *Water Resources Research*, 37(9):2411–2424.

Tarboton, D. G. (2001). TauDEM, terrain analysis using digital elevation models. *ArcGIS Extension. Versão*, 5.

Tarboton, D. G., Bras, R. L., and Rodriguez-Iturbe, I. (1992). A physical basis for drainage density. *Geomorphology*, 5(1):59–76.

Tarolli, P. and Dalla Fontana, G. (2009). Hillslope-to-valley transition morphology: new opportunities from high resolution DTMs. *Geomorphology*, 113(1):47–56.

Torri, D., Poesen, J., Borselli, L., and Knapen, A. (2006). Channel width/flow discharge relationships for rills and gullies. *Geomorphology*, 76(3–4):273–279.

Tucker, G. E. and Bras, R. L. (1998). Hillslope processes, drainage density, and landscape morphology. *Water Resources Research*, 34(10):2751–2764.

Turnage, K. M., Lee, S. Y., Foss, J. E., Kim, K. H., and Larsen, I. L. (1997). Comparison of soil erosion and deposition rates using radiocesium, RUSLE, and buried soils in dolines in East Tennessee. *Environmental Geology*, 29(1):1–10.

Ullah, M. S., Bhattacharya, J. P., and Dupre, W. R. (2015). Confluence Scours Versus Incised Valleys: Examples From the Cretaceous Ferron Notom Delta, Southeastern Utah, US. *Journal of Sedimentary Research*, 85(5):445–458.

Vinci, A., Brigante, R., Todisco, F., Mannocchi, F., and Radicioni, F. (2015). Measuring rill erosion by laser scanning. *Catena*, 124:97–108.

Walling, D. E. (1983). The sediment delivery problem. *Journal of hydrology*, 65(1–3):209–237.

Wester, T., Wasklewicz, T., and Staley, D. (2014). Functional and structural connectivity within a recently burned drainage basin. *Geomorphology*, 206:362–373.

Wethered, A. S., Ralph, T. J., Smith, H. G., Fryirs, K. A., and Heijnis, H. (2015). Quantifying fluvial (dis) connectivity in an agricultural catchment using a geomorphic approach and sediment source tracing. *Journal of soils and sediments*, 15(10):2052–2066.

Wheaton, J. M., Brasington, J., Darby, S. E., and Sear, D. A. (2010). Accounting for uncertainty in DEMs from repeat topographic surveys: improved sediment budgets. *Earth Surface Processes and Landforms*, 35(2):136–156.

Wohl, E. E. and Pearthree, P. P. (1991). Debris flows as geomorphic agents in the Huachuca Mountains of southeastern Arizona. *Geomorphology*, 4(3–4):273–292.

Wu, Z., Huang, N. E., Long, S. R., and Peng, C.-K. (2007). On the trend, detrending, and variability of nonlinear and nonstationary time series. *Proceedings of the national academy of sciences*, 104(38):14889–14894.

Appendix for Chapter 4

Table 4.1: The summary statistics of 7 surveys and quality of intra-/between-survey registration

Dataset	Number of points	Avg. point density (pts/cm^2)	Intra-survey RMSE (mm)*	Between-survey RMSE (cm)*
12/2014	7671276	1.91	3.46 ± 1.13	0 (reference)
03/2015	8983232	2.25	3.51 ± 1.28	0.53 ± 0.08
06/2015	8223775	2.06	3.35 ± 1.11	0.41 ± 0.08
09/2015	8059708	2.02	3.34 ± 1.20	0.44 ± 0.05
12/2015	7931839	1.99	3.47 ± 1.38	0.40 ± 0.07
05/2016	7812266	1.96	3.75 ± 1.37	0.46 ± 0.08
12/2016	7891978	1.98	3.66 ± 1.32	0.45 ± 0.06

* mean ± standard error

Table 4.2: The areal and volumetric changes within our study area during the 7 scans

Time	12/2014 – 03/2015	03/2015 – 06/2015	06/2015 – 09/2015	09/2015 – 12/2015	12/2015 – 05/2016	05/2016 – 12/2016	Total
AREAL							
Area w. Detectable Change (m^2)	5.83	8.73	6.86	8.75	8.43	8.96	–
Area of Erosion (m^2)	3.80	8.59	6.35	7.37	8.04	8.10	–
Area of Deposition (m^2)	2.03	0.14	0.52	1.38	0.39	0.86	–
Percent of Area w. Detectable Change	3.76%	5.63%	4.42%	5.65%	5.44%	5.78%	–
VOLUMETRIC							
Volume of Erosion (m^3)	0.18 ± 0.07	0.38 ± 0.16	0.27 ± 0.10	0.36 ± 0.13	0.58 ± 0.17	0.62 ± 0.16	2.49 ± 0.79
Volume of Deposition (m^3)	0.05 ± 0.03	0.03 ± 0.01	0.04 ± 0.02	0.05 ± 0.02	0.03 ± 0.01	0.03 ±0.01	0.25 ± 0.10
Net sediment change (m^3)	-0.13 ± 0.10	-0.35 ± 0.17	-0.23 ± 0.12	-0.31 ± 0.15	-0.55 ± 0.18	-0.59 ± 0.17	2.24 ± 0.89

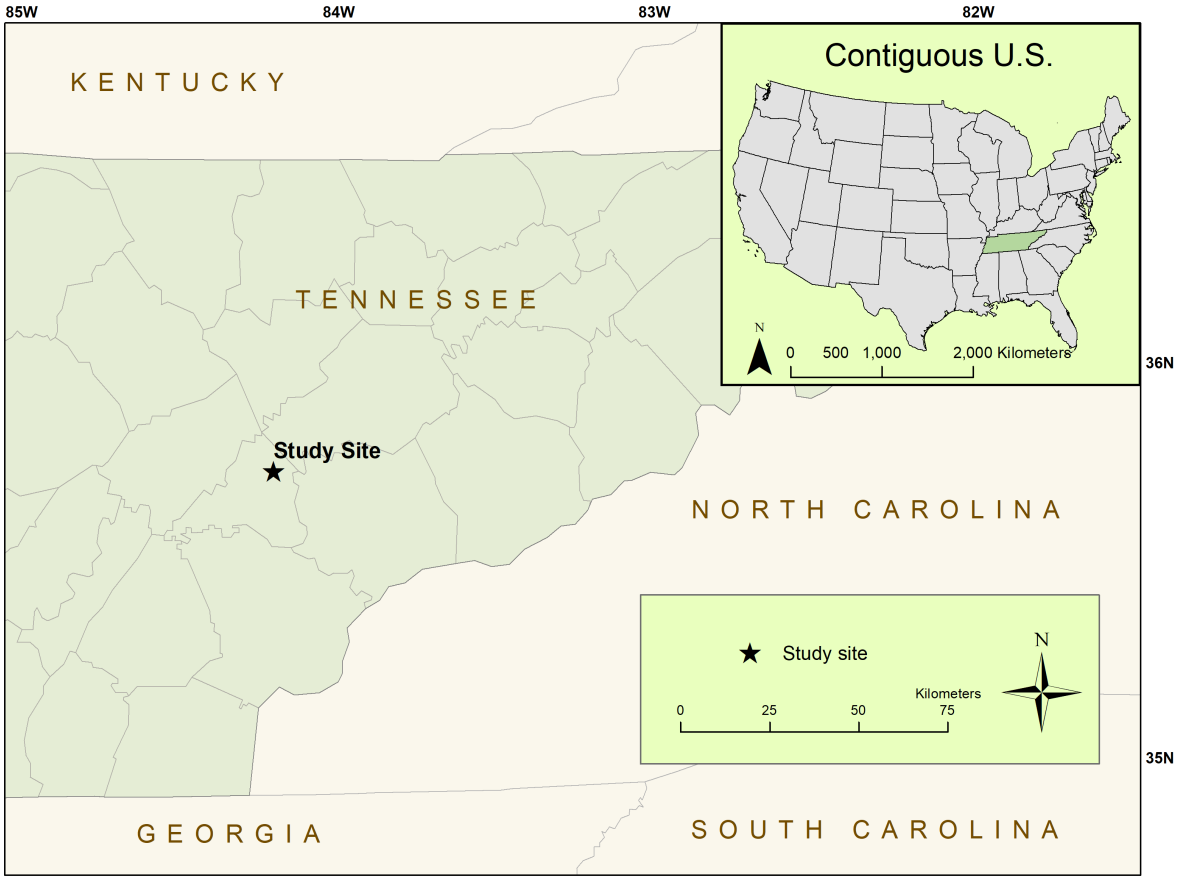

Figure 4.1: Study area

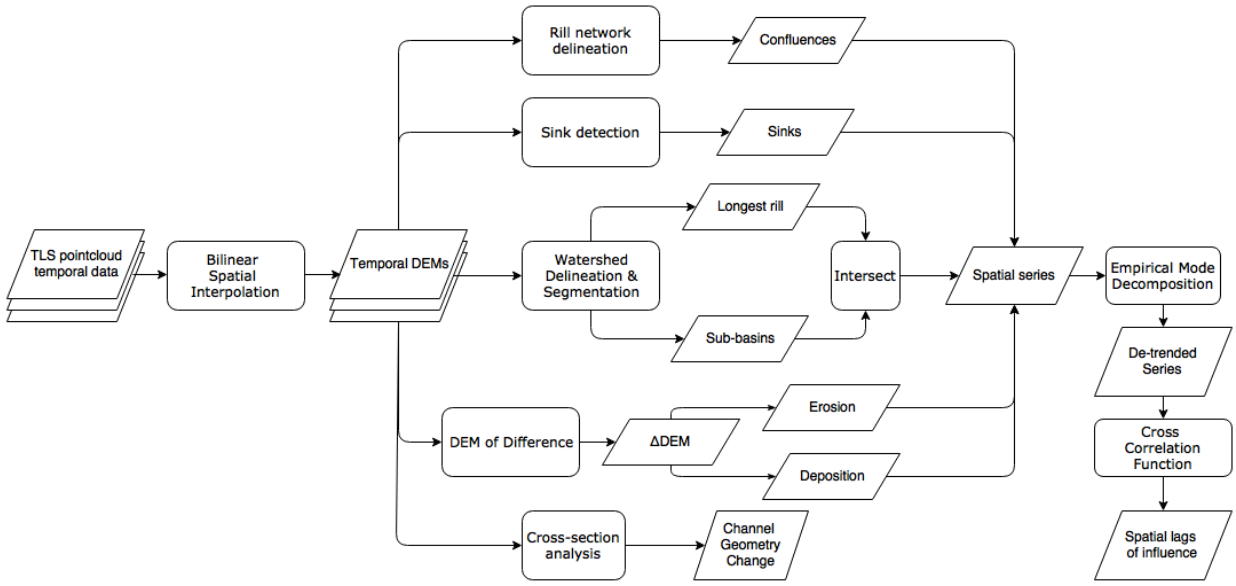

Figure 4.2: The workflow of data processing and analyses in this research.

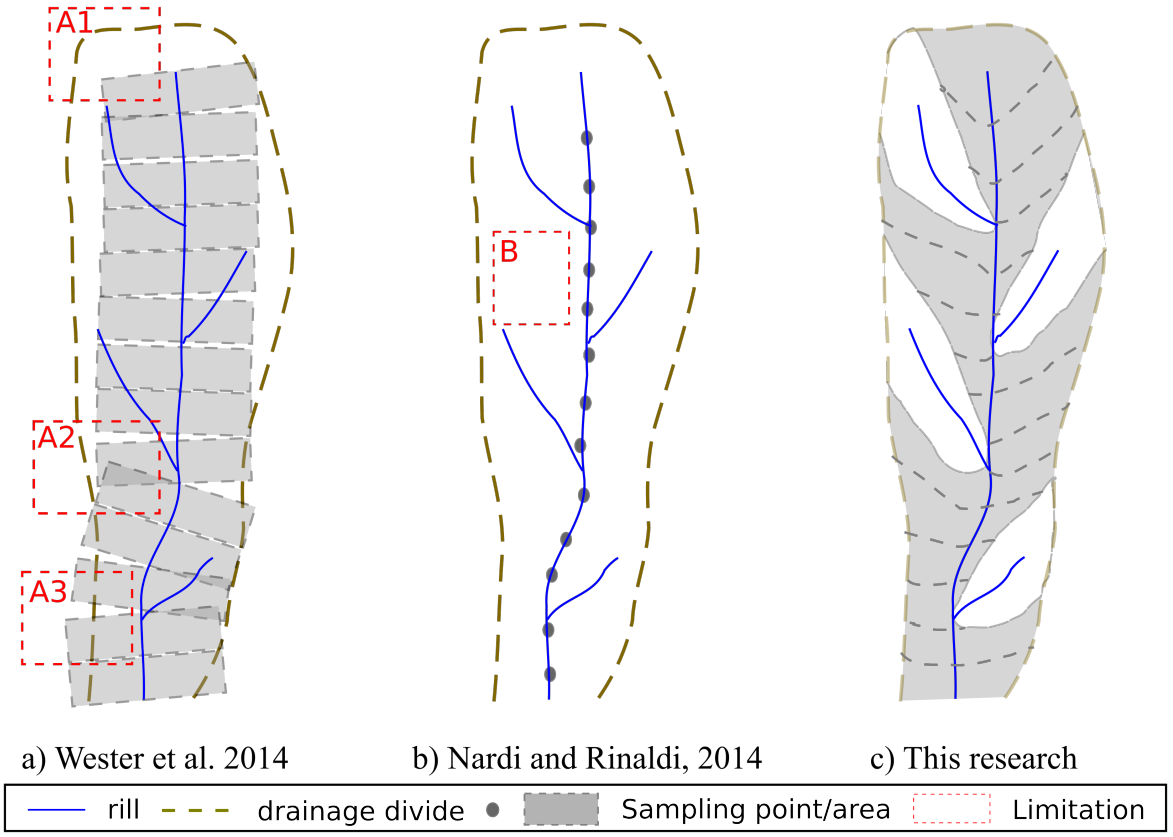

Figure 4.3: The comparison between the methods used in a) Wester et al. (2014), b) Brierley and Fryirs (2013), and c) this research. The sizes of the visual elements in this figure are for demonstration purposes only and may not be of the true scale. Limitations of a) and b) include: A1 – areas contributing to the rill channel are not captured; A2 – overlapping areas and gaps exist where rills are sinuous; A3 – sampling polygons are outside of the drainage divide; B – changes in interfluve are not captured.

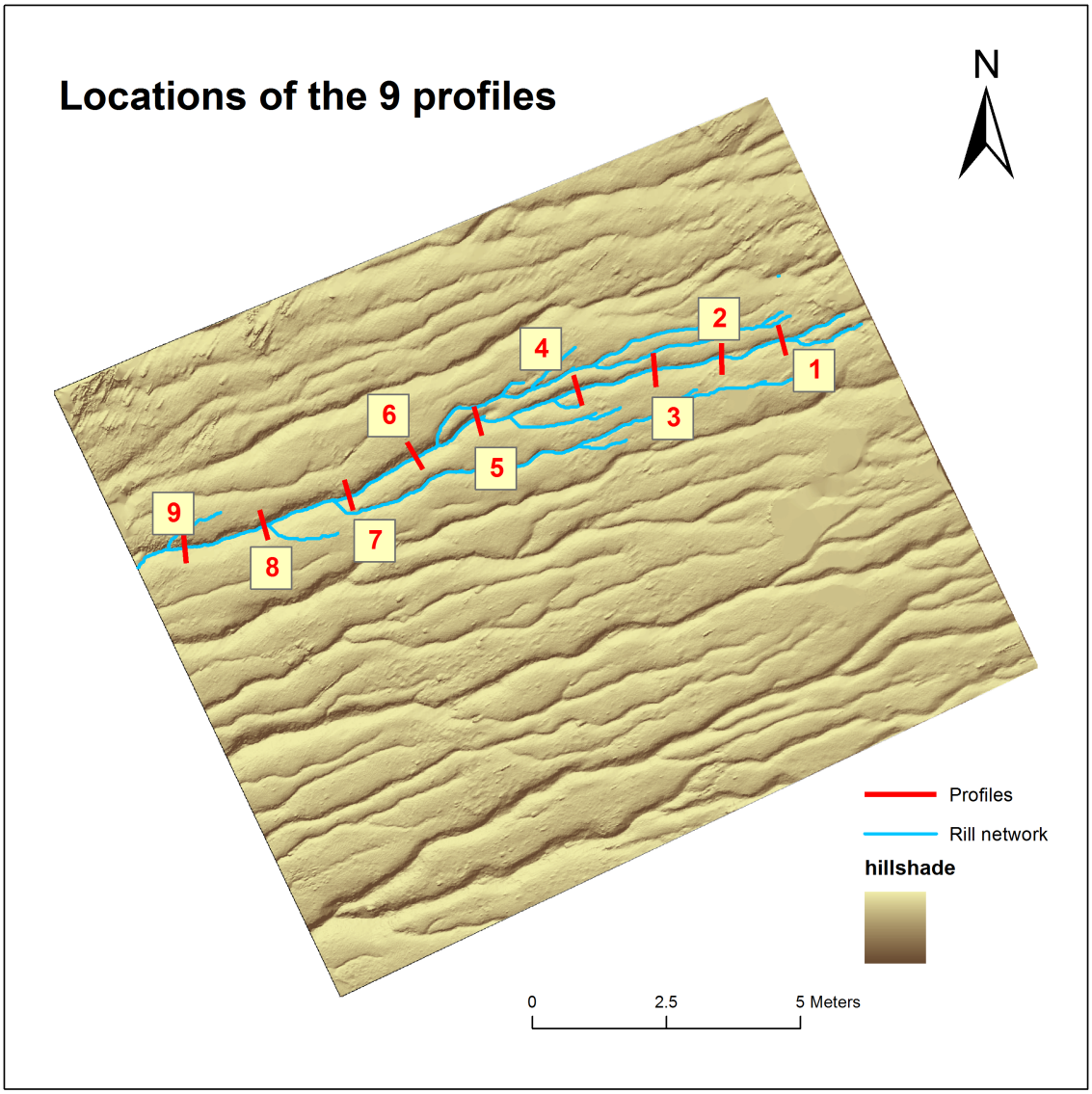

Figure 4.4: Locations of 9 cross-sections along a representative rill in our study area. Each cross-section is 60 cm long.

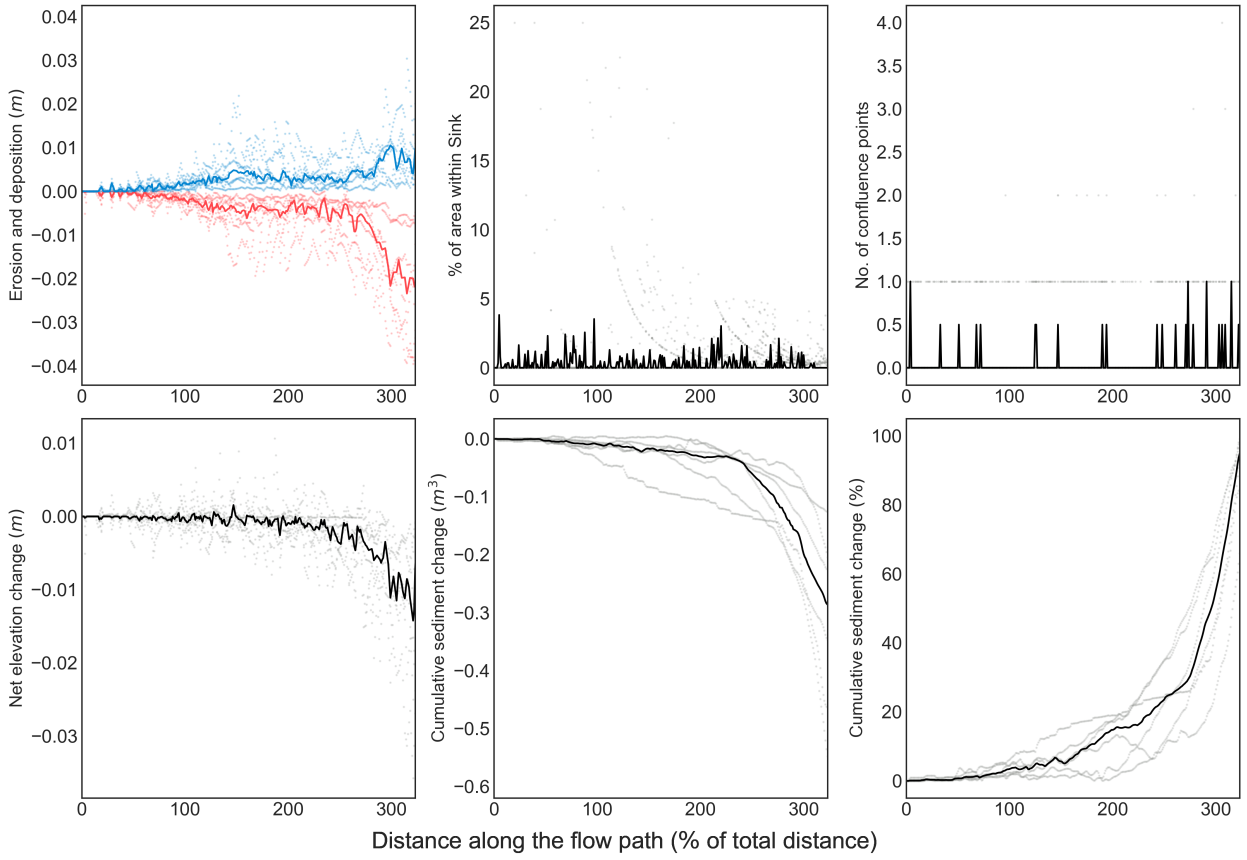

Figure 4.5: The summary of erosion/deposition, depression, confluence points, net elevation change, cumulative sediment change (m^3) and cumulative sediment change (%) along the rills. The dots specify the values for individual series, while the solid line represents the median of values at each distance.

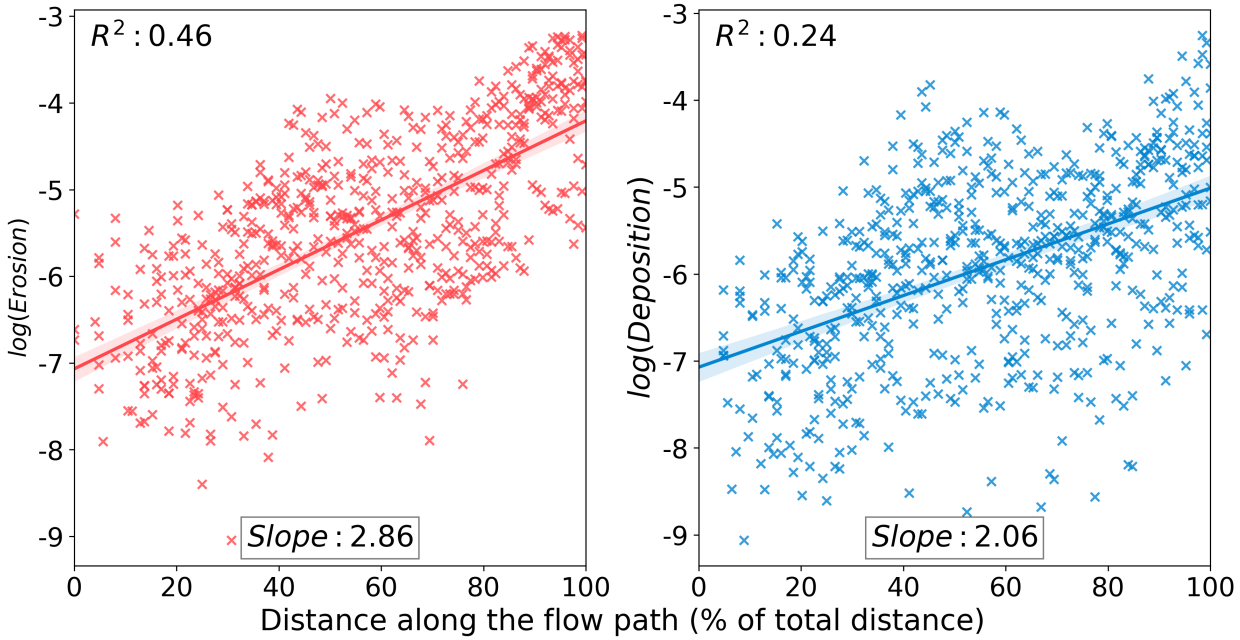

Figure 4.6: Regression results between the log-transformed erosion/deposition and downslope distance along the rills. The solid line represents the regression line, and shaded area represents the estimated line at 0.95 confidence interval.

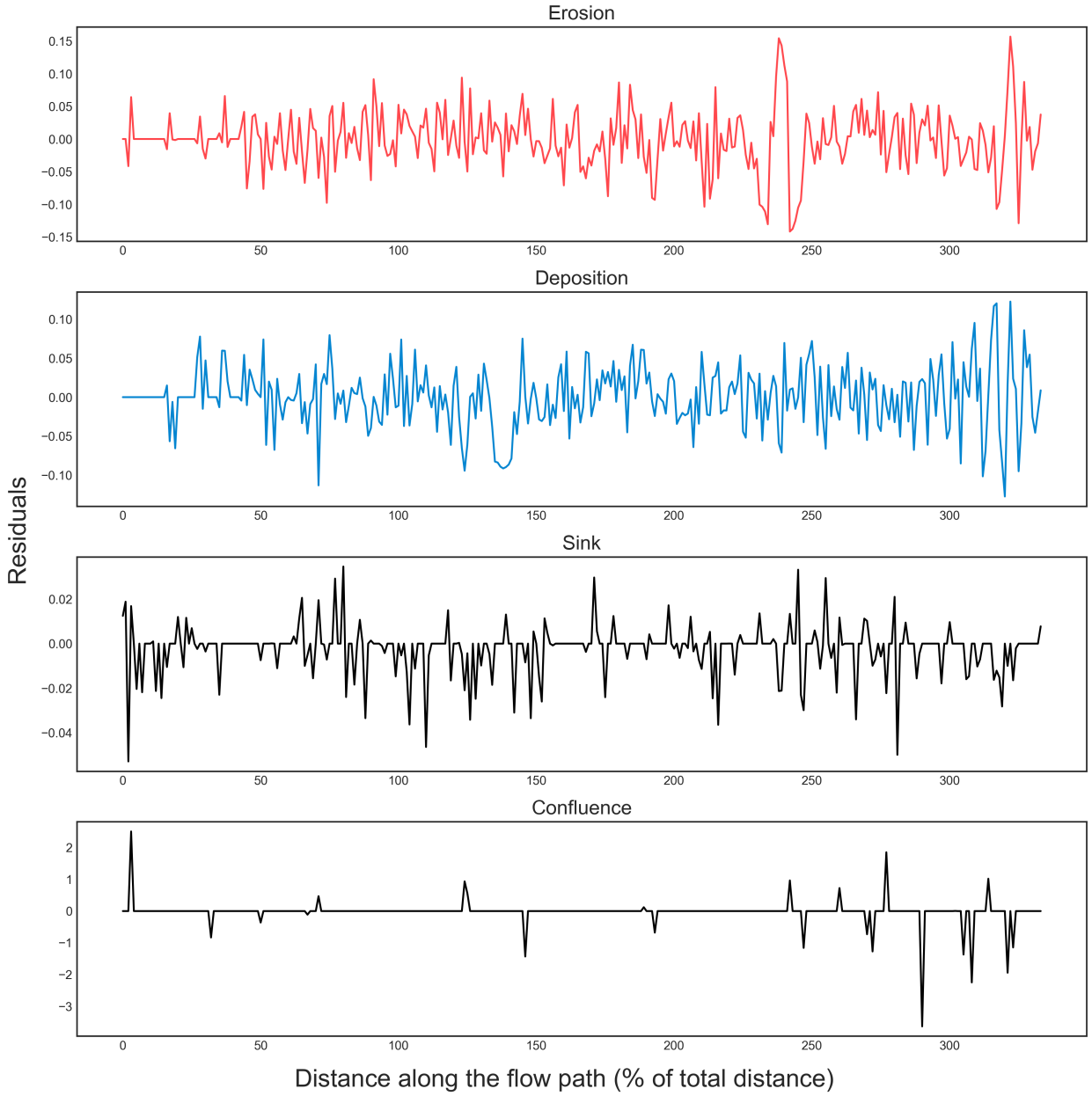

Figure 4.7: Residuals of the 4 series (erosion, deposition, sink, and confluence) obtained using the EMD. The EMD removes the trends and makes the series stationary. The values represent the residuals from the general trend.

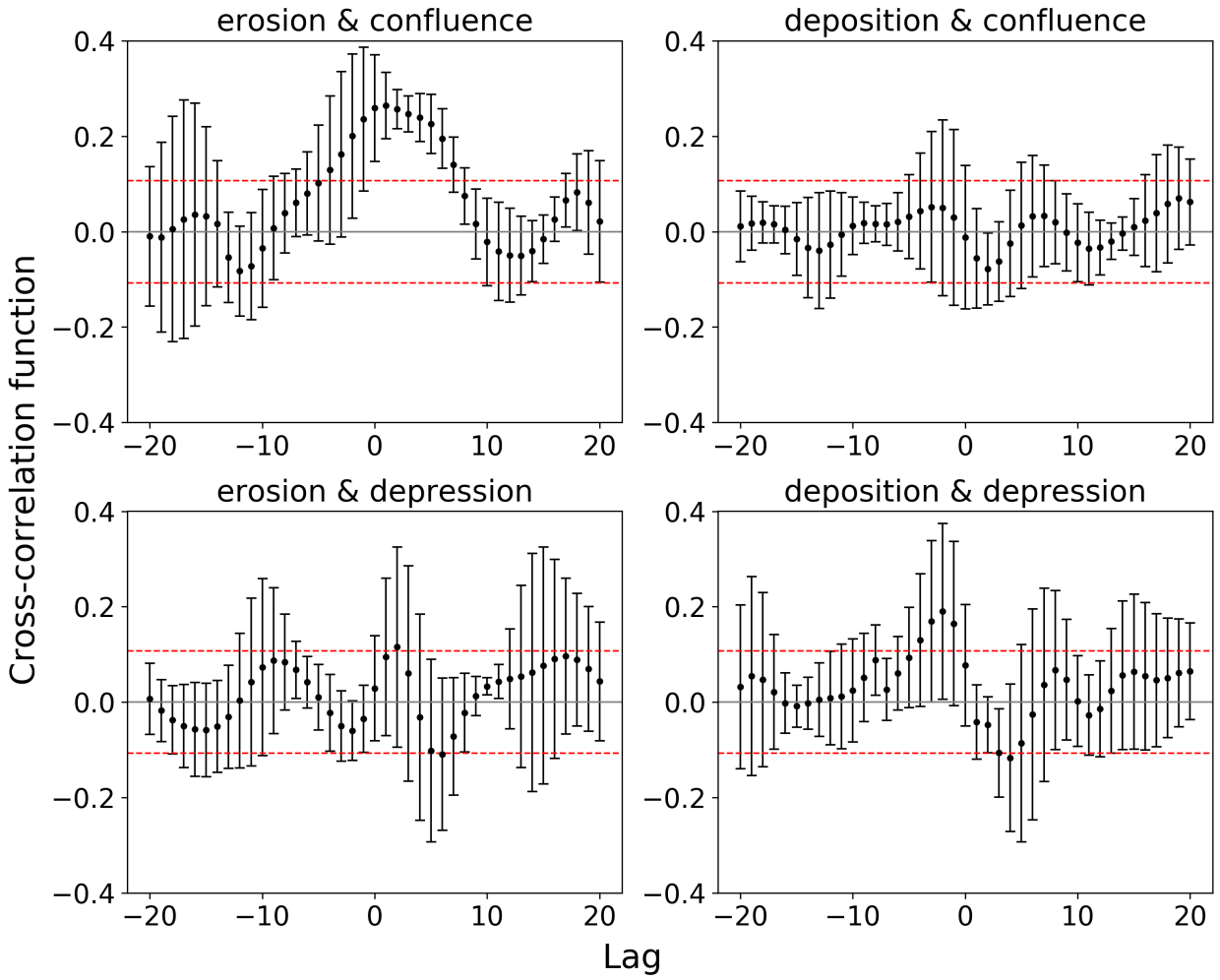

Figure 4.8: Results of the CCF between two sedimentological series (erosion and deposition) and two topographic series (confluence and depressions). Red dashed lines represent the 0.95 confidence interval. The spatial distance between any two adjacent locations of the same series is 0.05 m.

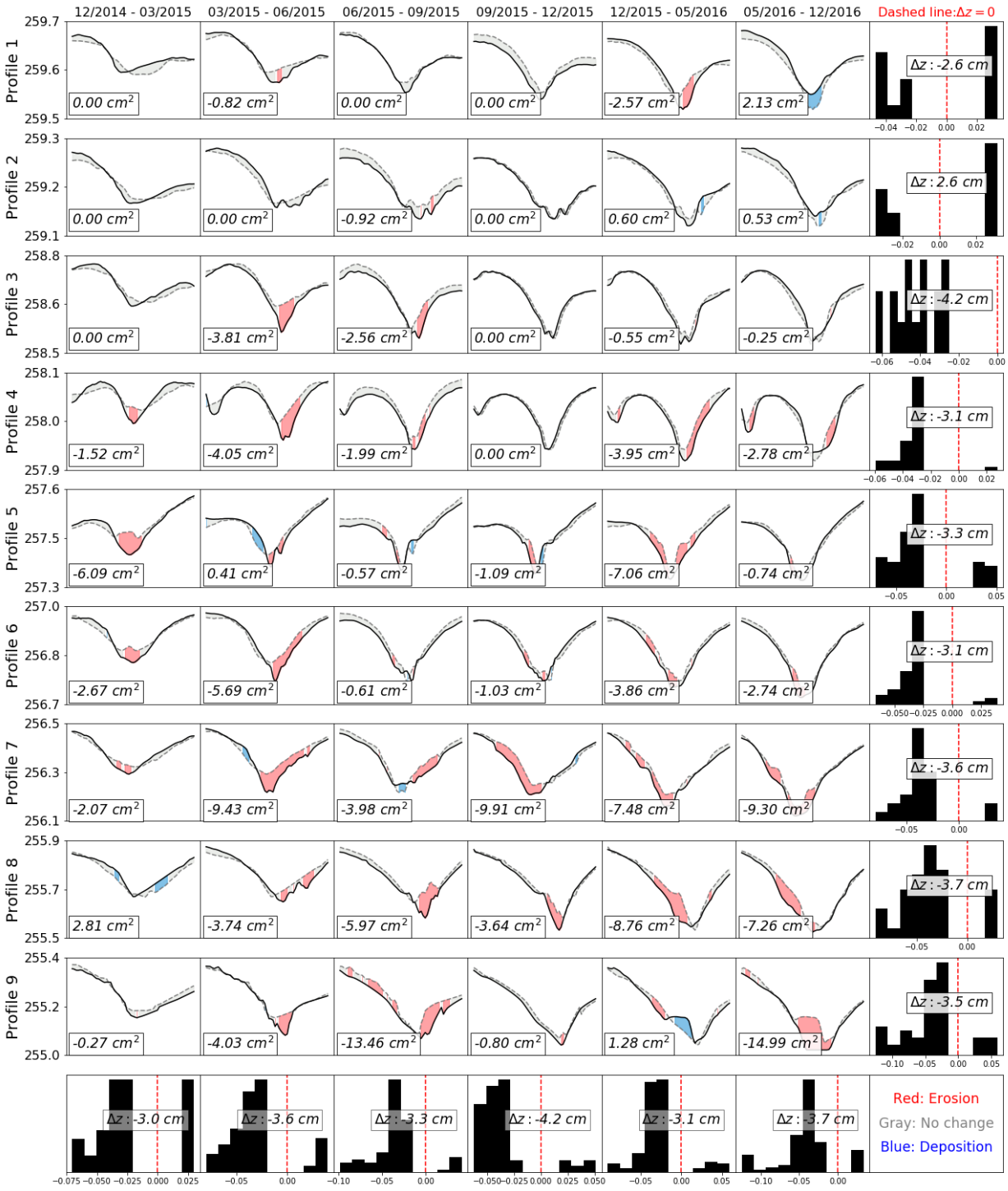

Figure 4.9: The changes along the 9 cross-sections. Red represents erosion, blue represents depositions, and gray represents area with no detectable changes. Histograms on the bottoms summarizes the changes during each time period; ones on the right summarizes the changes occurred for each profile. Each profile is 60 cm in length.

Chapter 5

Summary and future work

This dissertation research examined the sediment and channel change on a rilled hillslope in Loudon, TN. Fine resolution (cm level) DEMs were used to map the sediment redistribution within the study area and quantify the temporal changes of sediment and rills over time. Chapters 2 – 5 of this dissertation are stand-alone manuscripts that examined the influence of grid size on the change detection and rill delineation, the influence of micro-topographic variation on the erosion and deposition, and the impact of structural connectivity on the sedimentological connectivity in the study area. This chapter summarizes the major findings of this dissertation, and I would also discuss some future topics that might be extended from this research.

5.1 Summary and major findings

TLS is suitable for collecting high-resolution, high-accuracy temporal DEMs for the study of rill erosion, and the application of the TLS is subjective to the influence of both temporal and spatial resolution. Based on the pattern of the sediment redistribution, it was concluded that the erosion mainly occurred on rill sidewalls with some patches of erosion in interrill areas; the deposition occurred on some rill floors and also on some spots on the interrill areas. The changes occurred in the interrill areas are of smaller magnitude compared to those in the rills. Therefore, it is less likely to be captured if the time interval between two consecutive time periods is short. The interpretation of the results is also subjective to the spatial resolution. The point cloud dataset collected by the TLS is likely to have non-uniform density due to the occlusion of terrain ruggedness and the distance between the scanner and the intercepting surface. The dataset would be more manageable if sub-sampled to the similar spatial resolution (point spacing for point cloud dataset, and grid size for data in raster format). This research sought to identify the later one, and it was concluded that as the DEM resolution progressively reduces, the spatial variations of elevation change at a finer scale would be averaged across larger pixels, making it difficult to visually represent the continuous pattern of sediment redistribution along the rills. The absolute values of the area and volume of sediment change tend to decrease as the grid size increases, due to the

smoothing effect introduced by larger grid size. Such results reflect the critical role of scale in geomorphology and the fractal nature of the Earth surface.

A grid size equal to, or finer than 1-cm is recommended for mapping erosion and deposition in a rilled hillslope. The overall area of detectable change reduces to less than 50% of the 1-cm DEM when the grid size increased to 2-cm. Both the area and volume of erosion in the study are less sensitive to resolution reduction compared to deposition, presumably due to the different spatial patterns. The deposition mainly occurred at the rill floors, as a narrow band following the thalweg; while rill erosion occurred on the sidewalls of rills, and the erosional areas are relatively less elongated in shape compared to depositional areas. A grid size equal to, or finer than 1-cm is recommended for monitoring sediment delivery of rill/interrill erosions, although a grid size of 5-cm is sufficient if an estimation of 85% for the volume is acceptable. In this research, the relative value of sediment change (shown as the percent compared to the reference) is the least sensitive, and 81.97% of the sediment change is observed at the 10 cm grid size. From an areal perspective, however, the area of detectable change reduces to 67.63% when using a grid size of 2 cm, and 44.58% when using a grid size of 10 cm. In my study area, the total volume of deposited sediment was $0.23 \pm 0.15\ m^3$, which is much less compared to the volume of the sediment that was eroded ($0.81 \pm 0.53\ m^3$). Although the deposition is more sensitive to the increased grid size, the net difference between the volume of deposition and erosion is decreasing at a slower rate, and even at the grid size of 5-cm, it is able to obtain 86.89% of the net sediment volume change. The total length and the total number of rill segments show a decreasing trend, while the average length of rills increases with greater DEM grid size. As the spatial resolution gets coarser, the detailed shape of rills can be smoothed by the generalization. The RAPCA method was used to compare the offset between rill networks delineated using the resampled DEMs (with grid size larger than 1-cm) and the reference DEM (1-cm). The results show that although the mean and maximum offset increases as the grid size get larger, the relative offset is always within one pixel. Therefore, using a larger grid size might reduce the accuracy of the mapped rill networks in the slope, but the effect is always within one pixel.

Chapter 2 used used QR to examine the micro-topographic factors and its influence on sediment movement across a rilled hillslope. Generally, the QR showed stronger predictive ability compare to the OLS regression models, that 29% of the variability for erosion and 34% for deposition can be explained by the micro-topographic variables. A larger CA leads to higher erosion and deposition, although the absolute value of the coefficient for CA in the erosion model is relatively higher. A steeper slope is associated with higher erosion and lower deposition. The coefficient of slope is -0.052 for erosion and -0.076 for deposition, and this suggests that one degree of slope change will have an effect of -0.128 cm on the average elevation change. Ruggedness is positively related to deposition and negatively related to erosion. Rill floors with larger depth value tend to have less erosion and more deposition. The cosine component of the aspect is associated with higher erosion and lower deposition, possibly due to higher soil moisture on the north-facing slopes with limited solar insolation. The Topographic Wetness Index (TWI), another index that is positively associated with the soil moisture, also leads to higher erosion and lower deposition.

Chapter 3 investigated the longitudinal sedimentological connectivity and how it is influenced by the structural connectivity. The depressions within the rills and the confluences of the rills are closely related to the sedimentological connectivity on a rilled hillslope. The general trend of both the erosion and deposition increases exponentially along the profile of the rills, while the magnitude of the increase of erosion is greater than that of the deposition. The coefficient of erosion (2.86) is greater than that of deposition (2.06), suggesting that erosion tend to be dominant compared to deposition along the rill profile. The rill length accounts for 46% of the variability for erosion and 24% of the variability for deposition. The longitudinal erosion, deposition, depressions, and confluence locations are represented using series of measurements at a 5 cm interval. By removing the general trend, I extracted the variations of the series and examined the relationship between any two paired series using the cross-correlation analyses. The results of the cross-correlation analyses suggest that the confluences of rills lead to higher amount of erosion in both upstream and downstream directions. The effect is the strongest at the location of confluence, and attenuates as it gets further away from the confluence point until becoming statistically insignificant. The

depressions within the rills lead to higher magnitude of deposition, and such influence is only observed in the upstream direction.

5.2 Future work

This dissertation research addressed three issues (scale, micro-topographic control, and channel connectivity) associated with the application of high-resolution DEMs for the study of sediment and channel dynamics on rilled hillslopes. The findings of this research may serve as a good starting point for future studies on similar topics. On the other hand, this work also has limitations that might be addressed in the future studies. A few possible topics of interest are listed in this section.

5.2.1 Field validation and measurement

This research was based on the fine resolution (cm level) elevation data collected using the Terrestrial Laser Scanner (TLS). Although the TLS has demonstrated some major advantages including fast data acquisition and high accuracy, it also has limitations. For the study area, rills have developed over time and incised the hillslope surface. The ruggedness of the terrain surface will introduce occlusion, leading to gaps in our survey data. Switching to multiple scan location can address this problem to a certain degree, but the areas within the rills are likely to have relatively lower point density, reducing the validity of the elevation measurements. We used the Fuzzy Inference Systems in the Geomorphic Change Detection tool (Wheaton et al., 2010) in ArcGIS to account for the uncertainty associated with the temporal DEMs. This method provides a convenient and computationally simple way to address the uncertainty associated with the calculation. Future research could possibly provide better ways to propagate error and expand our ability to capture the surface changes, especially in areas with low elevation changes (e.g. interrill areas).

Future research can incorporate data from other sources to enhance the validity of the data, and the fusion of multi-source dataset may also provide insights into the data management and processing. Previous works have shown the merit of validation using field

measurements and other remotely-sensed technologies (Di Stefano et al., 2017; Vinci et al., 2015, 2016). Di Stefano et al. (2017) measured the geometry of the cross-sections of the rills using the gypsum cast and the profilometer, to validate the result of the digital terrain model (DTM) captured by structure-from-motion (SFM). Vinci et al. (2015) also used the DTM generated using the SFM to measure the rill erosion. More efforts on the validation and calibration are necessary to improve the quality assessment and control in future research. Data of other valid sources do not have to be limited to elevation. Images collected either by the Unmanned Aerial Systems or handheld camera can be used to assist the DEM-based analyses. Measurements on other properties of the soil including the soil moisture and the organic matter can also be included.

5.2.2 Physical processes and heuristic implications

The major source of data used in this research is elevation data in the form of DEMs. We used different approaches to address the selected research topics, but the research is heuristic and the majority of the findings in this research are data-driven. One limitation to this research design is that factors including the precipitation, soil, vegetation, and the topography are not within a controlled environment. That means we cannot set up specific experimental conditions with some factors fixed. It would be more ideal if in future studies, the conditions of precipitation, topography, and soil can be controlled either in a natural or lab setting. Furthermore, with the controlled precipitation conditions, the duration, intensity, and frequency of the precipitation events can all be adjusted based on the need of the researcher. The processes can be greatly accelerated, and the controlled experiments with the same conditions can be performed for multiple times.

Currently, the majority of the TLS-based erosion studies still focus on the statistical inferences of the surface characteristics and the channel properties on the erosion and/or deposition. Several attempts to build the linkages between the statistical implications and the physical processes are present in existing literatures. Eitel et al. (2011) used the flow regulator to simulate concentrated runoff on several experimental plots, and concluded that TLS-measured surface roughness yields better results compared to the manually measurements.

Di Stefano et al. (2017) re-visited the power relationship between the erosional volume and the contributing area based on the data collected using the TLS. Zhang et al. (2016) used the TLS to capture the morphological variations of the rills over time during simulated rainfall events. These attempts exhibit promising perspectives for future applications, and future researchers would have more opportunities to revisit previous theories and concepts to test if the incorporation of high-resolution elevation data could help our understanding in the physical processes, as well as improve our ability to predict erosion and deposition for land management purposes.

5.2.3 Expanding the time and geographic scale of hillslope processes

This dissertation research has a focus on a rilled hillslope in the East Tennessee. The data collection has not started until the hillslope has well-developed rill networks that are already of 10s of centimeters wide and deep. Important questions have yet to be answered as how our observations and conclusions would differ if the rills were in the early stages of developing. It has been widely accepted that where the rills emerge on the hillslope is controlled by the initial condition of the micro-topography (Favis-Mortlock et al., 2000; Bennett et al., 2015; Gessesse et al., 2010). Through observation of the elevation changes overtime, it would be possible to bridge the gap between the rill formation and the micro-topographic characteristics.

The topics investigated in this dissertation research can be expanded to larger hillslope channels such as gullies as well. Gullies usually form where the contributing area is large and the vegetation is absent (Knighton, 1998). Therefore, surveying the gullies would be labor intensive and time consuming if the entire contributing area is to be captured. But for large permanent gullies (sometimes also referred to as classic gullies) (Haan et al., 1994), the advantage of the TLS compared to satellite-based or airborne remote sensing technologies is that the scanner can be mounted within the gully and the entire features on the sidewall can be captured. McNelis (2016) surveyed a permanent gully in the West Tennessee by mounting the scanner at different locations within the gully to capture the expansion of gully head, failures on the sidewall, and within-gully depositions. Traditional raster format

DEMs would be not optimal since a single value has to be assigned for every horizontal spatial unit (a pixel/cell in raster dataset), but the point cloud would be able to capture the varied geometries on the vertical perspective. Consequently, better analytical algorithms and tools should be developed. In recent years, tools including the CANUPO (Brodu and Lague, 2012) and M3C2 (Lague et al., 2013) have extended our ability to analyze the 3-D structural changes in the point cloud dataset. In the future, researchers should seek to develop and employ more advanced tools to improve the processing, analyzing, and visualizing capabilities.

5.2.4 Other factors to be considered

Soil erosion and deposition are complex processes driven by topography, climate, soil, vegetation, and human activities. This dissertation only examined the influence of topography on the erosion and deposition. The other factors were either not showing much variability in our study site (vegetation, soil, and human activities), cannot be measured at such fine-scale (climate and soil), or not included due to logistic limitations. The absence of these variables in this research by no means suggests these factors are of lesser significance. Future work, given logistic, financial, and technological feasibility, should incorporate some factors describing conditions of climate, soil, vegetation, and human activities in the erosion and deposition modeling efforts.

References

Bennett, S. J., Gordon, L. M., Neroni, V., and Wells, R. R. (2015). Emergence, persistence, and organization of rill networks on a soil-mantled experimental landscape. *Natural Hazards*, 79(1):7–24.

Brodu, N. and Lague, D. (2012). 3D terrestrial lidar data classification of complex natural scenes using a multi-scale dimensionality criterion: Applications in geomorphology. *ISPRS Journal of Photogrammetry and Remote Sensing*, 68:121–134.

Di Stefano, C., Ferro, V., Palmeri, V., and Pampalone, V. (2017). Measuring rill erosion using structure from motion: A plot experiment. *Catena*, 156:383–392.

Eitel, J. U. H., Williams, C. J., Vierling, L. A., Al-Hamdan, O. Z., and Pierson, F. B. (2011). Suitability of terrestrial laser scanning for studying surface roughness effects on concentrated flow erosion processes in rangelands. *Catena*, 87(3):398–407.

Favis-Mortlock, D. T., Boardman, J., Parsons, A. J., and Lascelles, B. (2000). Emergence and erosion: a model for rill initiation and development. *Hydrological Processes*, 14(11-12):2173–2205.

Gessesse, G. D., Fuchs, H., Mansberger, R., Klik, A., and Rieke-Zapp, D. H. (2010). Assessment of erosion, deposition and rill development on irregular soil surfaces using close range digital photogrammetry. *The Photogrammetric Record*, 25(131):299–318.

Haan, C. T., Barfield, B. J., and Hayes, J. C. (1994). *Design Hydrology and Sedimentology for Small Catchments*. Academic Press, London.

Knighton, D. (1998). *Fluvial Forms and Processes: A New Perspective*. Number Ed. 2. Edward Arnold, London, UK.

Lague, D., Brodu, N., and Leroux, J. (2013). Accurate 3D comparison of complex topography with terrestrial laser scanner: Application to the Rangitikei canyon (N-Z). *ISPRS Journal of Photogrammetry and Remote Sensing*, 82:10–26.

McNelis, J. J. (2016). Quantifying Gully Erosion in West Tennessee using High Resolution LiDAR Data. Master's thesis, Knoxville, Tennessee.

Vinci, A., Brigante, R., Todisco, F., Mannocchi, F., and Radicioni, F. (2015). Measuring rill erosion by laser scanning. *Catena*, 124:97–108.

Vinci, A., Todisco, F., and Mannocchi, F. (2016). Calibration of manual measurements of rills using Terrestrial Laser Scanning. *Catena*, 140:164–168.

Wheaton, J. M., Brasington, J., Darby, S. E., and Sear, D. A. (2010). Accounting for uncertainty in DEMs from repeat topographic surveys: improved sediment budgets. *Earth Surface Processes and Landforms*, 35(2):136–156.

Zhang, P., Tang, H., Yao, W., Zhang, N., and Xizhi, L. V. (2016). Experimental investigation of morphological characteristics of rill evolution on loess slope. *Catena*, 137:536–544.

Appendices

The appendices include key Python scripts used for the data analyses and visualization in this Research. All scripts were produced in Python 3.6 unless otherwise noted.

Appendix 1. Sample script used for Chapter 3

```
from statsmodels.regression.quantile_regression import QuantReg
import pandas as pd
import numpy as np
import matplotlib.pyplot as plt
from sklearn import metrics
from operator import itemgetter
from sklearn.model_selection import cross_validate, KFold, RFE

%matplotlib inline
```

```
def rfe_select(rfe_result_list,data,target, x):
    """[function for variable selection]

    Arguments:
        rfe_result_list {[type:list]} -- [list of variables]
        data {[type:pandas DataFrame]} -- [data]
        target {[type:string]} -- [the dependent variable]
        x {[type:array-like]} -- [features used in the model]

    Returns:
        mse_min {[type:float]} -- [minimal mse]
        no_features {[type:int]} -- [the number of features selected]
    """

    mse_dict = dict()
    features = list()
    for i in np.arange(len(rfe_result_list))+1:
        feature_index = list(np.arange(i)+1)
        feature_select = [rfe_result_list[x] for x in feature_index]
        model = QuantReg()
        mse_dict[i] = kgf_cv(data = data,
                             target = target,
                             features = feature_select)
    mse_min = min(mse_dict.values())
    f_list = list(mse_dict.keys())
    no_features = f_list[list(mse_dict.values()).index(mse_min)]
    return (mse_min, no_features)
```

```
def kgf_cv(data, target, features, split):
    """[group k-fold cross-validation]

    Arguments:
        data {[type:pandas DataFrame]} -- [data]
        target {[type:string]} -- [the dependent variable]
        features {[type:array-like]} -- [features used in the model]
        split {[type:int]} -- [how many folds to split]
    Returns:
        [test_score] -- [score of model]
    """

    model = QuantReg()
    y = data[target]
    x = data[features]
    gkf = KFold(n_splits=2, shuffle=True)
    cv = cross_validate(estimator=model, cv=gkf,
                        X=x, y=y,scoring='neg_mean_squared_error')
    test_score = -np.mean(cv['test_score'])
    return (test_score)
```

```
def pred_ints(model, X, percentile=95.):
    """[predicting at a given quantile]

    Arguments:
        model {[type:model.class]} -- [fitted model]
        X {[type: array-like]} -- [features to be used]

    Keyword Arguments:
        percentile {float} -- [quantile] (default: {95})

    Returns:
        quantile [type:float] -- [quantile predictions]
    """

    quantile = []
    for x in range(len(X)):
        preds = []
        for pred in model.estimators_:
            preds.append(pred.predict(X[x].flatten().reshape(1,-1)))
        quantile.append(np.percentile(preds, (100 - percentile) / 2. ))
    return (quantile)
```

```
def quantile_prediction_graph(target, quantile=50., randomstate=42):
    """[quantile predictions]

    Arguments:
        target {[type:string]} -- [independent variable]

    Keyword Arguments:
        quantile {[type:float]} -- [quantile] (default: {50.})
        randomstate {int} -- [random seeds] (default: {42})

    Returns:
        y_test [type:array-like] -- [y_test]
        prediction [type:array-like] -- [y_hat]
        r2 [type:float] -- [r-squared]
        slope [type:float] -- [coefficient]
        intercept [type:float] -- [intercept]
    """

    X_train, X_test, y_train, y_test = train_test_split
    (data[features], data[target], test_size=0.1, random_state=12)
    X_train = X_train.as_matrix()
    y_train = y_train.as_matrix()
    X_test = X_test.as_matrix()
    y_test = y_test.as_matrix()
    model = QuantReg(quantile = 50.)
    model.fit(X_train, y_train)
    regr = linear_model.LinearRegression()
    prediction = pred_ints(model, X_test, percentile = quantile)
    regr.fit(X=y_test.reshape(-1,1),y=prediction)
    r2 = r2_score(y_pred=prediction, y_true=y_test)
    slope = regr.coef_
    intercept = regr.intercept_
    return (y_test, prediction, r2, slope, intercept)
```

Appendix 2. Sample script used for Chapter 4

```
import pandas as pd
import matplotlib.pyplot as plt
import numpy as np
import seaborn as sns
from matplotlib.ticker import FormatStrFormatter
from PyEMD import EMD

%matplotlib inline
```

```
#script used to plot residuals
f,ax = plt.subplots(ncols=1, nrows=4, figsize=(12,12),dpi=300)
col_list=['#ff474c','#0485d1','black','black']
df_new = df.groupby('Distance').agg('median')
res_dict = {}
for index,ax in enumerate(f.axes):
    if index ==0:
        target = 'Erosion'
    if index ==1:
        target = 'Deposition'
    if index ==2:
        target = 'Sink'
    if index ==3:
        target = 'Confluence'
    data=df_new[target]

    if index == 2:
        d = np.abs(np.array(data))
    else:
        d = np.log(np.abs(np.array(data)))

    x = np.arange(len(d))
    emd = EMD()
    res = emd(d)[0]

    ax.plot(x, res,c=col_list[index])
    ax.set_ylabel('')
    ax.set_xlabel('')

f.tight_layout()
```

```
#script used to produce series figures
sns.set_style('white')
nrow, ncol = 2, 3
fig, axs = plt.subplots(nrows=nrow, ncols=ncol, figsize = (15,10), dpi=300)
Feature_list = #list of features
y_label_list = #list of labels

for f, ax in enumerate(fig.axes):
    df_j = df[df['Date'] == Date_list[0]]
    if f == 0:
        ax.scatter(df['Distance'], df['Erosion'],
                   c='#ff474c', alpha=0.2, s = 1)
        ax.scatter(df['Distance'], df['Deposition'],
                   c='#0485d1', alpha=0.2, s = 1)
        dep = df.groupby('Distance')['Deposition'].agg('median')
        ero = df.groupby('Distance')['Erosion'].agg('median')
        ax.plot(df_j['Distance'], ero, c='#ff474c', alpha=1)
        ax.plot(df_j['Distance'], dep, c='#0485d1', alpha=1)
    else:
        df_j = df[df['Date'] == Date_list[0]]
        feature = Feature_list[f-1]
        if f not in [1, 5]:
            ax.scatter(df['Distance'], df[feature], c='#929591',
                       alpha=0.2, s = 1)
            med = df.groupby('Distance')[feature].agg('median')
            ax.plot(df_j['Distance'], med, c='black', alpha=1)

        else:
            ax.scatter(df['Distance'], df[feature]*100, c='#929591',
                       alpha=0.2, s = 1)
            med = df.groupby('Distance')[feature].agg('median')*100
            ax.plot(df_j['Distance'], med, c='black', alpha=1)

        ymax, ymin = ax.get_ylim()
    ax.set_ylabel(y_label_list[f], fontsize = 15)
    ax.tick_params(labelsize=16)

fig.tight_layout()
```

Vita

Xiaoyu Lu was born and raised in Wuwei, China. He attended the Beijing Forestry University in 2006. He received a Bachelor of Science degree in *Urban and Rural Planning and Resources Management* (now *Physical Geography*) in July 2010, and a Master of Agricultural Sciences degree in *Soil and Water Conservation and Resources Management* in July 2013. Xiaoyu came to the United States in 2014 to attend the University of Tennessee for a Ph.D. degree in *Geography* under the advising of Dr. Yingkui Li. Xiaoyu's research interests center around the application of geo-spatial sciences and technology in the study of Earth-surface processes.